2024-03-15

Viscous Fingering Instability of Complex Fluids in a Radial Hele-Shaw Cell

Lee, Young Hoon

UNIVERSITY OF CALGARY

Viscous Fingering Instability of Complex Fluids in a Radial Hele-Shaw Cell

by

Young Hoon Lee

A THESIS

SUBMITTED TO THE FACULTY OF GRADUATE STUDIES

IN PARTIAL FULFILMENT OF THE REQUIREMENTS FOR THE

DEGREE OF DOCTOR OF PHILOSOPHY

GRADUATE PROGRAM IN CHEMICAL AND PETROLEUM ENGINEERING

CALGARY, ALBERTA

MARCH, 2024

Abstract

When a less-viscous fluid displaces another fluid of higher viscosity in a porous medium, instability can develop at the interface between the two fluids. The instability manifests itself in the form of finger-like patterns of the displacing fluid propagating through the displaced one. In this work, viscous fingering instabilities involving complex fluids in a radial Hele-Shaw is investigated. Many fluids in our lives such as shaving foams, glues, flour-water dough, mayonnaise, and paints are complex fluids which exhibit multiple non-Newtonian properties simultaneously such as shear-thinning or shear-thickening, yield stress, and viscoelastic effects. First, the effects of normal stress differences of dilute low molecular weight poly(ethylene oxide) (PEO) solutions on viscous fingering instability are studied. Second, we investigate the instabilities associated with air invading foam in Hele-Shaw cell. Third, we examine the effects of water in viscous fingering instabilities of air displacing mineral oil. Fourth, the instability at the interface between two parallel flows of immiscible liquids through a uniform planar pore is studied by using linear stability analysis. We pose important questions: How does normal stresses affect immiscible radial viscous fingering? How does fingering occur into foam? Is it similar to that of a single-phase liquid? The experimental observations reveal nonmonotonic and opposing effects are evident depending on the molecular weight of the PEO and the stage of the radial viscous fingering evolution. We have identified three different flow regimes in the immiscible radial displacement flows of air invading foam in Hele-Shaw cell. The presence of a small volume of water leads to significantly different fingering patterns than that when no water is present. The outcomes are significant because the results demonstrate new behaviors for displacement flow of complex fluids.

Preface

The thesis is based on four manuscripts, which have either been published or are currently in the process of preparation for submission.

1. Chapter 3 is published as “Lee, Y. H., Wang, J., & Gates, I. D. (2023). Effects of dilute low molecular weight poly (ethylene oxide) solutions in immiscible radial viscous fingering instabilities. Physics of Fluids, 35(8).”
2. Chapter 4 is based on a manuscript “Lee, Y. H., Wang, J., Kannaiyan R., Su Y., & Gates, I. D. (2024). Air invasion into three-dimensional foam induces viscous fingering instabilities. Scientific Reports, 14.”
3. Chapter 5 is based on a manuscript “Lee, Y. H., Wang, J., Kannaiyan R., & Gates, I. D. (2024). Viscous fingering and interface splitting instabilities in air-water-oil systems” which is under review in a peer-reviewed journal.
4. Chapter 6 is published as “Lee, Y. H., & Gates, I. D. (2022). Instability of parallel flow of two immiscible liquids in a pore and application to steam-assisted gravity drainage. The Canadian Journal of Chemical Engineering, 100, S302-S311.”

Acknowledgements

I am deeply thankful for the enormous support and guidance provided by my supervisor, Dr. Ian Gates. I am very grateful for his dedication in the late-night and weekend efforts to revise my manuscripts. I am also very thankful for Dr. Jingyi Wang and Dr. Ranjani Kannaiyan for their assistance in my experiments.

I am also grateful to my supervisory committee members, Dr. Jalel Azaiez and Dr. Qingye Gemma Lu, and Dr. Hossein Hejazi, who served as an internal examiner, for dedicating their time and offering valuable suggestions. I am also very appreciative of Arthur De Vera and Suha Abusalim in the Department of Chemical & Petroleum Engineering for their assistance and support.

I gratefully acknowledge the financial support received from the University of Calgary's Canada First Research Excellence Fund program, titled the Global Research Initiative in Sustainable Low Carbon Unconventional Resources. Also, I acknowledge Alberta Innovates for graduate student scholarship funding.

I am delighted to express my gratitude to my wife, Eun Ok, and my daughters, Rachel, Esther, and Sophia, for their support and prayers.

Lastly, I express deep gratitude to the Lord for everything.

Dedicated to the loves of my life

My wife Eun Ok Kim

My daughters Seoyeon (Rachel), Hyeona (Esther), and Sujung (Sophia)

My parents,

Donghu Lee and Jeonghui Lee

Table of Contents

List of Tables

List of Figures

Chapter One: Introduction

1.1 Background

Instabilities of the interface between two phases flowing through porous media are commonly found in many technological processes and have been investigated extensively. When a less-viscous fluid displaces another fluid of higher viscosity in a porous medium, instability can develop at the interface between the two fluids. Hill examined the instability for the first time in an experiment to displace sugar liquors with water in a vertical uniformly packed column of charcoal [1]. The instability, which manifests itself in the form of fingerlike patterns with the displacing fluid propagating through the displaced fluid, is known as viscous fingering instability. In a seminal study, Saffman and Taylor investigated interfacial instability between two immiscible fluids with different densities and viscosities in a Hele-Shaw cell arranged both horizontally and vertically [2]. They injected air from the top to displace the more viscous glycerin in a vertically configured rectilinear Hele-Shaw cell. Slobod and Caudle investigated the effects of mobility ratio on areal sweep efficiencies using a radiographic method during both miscible and immiscible displacement flows in a five-spot configuration and a straight-line drive using a porous media made of fused alundum plate with a thickness of 0.25 inches [3]. They determined the mobility ratios for the miscible phases directly from the viscosity ratios since the permeabilities ahead of and behind the front are equal. However, the mobility ratios for the immiscible phases were estimated using relative permeability measurement data from a core plug of similar material and the average saturation behind water front. The results of experiments,

whether miscible or immiscible, consistently showed that the mobility ratio significantly affects the areal sweep efficiency. The quarter five-spot configuration with localized injection and production wells has been widely utilized in numerous studies [4] [5] [6]. Paterson conducted a study on radial fingering using Hele-Shaw cell, where air injection at the center displaced more viscous glycerin [7]. An equation determining the minimum wavelength necessary for finger growth in a radial outward displacement was derived. Furthermore, approximate equations were presented for the growth rate of the fingers and the shape of an elongated finger. Chen investigated the impact of plate roughness on viscous fingering in a radial Hele-Shaw cell by injecting a liquid to radially displace a significantly more viscous liquid [8]. The impact of flow rate and interfacial tension was also examined. The patterns of immiscible fingers were less branched compared to miscible patterns due to interfacial tension and were more susceptible to changes in the flow rate. Banpurkar et al. investigated the viscous fingering behavior of the immiscible kerosene-glycerin system using an anisotropic radial Hele-Shaw cell, which was prepared by affixing a patterned copper circuit board on the bottom plate [9]. Tsuzuki et al. studied the effects of injecting Newtonian surfactant solution to displace viscous oil in a radial Hele-Shaw cell [10]. Nagatsu and his colleagues conducted studies on non-isothermal miscible displacements [11] and examined the impact of chemical reactions that alter the viscosity of the more-viscous liquid [12] in a radial Hele-Shaw cell.

Viscous fingering instabilities are commonly observed in a wide spectrum of applications such as filtration, fluidization, enhanced oil recovery (EOR) processes, groundwater infiltration, soil remediation, geothermal energy production, CO_2 sequestration, production of hollow fiber membranes, and air-assisted injection molding [13] [14] [15] [16] [17]. The vast majority of

existing literature on viscous fingering instabilities has focused on Newtonian fluids. However, experimental studies showed that the fingering patterns for non-Newtonian fluids are very different from those with Newtonian fluids [18] [19]. Nittmann et al. observed a fractal growth of viscous fingers from rectilinear miscible displacement experiments in a Hele-Shaw cell where water displaced non-Newtonian polymer solutions [20]. Daccord and Nittmann also found fractal viscous fingers when water displaced high-viscosity non-Newtonian polymer solutions in a radial Hele-Shaw cell [21]. Most real fluids such as shaving foams, glues, flour-water dough, mayonnaise, and paints are non-Newtonian, and most of them exhibit multiple non-Newtonian properties simultaneously such as shear-thinning or shear-thickening, yield stress, and viscoelastic effects [16] [22]. This makes the viscous fingering instabilities in non-Newtonian fluids more complex and difficult to understand [23].

1.2 Objectives

In the research documented in this thesis, viscous fingering instabilities involving complex fluids such as dilute low molecular weight poly(ethylene oxide) (PEO) solutions and liquid-based foam in a radial Hele-Shaw cell are examined.

Existing studies on the viscous fingering instabilities involving non-Newtonian fluids suggest that elastic properties can have several different effects on the evolution of viscous fingering interface [16] [24] [25]. These include narrowing or widening the width of fingers and tip splitting. The effects of normal stress differences on immiscible radial viscous fingering instability in a Hele-Shaw is investigated. To separate shear-thinning viscosity, dilute low

molecular weight PEO solutions are used as more viscous fluids. In addition, only the molecular weight of PEO is varied to precisely investigate the effects of normal stress differences. This study's outcomes are significant because the results demonstrate new behaviors for displacement of elastic fluids. The results have importance for the oil and gas industry (cold bitumen and heavy exhibits elastic contributions) and the manufacturing industry (injection molding). The research question associated with this objective is: how does normal stresses affect immiscible radial viscous fingering?

Liquid-based foam is a non-Newtonian fluid composed of gas bubbles randomly dispersed in a liquid where typically, the volume fraction of gas far exceeds the volume fraction of liquid [26] [27]. Foams are used in many household and industrial products where a liquid foam is allowed to solidify to form a solid form, e.g., polyurethane foams. The quasi-two-dimensional foam which consists of bubbles squeezed between two plates is widely used in existing studies [28] [29]. This research investigates the instabilities associated with three-dimensional foam displacement in a radial Hele-Shaw cell. These flows are important in manufacturing processes for foamed products (after they have cured) which are increasingly used for products due to their remarkable elastic properties. The research question associated with this objective is: how does fingering occur into foam and is it similar to that of a single-phase liquid? This research investigates radial displacement flow of three-dimensional foam which contains many bubbles in the thickness direction, while the quasi-two-dimensional foam in the previous studies consists of bubbles squeezed between two plates. In addition, higher air injection pressures are covered in using a rigid Hele-Shaw cell to avoid flexing of the glass plates. This research provides the first detailed investigation of the fingertip velocity, number of fingers, and other quantitative values

on fingering patterns as a function of the air injection pressure for the radial viscous fingering of three-dimensional foam.

Few studies have been done on viscous fingering instabilities involving three fluid phases in porous media even though three-phase flows in porous media are frequently encountered in various applications such as enhanced oil recovery (EOR) [30] and ground water remediation [31]. This research examines radial viscous fingering instability involving three immiscible phases in a Hele-Shaw cell. A small volume of water is slowly introduced through the injection hole into Hele-Shaw cell initially filled with mineral oil before the injection of air. Subsequently, air is injected to displace both water and mineral oil. The evolution of fingering patterns is then compared to the reference cases in which air displaces mineral oil without the presence of water. The research question associated with this objective is: how does the presence of water influence viscous fingering instabilities when air displaces mineral oil in a radial Hele-Shaw cell? This research provides the first comprehensive examination of the fingering patterns, finger area, and fingertip velocity as a function of the air injection pressure and time for the radial viscous fingering process of air displacing water and mineral oil in a Hele-Shaw cell.

Moreover, there have not been many studies on the instability at the interface between two parallel flows of immiscible liquids in porous media despite the common occurrence of parallel flows in numerous applications. This research studies the instability in thin film flows associated with condensate and bitumen flows. This flow is important for oil sands recovery processes where instability of the interface could help with heat transfer which can help to mobilize greater bitumen drainage but also could also adversely lead to the formation of oil-water emulsions. The

research question associated with this objective is: how does instability occur at pore scale in condensate-bitumen systems? In research, the instability at the interface between two parallel flows of immiscible liquids with a flat interface within a pore is studied following the linear stability analysis performed by Chuoke et al [32]. In formulating the problem, two constant parallel velocities are used to describe the base state of the parallel flow. A characteristic equation which determines the growth rate as a function of the wavenumber is derived, and the instability conditions are determined. In the results and discussion section, the instability of the parallel flow of steam condensate and mobilized bitumen in the SAGD process is examined using the instability conditions. The importance of this study is that it gives well-defined instability conditions for the two non-horizontal parallel flows in a pore and applies them to SAGD. This study determines that the instability depends on the temperature and there exist optimum and minimum temperatures in SAGD.

The results of the research are of interest to researchers in fluid mechanics, fingering phenomena, and interfacial behaviors. The research is significant since it resolves and adds new understanding on viscous fingering of complex fluids.

1.3 Outline

The thesis is composed of seven chapters. Chapter Two presents a literature review of viscous fingering instabilities involving elastic fluids, displacement of liquid foam by gas in a Hele-Shaw cell, viscous fingering instabilities of three fluid phases, and instability of the interface between two parallel flows. Chapter 3 mainly focuses on the effects of dilute low molecular weight

poly(ethylene oxide) solutions in immiscible radial viscous fingering instabilities. Chapter 4 presents the study of air invasion into three-dimensional foam inducing viscous fingering instabilities. Chapter 5 concentrates on viscous fingering instabilities of air displacing water surrounded by mineral oil in a radial Hele-Shaw cell. Chapter 6 presents instability of parallel flow of two immiscible liquids in a pore and application to Steam-Assisted Gravity Drainage. Chapter 7 summarizes the main research conclusions and provides recommendations.

Chapter Two: Literature Review

2.1 Viscous fingering

Viscous fingering commonly describes the emergence and progression of the interfacial instability between two miscible or immiscible fluids that can arise when a less-viscous fluid displaces a higher-viscous fluid in a porous medium [13]. Fingering instabilities typically arise from differences in viscosity and/or density at the interface [33]. Because the majority of porous materials are not transparent, a practical analogous model for the study of viscous fingering is the Hele-Shaw cell model which consists of two parallel transparent plates with a small gap between them [13] [32]. Common displacement flows employed in Hele-Shaw cell experiments are rectilinear, radial, and quarter five-spot displacements [13]. Chuoke et al. performed rectilinear immiscible displacement experiments in a tilted Hele-Shaw cell where less-viscous water-glycerine solutions with higher density was injected at the lower end with uniform speed to displace more-viscous oil with lower density [32] (see Figure 2.1-a). They observed that viscous fingering occurred only at speeds above a critical rate. Petitjeans and colleagues investigated miscible quarter five-spot displacements in a Hele-Shaw cell [4]. They introduced water-dye or glycerin-water-dye solutions with a reduced glycerin concentration to displace an existing, more viscous glycerin-water solution, as depicted in Figure 2.1 (b). Dias et al. conducted immiscible radial displacement experiments in a Hele-Shaw cell as shown in Figure 2.1 (c) [34]. In these experiments, water was injected to displace mineral oil. Their objective was to investigate the impact of time-dependent injection rates.

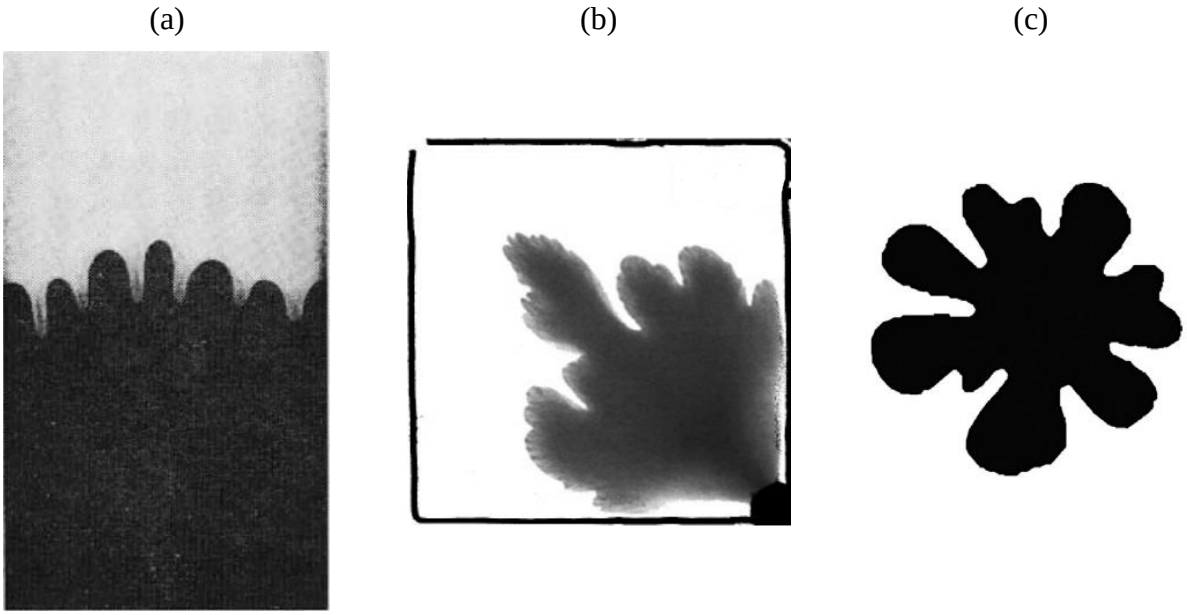

Figure 2.1. Viscous fingering experimental results using Hele-Shaw cell from (a) Chuoke et al. 1959, (b) Petitjeans et al. 1999, and (c) Dias et al. 2012.

Figure 2.2 depicts a typical evolution of an immiscible radial viscous fingering interface, involving two Newtonian fluids. In this case, a less viscous air is injected at a constant pressure to displace more viscous mineral oil radially in a Hele-Shaw cell. As shown in the figures, the initial fingers extend and evolve into a fan shape, with some of them splitting as the width of the fingers reaches a certain size [13] [35]. This tip-splitting process repeats as the fingers continue to grow.

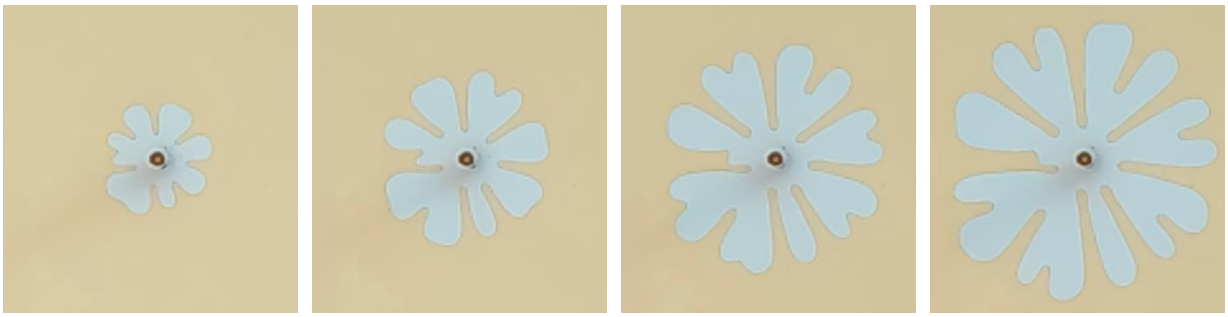

$t = 1.64$ s $t = 3.29$ s $t = 4.93$ s $t = 6.57$ s

Figure 2.2. Air displacing mineral oil in a radial Hele-Shaw cell: evolution of the viscous fingering interface under a constant air injection pressure of 0.5 psi.

When the mobility of the displacing fluid, M_1, is significantly greater than the mobility of the existing displaced fluid, M_2, the instability study of a circular immiscible interface in a Hele-Shaw cell determines the critical wavelength λ_c as follows [36] [7]:

$$\lambda_c = \frac{2\pi R}{\left[\sqrt{\frac{QR}{2\pi M_2 \sigma} + \frac{1}{4}} - \frac{1}{2}\right]} \tag{2.1}$$

where R is the radius, Q is the volume flowrate, M_2 is the mobility of the displaced outer fluid, and σ is surface tension. Mobility in a Hele-Shaw cell is determined as follows [36] [7]:

$$M = \frac{b^2}{12\mu} \tag{2.2}$$

where b is the plate spacing and μ is the viscosity. The wavelength of maximum growth rate is follows [36] [7]:

$$\lambda_m = \frac{2\sqrt{3}\pi R}{\sqrt{\frac{QR}{2\pi M_2 \sigma} + 1}}. \tag{2.3}$$

The instability of the interface arises only when the circumference of the interface is greater than the critical wavelength. An increase in the viscosity of the existing fluid or flow rate results in a

decrease in the critical wavelength. This implies that viscous fingering begins at an earlier stage when the circular interface is smaller. Conversely, an increase in the surface tension leads to a longer critical wavelength.

2.2 Viscous fingering instabilities of elastic fluids

Allen and Boger separated non-Newtonian shear-thinning viscosity and prepared ideal elastic fluids (referred to as Boger fluids) with constant viscosity by adding small amounts of high molecular weight rubber polymers in viscous Newtonian solvents [37] [16]. They studied the viscous fingering patterns for the rear interface between chasing waterflood and polymer slug in polymer flooding using a big one-meter diameter radial Hele-Shaw cell. The interface between water and the shear-thinning fluid became significantly more unstable. However, the constant viscosity elastic fluids showed negligible effects on the fingering pattern. They were inconclusive about the elastic effects. They suggested that the extensional flow in the formation of viscous fingers at the flow rates tested might not be fast enough to have elastic effects. Vlad and Maher further investigated the elastic effects on the fingering pattern using Boger fluids in a narrow linear Hele-Shaw cell [16]. They covered a wide range of Weissenberg numbers by using two different Boger fluids and varying gap thickness and air injection pressure. Two Boger fluids and one Newtonian fluid with similar viscosities were prepared, and the strength of viscoelasticity was controlled by changing the amount of polyisobutylene ($\mathrm{MW} = 1.2 \times 10^6$ Da) added to the viscous Newtonian solvent which was made by dissolving polybutene ($\mathrm{MW} =$ 600 Da) in kerosene. They observed a tip-splitting instability when the velocity of the finger tip exceeded a threshold value only for the Boger fluid where the threshold velocity depended on the

aspect ratio (gap thickness divided by the width of the Hele-Shaw cell) and the Boger fluids with the larger relaxation time showed smaller threshold velocities. They also analyzed the normal stress differences arising from the shear and extensional flows in front of the moving finger and showed that these stresses could become very large. They suggested that the strong elastic forces arising from the normal stress differences near the finger tip opposed the finger growth and caused the tip splitting. Malhotra and Sharma prepared aqueous Boger fluids using polyethylene glycol and poly(ethylene oxide) and performed miscible rectilinear viscous fingering experiments [38]. They observed thinner and longer fingers in fully developed flow, growth of multiple fingers, and higher dominant wave number at the onset of instabilities in elastic fluids. Jangir et al. experimentally studied the role of nonlinear rheology of poly(ethylene oxide) solutions in finger formation in miscible rectilinear displacement flows [39]. They found that normal stresses (or elasticity) promoted side branching, tip-splitting, and shielding due to local flow behavior.

A dilute poly(ethylene oxide) (PEO) solution is known to have non-Newtonian shear-thinning viscosity and normal stress differences while the elastic response is negligible in the flow in a thin gap [14]. Bonn and Meunier studied the effects of normal stress differences of dilute PEO solutions on the viscous fingering instability in a rectangular Hele-Shaw and the motion of long bubbles in capillary tubes [25]. To separate the shear-thinning behavior, Bonn and Meunier prepared dilute 5 and 50 wppm PEO solutions using a PEO product named WSR301 ($MW = 4 \times 10^6$ Da) which is known as the most effective drag-reducing polymer [40]. It was found that the viscous fingers widened when air displaced the dilute PEO solutions in a rectangular Hele-Shaw cell. Narrow and elongated bubbles were also observed when air displaced dilute PEO

solutions in a capillary tube. They concluded that the widened fingers and narrow bubbles were caused by the normal stress effects of PEO solutions. It is known that the force resulting from the variation in the first normal stress difference in the flow in a circular microchannel is directed toward the center which is the direction of decreasing shear rate [41]. Holzner et al. studied the cell focusing caused by normal stress effects in rectangular microfluidic channels using low molecular weight dilute PEO solutions [42]. They were able to achieve the cell focusing using lower molecular weight ($MW = 0.4 \times 10^6$ and 1.0×10^6 Da) dilute PEO solutions (500 ppm). Lindner et al. performed viscous fingering experiments in a rectilinear Hele-Shaw cell where the air was injected to displace two different polymer solutions [23] [24]. They were able to examine the separate effects of the shear thinning and elastic properties on the width of fingers by using two different solutions. Narrow fingers were observed for the solutions of stiff polymers with a shear-thinning property. However, wider fingers were found in the case of dilute solutions of flexible polymers with dominant elastic effects. Fast et al. presented viscous fingering patterns from an immiscible radial Hele-Shaw cell experiment where air at constant pressure was injected to displace a dilute shear-thinning PEO solution with two different gap thicknesses [14]. Narrow fingers with an apparent lack of tip splitting were observed with the thicker gap, and the emergence of tip splitting and a more densely branched pattern were observed by reducing the gap thickness by 2.5 times. They also studied pattern formation of an air bubble expanding into a non-Newtonian fluid in a radial Hele-Shaw cell through both linear stability analysis and nonlinear simulations. A special small-gap limit model based on the Johnson-Segalman-Oldroyd viscoelastic constitutive equation was derived to describe the flow. They found that the shear-thinning behavior of the displaced fluid tends to suppress tip-splitting. Shokri et al. studied viscoelastic effects modeled by the Oldroyd-B constitutive equation on miscible viscous

fingering through both linear stability analysis and nonlinear simulations [43]. It was reported that elasticity tends to attenuate viscous fingering instability.

2.3 Displacement of liquid foam by gas in a Hele-Shaw cell

Foams exhibits flow properties arising not only from the viscosity of the liquid and gas phases but also the interfacial forces at the interfaces and Plateau borders [44]. At particular conditions, foam acts elastically like a solid at low shear stress but flows like a liquid at high shear stress [26]. At other conditions, foam can also flow like a shear-thinning fluid [27]. When a foam undergoes deformation and flow, its internal resistance to flow arises from viscous forces within the phases (liquid, gas) and between the phases (liquid, gas, and solid bounding surfaces) but also the energy required to stretch or deform interfaces which will tend to evolve to a configuration where the overall surface energy is minimized [27] [45] [46] [47].

There are a few studies on the displacement of liquid foam by gas in a Hele-Shaw cell. Injecting gas at a continuous flow rate or constant pressure into a body of liquid foam in a Hele-Shaw cell leads to finger-like gas/foam interfaces [48]. This behavior is the well-known Saffman-Taylor instability because viscous foam is pushed by a less viscous gas in a porous medium [49] [50]. Hilgenfeldt et al. examined foam dynamics of a quasi-two-dimensional liquid foam in a rectangular Hele-Shaw cell by injecting air at constant pressure at one end of the cell [28]. At very low pressures, the entire foam was uniformly displaced. A fingering of air in the foam propagating by the neighbor swapping mechanism of bubbles (T1 process) was observed for pressures larger than a critical value. They also found a foam yielding to the injected air by

breaking the thin films between bubbles. Arif et al. explored crack propagation in dry, quasi-two-dimensional aqueous soap foam in a rectangular Hele-Shaw cell by injecting air at constant pressure [29]. They observed a finger-like propagation of ductile fracture by T1 process around the fingertip at moderate speed and a propagation of brittle crack by breaking films at much higher speed. They also found that there is an upper limit to the ductile crack speed and a lower limit to the brittle crack speed. The fracture of a quasi-two-dimensional aqueous foam under an applied driving pressure was also investigated through simulations using a network modelling approach [51]. Salem et al. investigated the response of a quasi-two-dimensional liquid foam to air injection in a radial Hele-Shaw cell [50]. They identified swelling regime with fingering patterns and high-speed regime with a series of film ruptures. They examined the dependence among the swelling rate (increasing rate of fingering area), injection pressure, and other parameters. In a subsequent study, Salem et al. examined influence of surfactants on the response of a quasi-two-dimensional liquid foam in a radial Hele-Shaw cell [52]. Yanagisawa and Kurita examined the collective relaxation response of a two-dimensional wet foam to a disturbance [53]. A perturbation was made by injecting a constant amount of additional solution from the outside. They observed two sharp peaks in the movements of foam bubbles during the relaxing process. The first peak movement was just T1 event. The second peak movement was a localized collective movement of bubbles occurring at the same time. They focused on the second peak collective movement and defined the relaxation time as the duration of the second peak movement. They found that the relaxation time and correlation lengths for the collective movements increase with ϕ. They also found that monodisperse foams showed slip-like motion in one direction while polydisperse foams showed random motion. Park and Durian investigated pattern formation in the immiscible radial displacement of Gillette shaving foam (Foamy regular)

in Hele-Shaw cell [54]. In their experiments, nitrogen gas at constant pressures between 1 and 20 kPa was injected into Hele-Shaw cell to displace foam. They found that the finger width scales with the driving pressure, and the proportionality constant increases with the gap thickness divided by bubble diameter. However, the Hele-Shaw cell was not rigid enough to inject nitrogen at pressures higher than 20 kPa. Lindner et al. studied the instability for a polymer gel and Gillette shaving foam (Foamy regular) in a rectilinear Hele-Shaw cell [22]. They observed very branched fingers in the gel, but the results for foams were very different because the foam slipped at the wall. The complexity of the displacement of foam arises from its multi-phase nature – a displacement could either push the foam structure through the space as a whole or potentially split an interface leading to a bubble 'poking' its way along bubble interfaces with little displacement of the bulk of the foam. Sliding of bubbles on the interfaces could also occur.

2.4 Viscous fingering instabilities of three fluid phases

There have been few studies on viscous fingering instabilities involving three fluid phases in porous media. Three-phase flows in porous media are frequently encountered in various applications including enhanced oil recovery (EOR) [30], ground water remediation [31], and microfluidic devices [55] [56]. Water-Alternating-Gas (WAG) injection is an EOR which combines water flooding and gas injection to enhance the overall sweep efficiency [57]. Some of the variations of WAG processes are Hybrid-WAG, Simultaneous WAG (SWAG), Water Alternating Steam Process (WASP), Foam Assistant WAG injection (FAWAG), Polymer Alternating Gas (PAG) injection, and Chemically Enhanced Water-Alternating-Gas (CWAG). Caudle and Dyes investigated the simultaneous gas-water injection process which involves three

regions of mobility [58]. The first region is the lowest mobility oil region, the second is the high mobility gas region, and the third is the lower mobility region in which both gas and water are flowing. They used a five-spot configuration using a porous plate with a thickness of 0.25 inch and a separation of 10 inches between wells. The three mobility regions were represented with three miscible oils. The mobility in the oil and gas-water regions was set to be identical, while the gas zone had a mobility 17 times higher. They tried two gas zone volumes, 5% and 20% of the reservoir volume. They were able to achieve about 90% sweep efficiency using the simultaneous gas-water injection process which was implemented by injecting miscible oil with an identical mobility with the oil in the experiments. They also found that there is a noticeable difference between the sweep efficiency curves for the 5% and 20% gas zones. Wang and his colleagues examined how the generation of gas bubbles, resulting from a chemical reaction between the displaced and displacing fluids, affects viscous fingering instabilities in a radial Hele-Shaw cell [59]. They found that the main characteristic times affecting the flow patterns are the displacement time and nucleation time of bubbles. If the displacement time was less than the nucleation time, the generation of bubbles did not follow the propagation of viscous fingering. Instead, gas bubbles formed within the fingers, and these bubbles within the fingers merged, growing larger and causing outward flow. This process hindered the mixing of the displacing and displaced fluids.

2.5 Instability of the interface between two parallel flows

Instabilities of the interface between two immiscible phases flowing through porous media are commonly found in many technological processes and have been investigated extensively. At

pore scale, these instabilities lead potentially to enhanced mass and heat transfer and phase mixing and formation of emulsions. Hill analyzed the stability of the interface for a small depression at the interface and derived an equation for the critical velocity using the densities and the viscosities of the fluids [1]. Saffman and Taylor performed linear stability analysis for the interface between two immiscible fluids of upward displacement in a homogeneous porous medium assuming continuous pressure at the interface [49]. The instability condition was derived for a wave-like perturbation on the interface and found that the wavelength of the disturbance did not affect the instability condition. They also investigated the effect of the pressure difference across the interface arising from surface tension. It was found that the surface tension limits the range of unstable disturbances to be greater than a critical wavelength. A similar linear stability analysis study of the interface for immiscible liquid-liquid vertical displacement in a tilted permeable media considering the pressure drop at the interface was carried out by Chuoke et al [32]. The authors derived equations for a critical velocity and critical wavelength. The instability occurs for all flow rates greater than the critical velocity if the initial disturbance of the interface contains modes with wavelengths greater than the critical wavelength. It was mentioned that a form of Helmholtz instability can be predicted from a second-order theory if the tangential components of gravitational force are included. However, detailed analyses are not provided.

There have not been many studies on the instability at the interface between two parallel flows of immiscible liquids in porous media at pore scale. Parallel flows are commonly observed in many applications such as packed bed reactors, micromixers, and enhanced oil recovery (EOR) processes. In EOR, the instability at the interface can significantly affect emulsion formation

[60] and for thermal oil recovery processes, it can also substantially enhance heat and mass transfer at the interface [61] [62] [63]. This is especially the case for steam-based oil sands recovery processes, such as Steam-Assisted Gravity Drainage (SAGD), where the main control on oil mobilization is heat transfer [64]. In oil sands reservoirs, the viscosity of the oil (referred to as bitumen) is of order of hundreds of thousands to millions of cP at original reservoir conditions. At more than 200°C, the viscosity drops to less than 10 cP and it can be drained from the reservoir [65]. In these processes, injected steam loses its latent heat to the oil sand raising the temperature of the oil with consequent formation of steam condensate. With greater mixing at the interface between mobilized (heated) oil and steam condensate, if instabilities occur, there is an opportunity for mixing with resulting enhanced heat transfer and emulsion formation. If the oil is hosted within the steam condensate as an emulsion, the overall viscosity of the mixture is lower than that of the heated oil alone which implies greater drainage rates. Moreover, the density of bitumen is very similar to that of the formation water, typically <20 kg/m^3 difference but their dependences on temperature are different, and thus, the density difference between the two phases is sensitive to temperature. Although enhanced heat transfer is desired to achieve higher oil drainage rates (raising the productivity of the recovery process), emulsion formation can lead to oil-water separation issues at surface.

Raghavan and Mardsen investigated the parallel flow of two immiscible fluids with one phase above the other [66]. They performed linear stability analysis to derive a characteristic equation that relates the growth rate of the perturbation to the wavenumber and solved it numerically. They concluded that the instability is only caused by the gravitational force due to the density difference between the top-heavier fluid and the bottom-lighter fluid. Bau examined the parallel

flow of two statically stable fluids with the lighter fluid on top of the heavier fluid using linear stability analysis [67]. The conditions for the onset of instability include special conditions for the viscosity ratio and a relatively high critical velocity which has a value beyond the validity of Darcy's law. Lateral interfaces of the parallel flow of two immiscible fluids in a horizontal Hele-Shaw cell were also examined both theoretically and experimentally by Zeybek and Yortsos [68]. The small-amplitude long-wave motion of lateral interfaces was found at large values of the capillary number. Gondret and Rabaud studied parallel flow of gas on top of a viscous liquid in a Hele-Shaw cell both experimentally and theoretically [69]. The interface became destabilized when the gas velocity was above a critical value, and the waves grew and propagated throughout the Hele-Shaw cell. They found that the critical velocity of the gas can be determined by an analysis of the inviscid Kelvin-Helmholtz instability. However, the wave velocity and the growth rate of the instability are governed by the linear stability analysis based on Darcy's law. This suggests that the onset of the instability is caused by inertia but the wave velocity and the growth rate themselves are governed by viscous effects.

2.6 What is missing in the literature?

Allen and Boger studied the effects of ideal elastic fluids on the radial viscous fingering [37]. However, their flow rate was not fast enough to have elastic effects. Vlad and Maher conducted additional investigations into the elastic effects on viscous fingering using Boger fluids [16]. However, they focused on the tip-splitting caused by strong elastic effects. They did not investigate weak and intermediate elastic effects on fingering. Bonn and Meunier prepared dilute

5 and 50 wppm PEO solutions using a PEO product named WSR301 ($MW = 4 \times 10^6$ Da) to focus on the effects of normal stress differences [25]. They observed wider fingers. Lindner et al. further studied the elastic effects that widens the finger width using 50 and 250 wppm solutions of WSR301 [24]. At higher velocities, fingers were no longer stable; they observed tip splitting at higher velocities. However, they focused on the widening width of fingers steadily moving ahead at lower velocities. Adjusting the concentration of PEO not only changes the strength of the elastic effect but also makes a significant change in viscosity. In this study, dilute solutions of low molecular weight PEO are used as elastic fluids without shear-thinning behavior. Additionally, only the molecular weight of PEO is varied to modulate the strength of elastic effects, rather than adjusting the concentration of one PEO product. This makes it possible to adjust the strength of elastic effects while minimizing changes in viscosity. In addition, the flatness, uniform wettability, and rigidity of the plates were considered as the most important factors in implementing the radial Hele-Shaw cell. To address these factors, SCHOTT Borofloat® 33, recognized for its excellent flatness and surface quality, was selected. A thickness of 19mm was chosen to avoid any bending or flexing of the glass plates.

The quasi-two-dimensional foam used in previous studies consists of bubbles squeezed between two plates [28] [29] [50] [51]. This study examines the radial displacement flow of three-dimensional foam, where numerous bubbles are present in the thickness direction. Park and Durian studied viscous fingering in three-dimensional foam [54]. They examined how the width of the finger scales proportionally with the applied driving pressure. However, the Hele-Shaw cell was not rigid enough to inject nitrogen at pressures higher than 20 kPa. In this research, higher air injection pressures are considered, and a rigid Hele-Shaw cell is employed to prevent

flexing of the glass plates. This study marks the first comprehensive examination of fingertip velocity, number of fingers, and other quantitative parameters including the width of fingers in the radial viscous fingering in three-dimensional foam, with a focus on their dependency on air injection pressure.

Limited research has been conducted on viscous fingering instabilities involving three fluid phases in porous media, despite the frequent occurrence of three-phase flows in various applications. This study specifically investigates radial viscous fingering instability with three immiscible phases in a Hele-Shaw cell. Furthermore, the instability at the interface between two parallel flows of immiscible liquids in porous media has not been extensively studied, despite the widespread existence of parallel flows in numerous applications. This research focuses on investigating the instability in thin film flows related to condensate and bitumen flows.

Chapter Three: Effects of dilute low molecular weight poly(ethylene oxide) solutions in immiscible radial viscous fingering instabilities

In this chapter, the effects of normal stress differences in the immiscible radial viscous fingering instability in a Hele-Shaw cell are experimentally investigated. Dilute low molecular weight poly(ethylene oxide) (PEO) solutions are used as the displaced fluid to focus on elastic effects without shear-thinning behaviour. The molecular weight of PEO is varied to investigate the effects of normal stress differences. The experimental observations reveal nonmonotonic and opposing effects are evident depending on the molecular weight of the PEO and the stage of the radial viscous fingering evolution. Decreases of the PEO molecular weight reduce the number of fingers and widen the finger width in the early stage. However, the increase of the PEO molecular weight promotes tip splitting and narrows finger width in the early stage but suppresses tip splitting in the intermediate stage. The Weissenberg numbers are estimated at different stages of the radial viscous fingering instabilities. Tip splitting occurs at the highest Weissenberg number covered in this study and suppression of tip splitting is observed at intermediate Weissenberg numbers. At low Weissenberg numbers, an increase finger width and a reduced number of fingers are observed.

3.1 Experiments

The viscous fingering (VF) experiments were performed in a radial Hele-Shaw cell consisting of two square borosilicate glass plates ($304.8\text{mm} \times 304.8\text{mm} \times 19\text{mm}$, SCHOTT Borofloat® 33) as shown in Figure 3.1. The gap thickness was set as $b = 0.0762$ mm by clamping the two plates

with stainless steel shims of 0.0762 mm (0.003 in) thickness between them at eight symmetrical positions. A high aspect ratio of the cell width to the gap thickness greater than 1000 is recommended to enable longer evolution of the viscous fingering interface [70] [71]. An injection hole with a diameter of 3.175 mm (0.125 in) is at the center of the top plate. The gap thickness is verified by comparing the actual volume of injected water and the area occupied by the water multiplied by the gap thickness. The volume of injected water was determined as $3.32 \pm 0.02\ cc$ by measuring the mass of water. The volume of water determined as $3.31\ cc$ by multiplying the area occupied by the water by the gap thickness. This yields a percent error of $-0.32\ \%$ in the volume calculated from a captured image. Air was injected into the cell with a constant volume flow rate using a mass flow controller (Sierra SmartTrack 100). Multiple experiments were performed under each condition to ensure their repeatability. The inner surfaces of the Hele-Shaw cell were polished using a random orbital polisher with a very fine steel wool pad (Grade #00) to have uniform and increased wettability. A light diffusing film is attached to the top of the Hele-Shaw cell under the LED lighting to improve the visibility of viscous fingering patterns without dying the existing fluid. The experiments were recorded by a video camera (GoPro HERO 10 Black) at 240 frames per second positioned vertically below the cell to hide the injection tube and maintain a constant distance from the cell. The constant air flow rate was determined as $q = 2.13 \pm 0.09\ \mathrm{cc/s}$ through experiments.

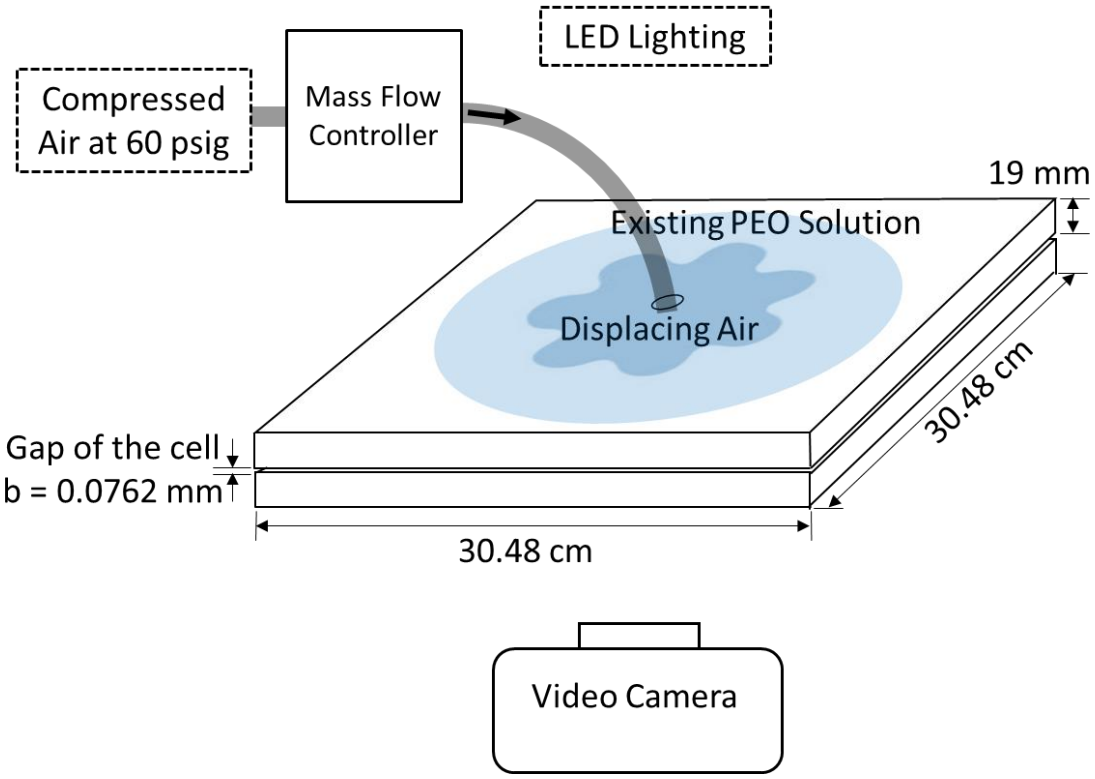

Figure 3.1. Schematic of the radial viscous fingering experimental setup.

Poly(ethylene oxide) (PEO) is an extensively studied and very widely used water-soluble polymer [72]. The degradation of PEO solutions has been examined by many researchers [73] [74] [75] [76]. It is known that PEO solutions are fragile, and many factors can cause degradation such as thermal, chemical, photochemical, and ultrasound [72]. The presence of metal in PEO solutions can also cause significant degradation [75]. Therefore, it is important to determine proper ways to prepare PEO solutions to maintain consistent sample properties for the experiments. Vanapalli et al. used a rolling apparatus at 3-6 rpm for 24-48 hours to dissolve 5M and 15M g/mol PEO in de-ionized water to avoid shear degradation [76]. 1 or 2 litre containers were used to prepare 1000-2000 ppm stock solutions. Samples of the desired concentration were made by diluting the stock solutions. They mentioned that there can be potential aggregates and

used a dynamic light-scattering analysis to check aggregates. They could not find any signs of aggregates. Bossard et al. used a to-and-from motion (30 mm amplitude) shaker at 175 rpm and a magnetic stirrer at the rotation speed of 500 rpm to mix PEO solutions [72]. They recommended a minimum of 4 days to mix low concentrated solutions and a maximum of 1 month for the most concentrated solutions. Visual inspection of the uniform natural light scattering of the sample is recommended to check the dissolution of PEO. Their goal was to compare rheological properties between shaken and stirred solutions. For solutions with MW $\geq$ 0.3M, degradations were found in stirred solutions, and aggregates were formed in shaken solutions. Holzner et al. prepared master stock solutions of 0.4M and 1M g/mol PEO to a concentration of 10g/L (9901 wppm) and aged them at room temperature for one month to achieve uniform solutions [42]. Rivero et al. prepared master solutions of 8M g/mol PEO by mild magnetic stirring for at least 24 h at room temperature [77].

In the viscous fingering experiments, deionized water was used as a standard Newtonian fluid. Three low molecular weight poly(ethylene oxide) (PEO) products supplied from Sigma-Aldrich (MW $= 0.3 \times 10^6, 0.6 \times 10^6,$ and 1.0×10^6 Da) were used to prepare dilute non-Newtonian solutions. The VWR standard orbital shaker was used to very gently mix 1000 wppm master PEO solutions at low rpm for four days, and dilute PEO solutions of 100 wppm were prepared by diluting the master solutions. The concentration of PEO solutions is determined by

$$wppm = \frac{m_{PEO}}{m_{PEO} + m_{water}} \times 10^6 \tag{3.1}$$

where m_{PEO} and m_{water} are the masses of the PEO and de-ionized water respectively. The steady shear viscosity measurements were performed on TA Instruments DHR-2 rheometer using a double gap rotor and cup geometry in a Peltier temperature system over the shear rate

range from 10 to 100 1/s at 20℃. Figure 3.2 shows viscosity as a function of shear rate for the fluids used in the experiments.

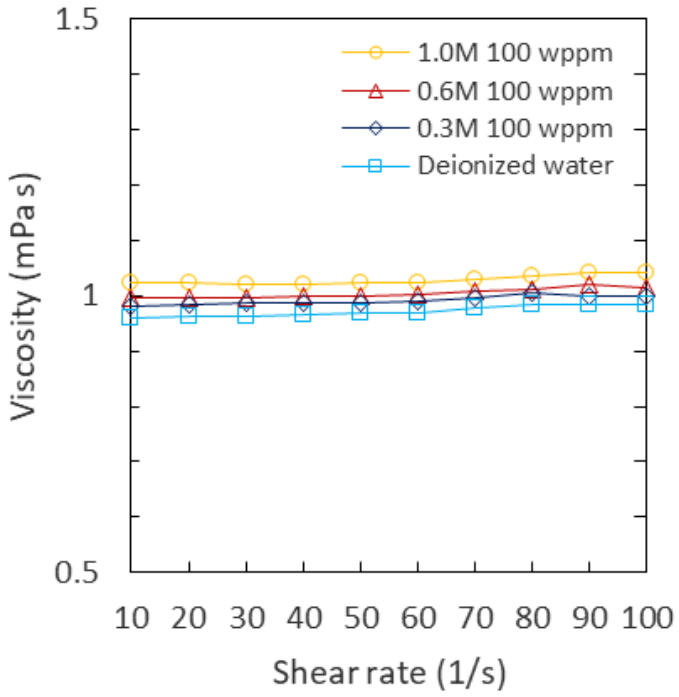

Figure 3.2. Viscosity as a function of shear rate for deionized water and dilute low molecular weight PEO solutions.

The dilute PEO solutions have viscosities very similar to that of deionized water. In addition, no shear-thinning behavior is found for the dilute PEO solutions as shown in Figure 3.2. According to the study on the surface tension of PEO solution with air as a function of molecular weight, the PEO molecule can form a self-assembled film at the interface [78]. In the dilute low molecular weight PEO solutions, there is a reduction of 9.8 $dyne/cm$ of the surface tension which is independent of the molecular weight [25] [78]. Relaxation times of dilute PEO solutions

were estimated using a relationship for the effective relaxation time in extension [42] [79]. The properties of the fluids used in the experiments are presented in Table 3.1.

Table 3.1. PEO molecular weight, concentration, viscosity η, surface tension γ and relaxation time λ of the fluids used in the viscous fingering experiments.

Fluid	PEO MW (Da)	Concentration (wppm)	η $(mPa\ s)$	γ (mN/m)	λ (ms)
Deionized water	⋯	⋯	0.97	72.3	⋯
0.3M 100wppm	$0.3 \times 10^6 (M)$	100	0.99	62.5	0.03
0.6M 100wppm	$0.6 \times 10^6 (M)$	100	1.00	62.5	0.12
1.0M 100wppm	$1.0 \times 10^6 (M)$	100	1.03	62.5	0.34

The modified capillary number which represents the ratio between the viscous force and the interfacial tension for a radial immiscible displacement in a Hele-Shaw cell is defined as

$$Ca' = \frac{\mu q}{\gamma b^2} \tag{3.2}$$

where μ is the viscosity of the more viscous fluid, q is the volume flow rate, γ is the interfacial tension, and b is the gap thickness [10]. This number is also referred to as a dimensionless flow rate [35]. The modified capillary number for the fluids used in the VF experiments at the constant air flow rate, $q = 2.13 \pm 0.09\ cc/s$, are shown in Table 3.2. The increase in Ca' for the dilute PEO solutions is mainly due to the reduction in surface tension. As the capillary number increases with a decrease in surface tension, the interface becomes more unstable so that the width of fingers is expected to decrease for PEO solutions[13] [10] [80]. The Weissenberg number Wi is defined as the ratio of a material relaxation time to the time scale of the flow which is typically the inverse shear rate in the thickness direction in a Hele-Shaw cell,

$$Wi = \lambda\dot{\gamma} = \lambda\frac{v}{b'} \tag{3.3}$$

where λ is the relaxation time of the dilute PEO solution and $\dot{\gamma}$ is the shear rate which is obtained by dividing the gap averaged longitudinal velocity v by $b' = b/2$ [14] [81]. Wi represents the strength of the elastic effects, and the larger the Wi, the greater the elastic effects [16].

Table 3.2. Modified capillary number Ca' for the fluids used in the viscous fingering experiments.

Fluid	Ca'
Deionized water	4.92 ± 0.21
0.3M 100wppm	5.81 ± 0.25
0.6M 100wppm	5.87 ± 0.25
1.0M 100wppm	6.05 ± 0.26

3.2 Results and Discussion

The fingering experiments were carried out at a constant volume flow rate of air while varying only the molecular weight of PEO in order to precisely investigate the effects of normal stress differences. Deionized water was used as a standard Newtonian fluid which provided a reference fingering pattern. The fingering patterns from the dilute PEO solutions were compared to the fingering pattern of deionized water. The immiscible VF is considered one of the most complex flows in porous media because it involves many pore-scale phenomena such as wetting behavior and interface tension [13]. Additionally, the immiscible VF in the radial geometry has significant differences compared to its rectilinear counterpart. These include an expanding interface and stronger spatial and temporal velocity variations [82]. Maximum velocity is expected near the injection point at the beginning, and the velocity gradually decreases as the interface expands

over time at a constant volume flow rate. As a result, it is expected to have strong variations in normal stress effects because the Weissenberg number proportionally changes with velocity as shown in Equation (3). For this reason, the fingering patterns were examined at four different time points. Figure 3.3 depicts time sequences of the interface for the dilute PEO solutions and deionized water at $\mathrm{t} = 0.038\mathrm{s}, 0.079\mathrm{s}, 0.163\mathrm{s}, \text{and } 0.329\mathrm{s}$.

(a) Deionized water

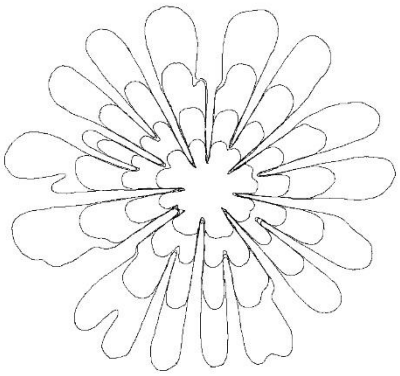

(b) 0.3M 100wppm

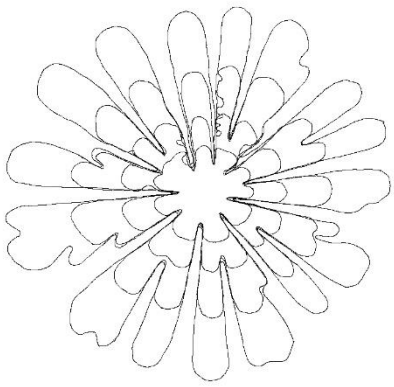

(c) 0.6M 100wppm

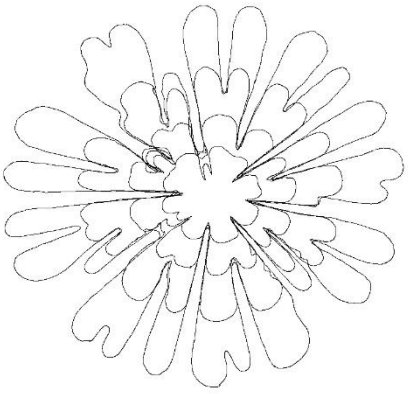

(d) 1.0M 100wppm

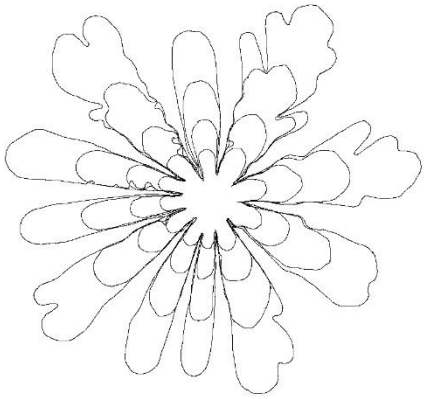

Figure 3.3. Time sequences of the interface taken at $t = 0.038s, 0.079s, 0.163s, and\ 0.329s$ for (a) deionized water, (b) 0.3M 100wppm, (c) 0.6M 100wppm, and (d) 1.0M 100wppm.

The VF evolution of deionized water shows a typical immiscible radial VF pattern where the initial fingers spread and develop into a fan shape and some of them split when the finger width becomes large enough [13] [35]. The 0.3M 100wppm solution shows no noticeable difference in the VF pattern compared to the VF pattern of deionized water. The early VF interface for 0.6M 100wppm shows that two dominant fingers at the top are widened and shielding a very small finger in between. A significantly different VF patterns are obtained for 1.0M 100wppm solution. At the early stage, some of the main fingers had already split, increasing the number of fingers. These fingers spread without tip splitting. Then, tip splitting and side branches are observed at the last VF pattern.

To quantitatively evaluate the instability of nonlinear VF interfaces, a number of quantitative criteria consisting of the effective number of fingers [82], the finger area density [35], and the representative finger width density [83] are adopted. The effective number of fingers is determined using the Fourier spectrum of the interface. The interface is considered as points of a radius versus angle function, and its discrete Fourier transform is determined. The effective number of fingers, k_{eff}, is obtained from:

$$k_{eff} = \frac{\sum_k |F(k)|^2 k}{\sum_k |F(k)|^2} \tag{3.4}$$

where $F(k)$ is the Fourier transform and k is the wavenumber in the transform space. The finger area density, FAD, is defined as the ratio of the fingering area to $\pi {r_{tip}}^2$, where r_{tip} is the radius of the point on the interface farthest from the center of the domain [35] [84]. A unit value of FAD represents the case of a stable circular interface, and the more complex the finger structures, the smaller the value of FAD. The representative finger width density $\bar{d}_w$ is determined by averaging the average finger width density $d_w(r)$ between r_{base} and r_{tip}. The

average finger width density $d_w(r)$ for a given r is obtained as $\bar{w}/2\pi r$ where $\bar{w}$ is the average finger width [83]. The average finger width $\bar{w}$ is obtained by dividing the length of the circumference where VF and a circle with radius r intersect by the number of fingers. Figure 3.4 illustrates how the above quantitative values are obtained using a VF pattern for deionized water at $t = 0.163s$.

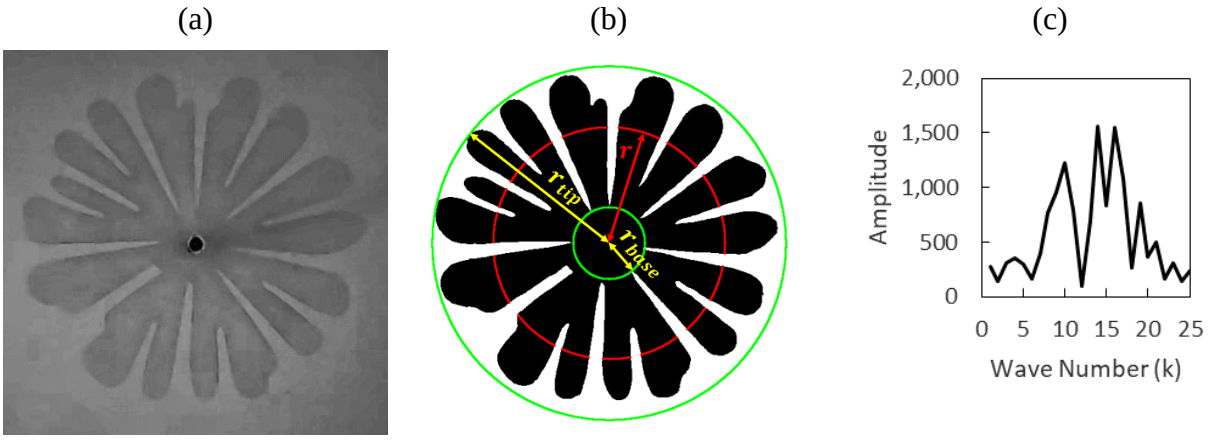

$$k_{eff} = 13.7 \qquad \bar{d}_w = 0.08 \qquad d_a = 0.66$$

Figure 3.4. (a)VF image for deionized water at $t = 0.163s$, (b) black and white VF image for processing in MATLAB, and (c) Fourier transform spectra of the VF interface (amplitude $|F(k)|$).

At least three experiments were performed under each condition to ensure their repeatability. The quantitative values, k_{eff}, $\bar{d}_w$, and d_a are determined from the experiment VF images at four different time points in MATLAB. The quantitative values are averaged, and the averaged values are plotted with error bars representing the standard deviations. Figure 3.5 depicts the effective number of fingers versus (a) time for different fluids and (b) PEO molecular weight at four different time points. The Newtonian reference case of deionized water is shown in a blue line in

Figure 3.5(a), and it is represented as 0 molecular weight in Figure 3.5(b). Both 0.3M 100wppm and 0.6M 100wppm show similar a pattern of growth to that of deionized water. However, the effective number of fingers of 0.6M 100wppm is smaller by 0.6 to 1.4. This difference gets smaller with time. Similarly, 0.3M 100wppm shows slightly larger number of fingers at the last time point, $t = 0.329s$. This can be because the surface tension of the dilute PEO solution is 9.8 $dyne/cm$ less than that of water. As surface tension becomes weak, the interface becomes more unstable [13]. As a result, the normal stress effects of 0.3M 100wppm and 0.6M 100wppm reduce the number of fingers, and the effects are strong initially and diminish over time.

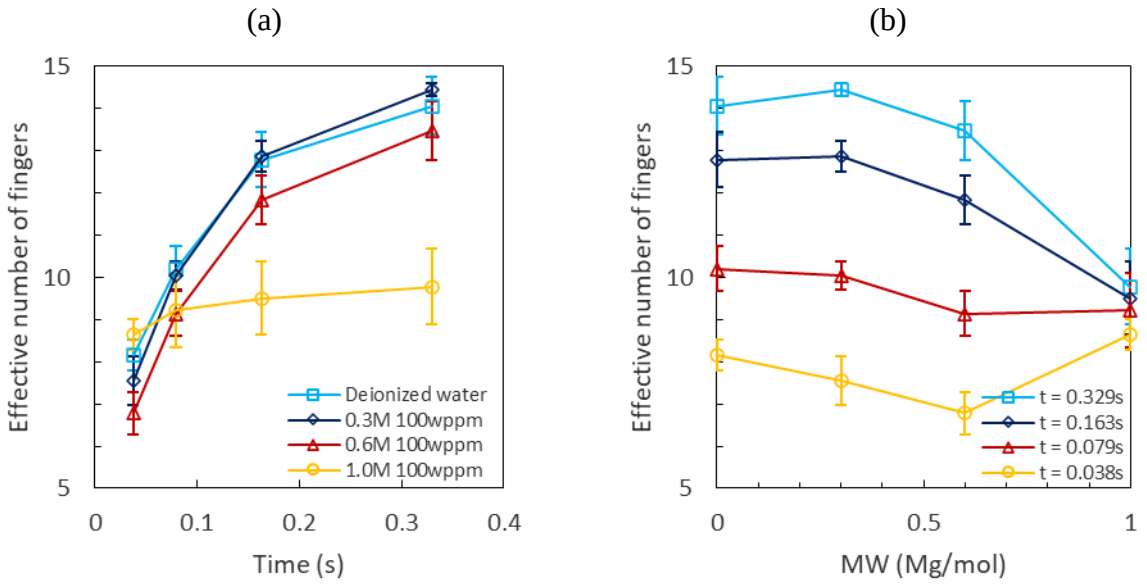

Figure 3.5. Effective number of fingers versus (a) time and (b) PEO molecular weight (Newtonian reference case of deionized water is represented as 0 molecular weight).

A significantly different pattern of VF evolution is observed for 1.0M 100wppm solution. At the early stage, some of the main fingers had already split as shown in Figure 3.6 resulting in

increased effective number of fingers at $t = 0.038s$. Then, it increases slowly by only 1.1 over time because the fingers spread without tip splitting as shown in Figures 3.6 and 3.7. Another noticeable result is that the effective number of fingers vary nonmonotonically with PEO molecular weight as shown in Figure 3.5(b) at $t = 0.038s$. 0.3M 100wppm and 0.6M 100wppm have the effect of lowering the number of fingers. However, 1.0M 100wppm has the effect of increasing the number of fingers by promoting tip splitting as shown in Figure 3.6. As a result, 1.0M 100wppm has two opposite effects, promoting tip splitting in the early stage and suppressing tip splitting in the intermediate stage.

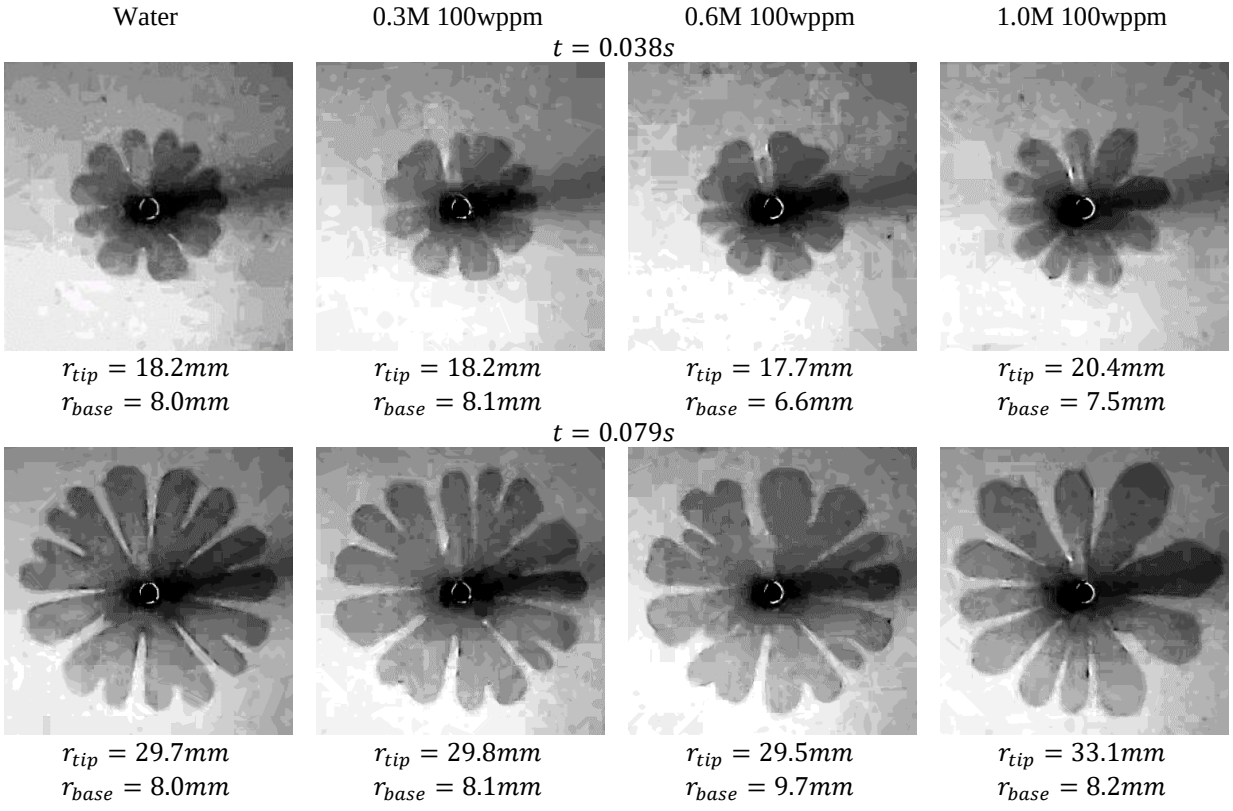

Figure 3.6. VF images at $t = 0.038s$ *and* $0.079s$.

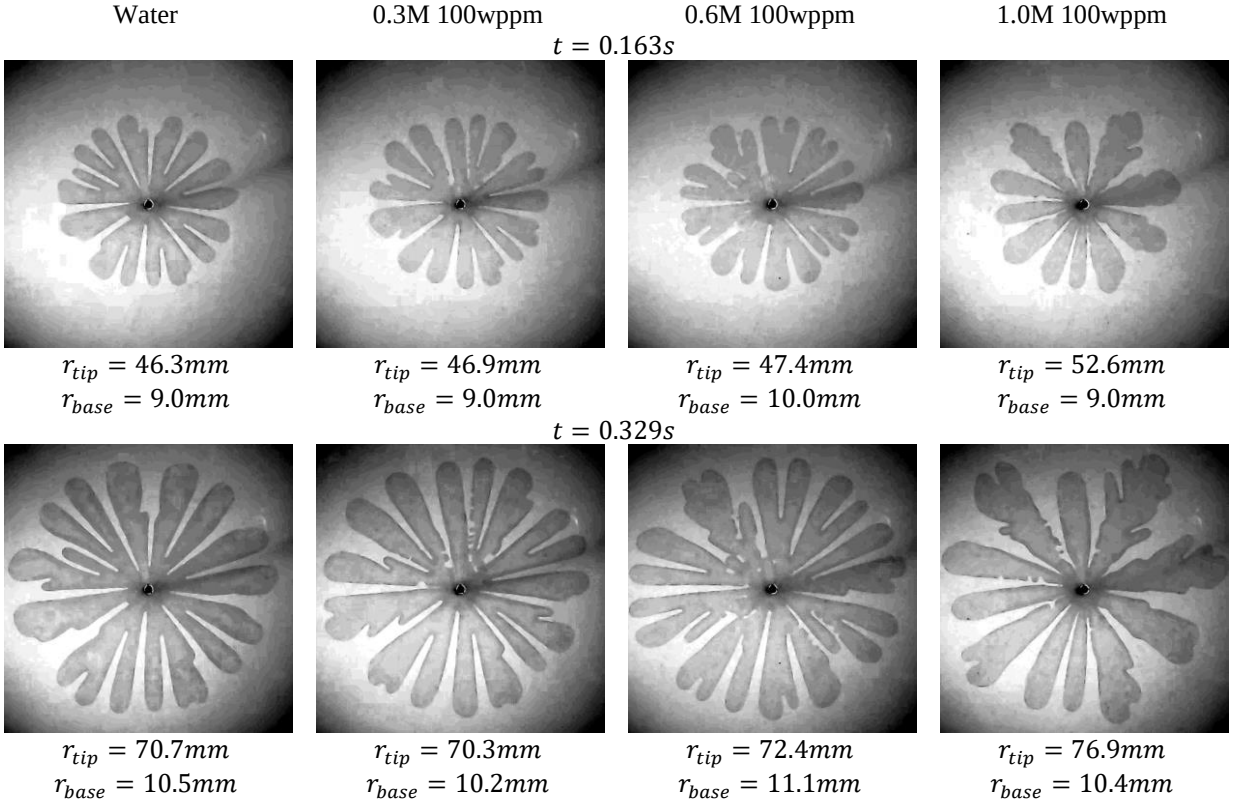

Figure 3.7. VF images at $t = 0.163s, and\ 0.329s$.

Figure 3.8 shows the variation of the average finger width density $\bar{d}_w$ with (a) time for the fluids and (b) PEO molecular weights at four different time points. There is noticeable increase of 0.09 in $\bar{d}_w$ for 0.6M 100wppm in the early stage. 0.3M 100wppm shows slight increase of 0.05 in $\bar{d}_w$in the early stage. This increases in $\bar{d}_w$ get smaller with time, and $\bar{d}_w$ of 0.3M 100wppm becomes slightly smaller at the last time point. On the other hand, $\bar{d}_w$ of 1.0M 100wppm is smaller than deionized water in the early stage because of the increased number of fingers. Then, it becomes almost the same as deionized water, and it gets slightly wider than deionized water. Like the effective number of fingers, the average finger width density varies nonmonotonically with PEO molecular weight in the early stage at $t = 0.038s$.

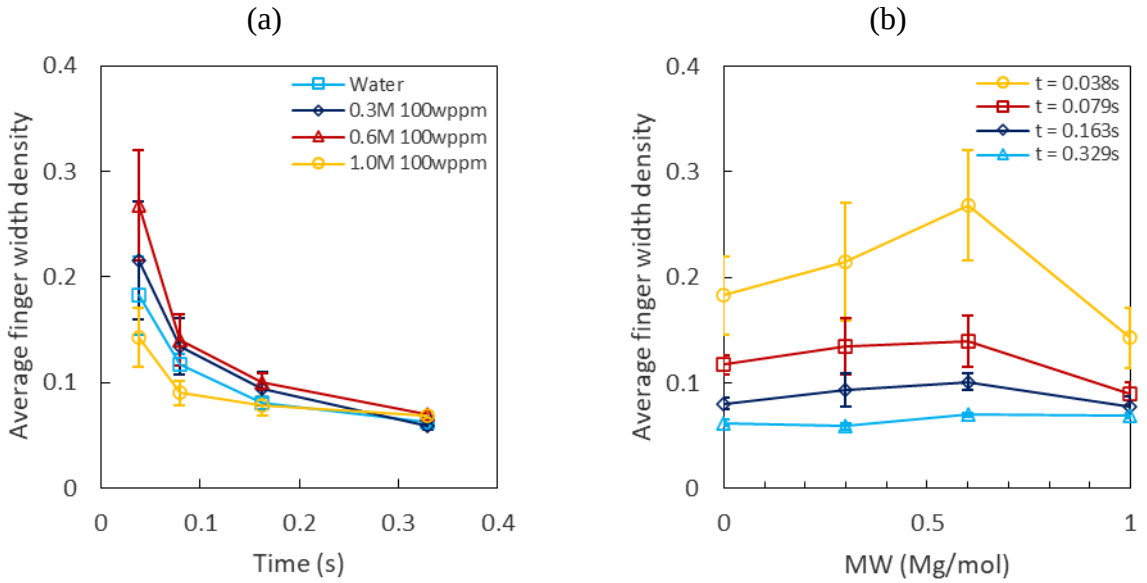

Figure 3.8. Average finger width density (m/m) versus (a) time and (b) PEO molecular weight (Newtonian reference case of deionized water is represented as 0 molecular weight).

Figure 3.9 shows the finger area density versus (a) time for different fluids and (b) PEO molecular weight at four different time points. There is no noticeable difference between deionized water, 0.3M 100wppm, and 0.6M 100wppm. However, 1.0M 100wppm shows significantly lower finger area density. The d_a of 1.0M 100wppm decreases more rapidly in the early stage and reaches a plateau.

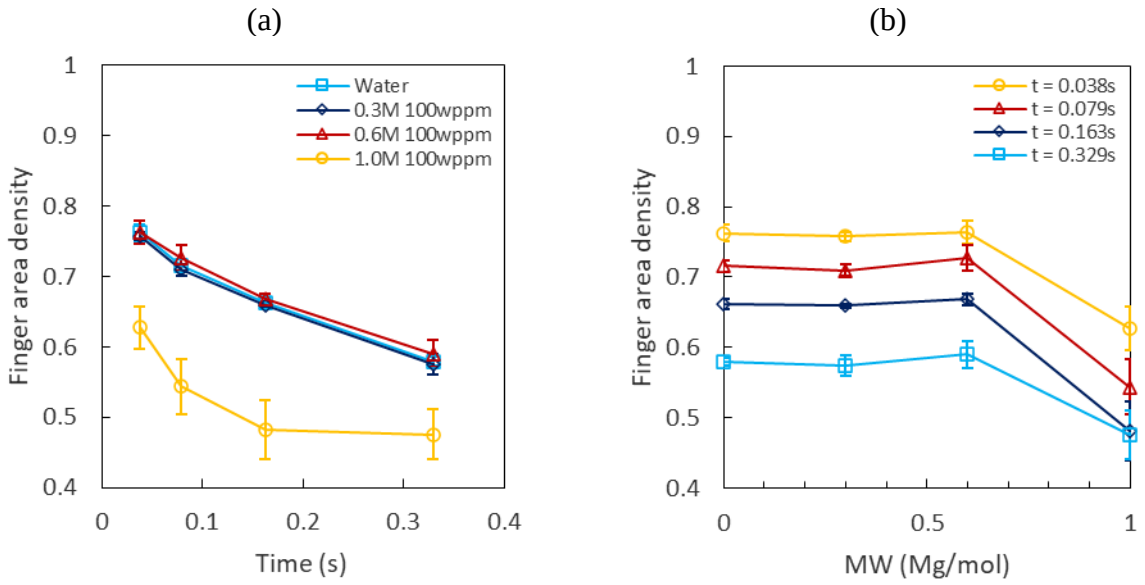

Figure 3.9. Finger area density (m^2/m^2) versus (a) time and (b) PEO molecular weight (Newtonian reference case of deionized water is represented as 0 molecular weight).

To estimate the magnitude of Wi, the representative tip velocity v_{tip} for each time period is determined from:

$$v_{tip} = \frac{\Delta r_{tip}}{\Delta t} \tag{3.5}$$

assuming r_{tip} is the same as the radius of the injection hole at $t = 0s$. The average tip velocities from multiple experiments are shown in Table 3. The tip velocity v_{tip} decreases over time as the fingers extend as shown in Table 3.

Table 3.3. Representative finger tip velocity for each time period.

Time (s)	Deionized water $v_{tip}(\mathrm{cm/s})$	0.3M 100wppm $v_{tip}(\mathrm{cm/s})$	0.6M 100wppm $v_{tip}(\mathrm{cm/s})$	1.0M 100wppm $v_{tip}(\mathrm{cm/s})$
0.038	42.87 ± 1.01	44.60 ± 0.28	42.92 ± 0.69	49.98 ± 0.45
0.079	26.61 ± 0.73	27.69 ± 0.19	27.45 ± 1.29	34.12 ± 2.78
0.163	19.55 ± 0.28	20.33 ± 0.46	20.41 ± 0.76	25.06 ± 1.57
0.329	14.50 ± 0.49	14.90 ± 0.61	14.75 ± 0.38	14.76 ± 0.72

The shear rate is estimated by dividing the tip velocity by b'which is the half of the gap thickness, and the Weissenberg number is determined by multiplying the shear rate by the relaxation time of the dilute PEO solutions as shown in Equation (3). The average Wi numbers from multiple experiments are listed in Table 4.

Table 3.4. Weissenberg number for each time period.

Time (s)	0.3M 100wppm Wi	0.6M 100wppm Wi	1.0M 100wppm Wi
0.038	0.33 ± 0.002	1.35 ± 0.022	4.52 ± 0.040
0.079	0.21 ± 0.001	0.86 ± 0.040	3.08 ± 0.251
0.163	0.15 ± 0.003	0.64 ± 0.024	2.26 ± 0.142
0.329	0.11 ± 0.005	0.46 ± 0.012	1.33 ± 0.065

As shown in Table 4, the VF experiments in this study covered the Weissenberg numbers from 0.11 to 4.52. Tip splitting was observed at the highest Wi, and suppression of tip splitting occurred at intermediate Weissenberg numbers. At small Weissenberg numbers, the width of fingers widened, and the number of fingers decreased. In these small Weissenberg numbers, the width of fingers further widened, and the number of fingers further decreased with the increase in Wi by increasing PEO MW from 0.3M to 0.6M. The highest Wi, 4.52 in this study, is similar

to the Weissenberg number at the onset of tip splitting in a linear Hele-Shaw cell from Vlad and Maher [16]. The range of Weissenberg numbers and their effects on the VF patterns are summarized in Table 5.

Table 3.5. Summary of the effects of the Weissenberg number on the evolution of VF interface in a radial Hele-Shaw cell.

Wi	Effects on VF pattern
$Wi > 4.52$	Cause tip splitting
$2.26 < Wi < 3.08$	Suppress tip splitting and narrow width of fingers
$0.11 < Wi < 1.35$	Widen width of fingers and reduce number of fingers

Vlad and Maher explained that the tip splitting of the finger moving at high velocities in the viscoelastic fluids is caused by the viscoelastic normal stresses arising in shear and extensional flows in front of the spreading finger [16]. The shear flow is the flow in the direction of the finger growth, and the first normal stress difference is the difference between the normal stress in the finger growth direction and the normal stress in the gap thickness direction (shearing direction) [40]. The extensional flow occurs in the direction perpendicular to the finger's advancing direction when the advancing finger stretches and splits the surrounding fluid, and the normal stress differences from the extensional flow resist the extensional motion [16]. The strong elastic forces arising from the normal stress differences near the finger tip oppose the finger growth and cause the tip-splitting [16]. It is also possible that the elastic forces arising from the normal stress differences near the finger tip are not strong enough to cause the tip-splitting, but they can still oppose the extensional motion. In this case, the finger can spread, but the finger width does not grow enough for tip splitting. This can explain the growth of finger without tip splitting at Wi numbers smaller than the Wi that caused tip splitting.

3.3 Conclusions

The elastic effects on the evolution of the viscous fingering interface in the immiscible radial displacement flows in Hele-Shaw cell were examined. To focus on elastic effects, dilute low molecular weight PEO solutions with constant viscosities similar to that of water were used as more viscous existing fluids. Air was injected to displace the dilute PEO solutions at a constant volume flowrate. Only the molecular weight of PEO was varied to precisely investigate the effects of normal stress differences. Three PEO products with different molecular weights (0.3M, 0.6M, and 1.0M) were used to adjust the strength of the elastic effects. The viscous fingering interfaces between dilute PEO solutions and air were examined at four different time points because of the strong velocity variation over time in the radial Hele-Shaw cell. The viscous fingering interfaces were quantitatively evaluated using the effective number of fingers, the finger area density, and the representative finger width density. Nonmonotonic and apparent opposite effects were observed depending on the molecular weight and the stage of the viscous fingering evolution. Decreases in PEO molecular weight (0.3M and 0.6M) reduced the number of fingers and widened the finger width in the early stage, and the effects are strong initially and diminish over time. Increasing PEO MW from 0.3M to 0.6M further widened the width of fingers and further decreased the number of fingers. However, significantly different viscous fingering patterns were observed for the dilute solution of 1.0M PEO. At the early stage, some of the main fingers had already split resulting in an increased number of fingers and narrow fingers. After early stage tip-splitting, fingers spread with an apparent lack of tip-splitting in the intermediate stage. Thereafter, tip-splitting and side branches were observed at the last stage.

The magnitude of the Weissenberg numbers was estimated from the representative tip velocities at four different time points in viscous fingering evolution. Tip-splitting occurred at the largest Wi number of 4.52, and this Wi number agreed with the Wi number at the onset of tip-splitting reported in other study. It was explained that the strong elastic forces arising from the normal stress differences near the finger tip moving at a high velocity opposed finger growth and caused tip splitting [16]. Narrow fingers with an apparent lack of tip splitting were observed at intermediate Wi numbers ($2.26 < Wi < 3.08$) smaller than the Wi with tip splitting. At weak Wi numbers ($0.11 < Wi < 1.35$), the width of fingers widened, and the number of fingers decreased.

Chapter Four: Air invasion into three-dimensional foam induces viscous fingering instabilities

An experimental investigation to examine the immiscible radial displacement flows of air invading three-dimensional foam in a Hele-Shaw cell was conducted. The study successfully identified three distinct flow regimes. In the initial regime, characterized by relatively low fingertip velocities, the foam underwent a slow displacement through plug flow. During this process, the three-phase contact lines slipped at the cell walls. Notably, we discovered that the air injection pressure exhibited a proportional relationship with the power of the fingertip velocity. This relationship demonstrated excellent agreement with a power law, where the exponent was determined to be 2/3. Transitioning to the second regime, we observed relatively high velocities, resulting in the displacement of the foam as a plug within single layers of foam bubbles. The movement of these bubbles near the cell walls was notably slower. Similar to the first regime, the behavior in this regime also adhered to a power law. In the third regime, which manifested at higher air injection pressures, the development of air fingers occurred through narrow channels. These channels had the potential to isolate the air fingers as they underwent a process of "healing." Furthermore, our results unveiled a significant finding that the width of the air fingers exhibited a continuous scaling with the air injection pressure, irrespective of the flow regimes being observed.

4.1 Experiments

In the study, viscous fingering (VF) experiments were conducted by using a radial Hele-Shaw cell apparatus. The cell consisted of two square borosilicate glass plates (304.8 mm × 304.8 mm × 19 mm, SCHOTT Borofloat® 33), as depicted in Figure 4.1(a). To achieve a controlled gap thickness, the two plates were clamped together using Polyester Plastic shims of 0.508 mm (0.02 inches) thickness. These shims were placed symmetrically at eight positions between the plates. An injection hole with a diameter of 3.175 mm (0.125 inches) was positioned at the center of the top plate. The accuracy of the gap thickness was verified by comparing the volume of injected water with the area occupied by the water multiplied by the gap thickness. A commercial shaving foam, Gillette Foamy Regular, was initially placed within the gap in the Hele-Shaw cell. The shaving foam was slowly injected to the Hele-Shaw cell using a 60cc syringe until it reached a radius, $R = 87.7 \pm 0.5mm$.

For the displacement process, constant pressure air injection was carried out into the Hele-Shaw cell through the upper plate. This was achieved by utilizing a 15-gallon (56.8 L) reservoir tank at the desired pressure. To ensure the reliability of the experiments, a minimum of three experiments were performed under each set of conditions.

To enhance wettability and ensure uniformity, the inner surfaces of the Hele-Shaw cell were meticulously polished using a random orbital polisher equipped with a fine steel wool pad (Grade #00). Additionally, a light diffusing film was affixed to the top of the Hele-Shaw cell, placed beneath the LED lighting. This arrangement aimed to improve the visibility of the viscous

fingering (VF) patterns during the experiments. Recording the experimental observations was accomplished using a vertically positioned video camera (GoPro HERO 10 Black) operating at a rate of 240 frames per second (time interval between each frame is about 4.2 milliseconds). The camera was placed below the cell, serving the purpose of concealing the injection tube and maintaining a consistent distance from the cell throughout the recording process.

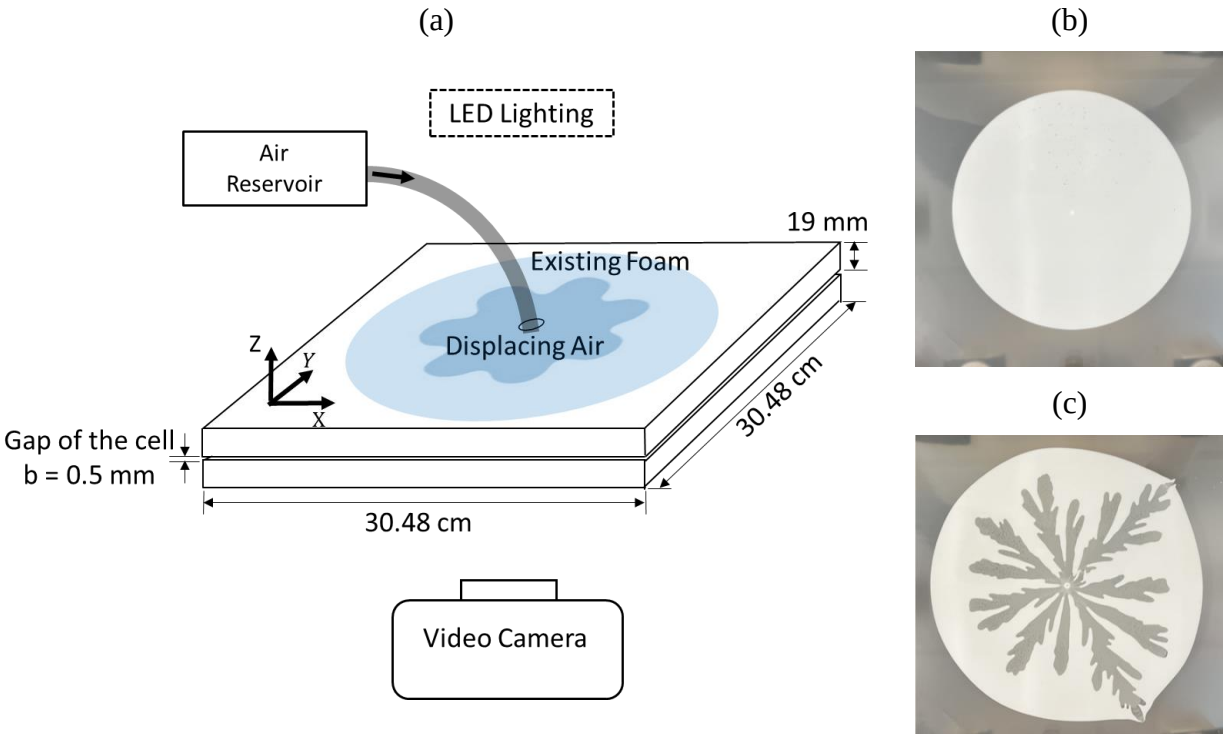

Figure 4.1. (a) Schematic of the radial viscous fingering experimental setup for air invading foam. (b) Gillette Foamy Regular shaving foam slowly injected using a 60cc syringe to a sample radius, $R = 87.7 \pm 0.5mm$, and (c) air is injected into the cell from a reservoir tank at constant pressure.

The Gillette Foamy Regular shaving foam has water, steric acid, triethanolamine, palmitic acid, isobutane, laureth-23, sodium lauryl sulfate, fragrance/parfum, and propane as its ingredients,

and it produces a gas-liquid foam with $92 \pm 1\%$ hydrocarbon gas bubbles by volume [26]. The bubbles have various random sizes without extraordinarily large or small sizes with average bubble diameter equal to about $30\ \mu m$ and standard deviation of about $14\ \mu m$ up to ~20 minutes which then increases due to coarsening [26]. The gap thickness of the Hele-Shaw cell is about 17 times the average bubble diameter. As a result, the shaving foam in this study is polydisperse three-dimensional. The surface tension of the shaving foam solution was determined as $\gamma = 24.1 \pm 0.1\ mN/m$ at 20°C measured by using a Wihelmy plate [85] [86]. The shaving foam solution (the liquid phase of the foam) is a Newtonian fluid, and its viscosity (measured using a DHR-2 rheometer, TA Instruments Inc.) is $\mu = 1.845\ cP$ at 21°C [86]. A three-dimensional foam is "dry foam" if the liquid volume fraction $\phi < 0.05$, it is "wet foam" if $\phi > 0.15$, and it is "bubbly liquid" if $\phi > 0.36$ [87]. The bubbles in "dry foam" are polyhedrons with very thin films, and bubbles in "wet foam" are round. The shaving foam used in this study has the liquid volume fraction of $\phi = 0.08 \pm 0.01$, and it lies between dry foam and wet foam. As a result, it is expected that the shaving foam bubbles are polyhedrons with thicker films and more roundness than dry foam bubbles. According to the study on collective relaxation dynamics in a two-dimensional foam, a wet foam with $\phi = 0.09$ showed simultaneous collective rearrangement of bubbles while separated T1 events propagated in dry foams [53] [88]. This suggests that the shaving foam with $\phi = 0.08 \pm 0.01$ can be considered as a wet foam.

To quantitatively assess the instability of the interfaces, the effective number of fingers [82], finger area density [35] [89] [83], representative finger width density [83], and representative fingertip velocity are examined. The effective number of fingers is calculated from the Fourier spectrum of the radial interface position. More specifically, the interface is rendered as a vector

of points, $\boldsymbol{X}$, of a radius versus angle, and its discrete Fourier transform is determined, given by $F(k)$ = fft($\boldsymbol{X}$) where the Matlab function fft is used, $F(k)$is the discrete Fourier transform, and k is the wave number. The amplitude spectrum is given by $|F(k)|$ (units cm). For X of length n, these transforms are defined as follows:

$$F(k) = \sum_{j=1}^{n} X(j) W_n^{(j-1)(k-1)} \tag{4.1}$$

where $W_m = e^{-\frac{2\pi j}{m}}$. This give the units of $F(k)$ being the same as that of $X(k)$. The amplitude spectrum is given by $|F(k)|$. The effective number of fingers, k_{eff}, is then determined from:

$$k_{eff} = \frac{\sum_k |F(k)|^2 k}{\sum_k |F(k)|^2} \tag{4.2}$$

The finger area density, FAD, is defined as the ratio of the overall finger area to $\pi {r_{tip}}^2$, where r_{tip} is the radius of the point on the interface farthest from the center of the domain [35] [84]. A FAD value of 1 is the case of a perfectly stable circular interface; the lower the value of FAD, the more complex is the fingering structure. The average finger width density $d_w(r)$ for a given r is obtained as $\overline{w}/2\pi r$ where $\overline{w}$ is the average finger width [83]. The representative finger width density for the entire pattern, $\bar{d}_w$, is the average of $d_w(r)$ between r_{base} and r_{tip}. The radius of the point on the interface closest from the center of the domain is r_{base}. The average finger width $\overline{w}$ is the quotient of the total widths of the fingers in a circle of radius r and the number of fingers encountered in the circle. Multiple runs were conducted at each condition to ensure repeatability. The quantitative values, k_{eff}, $\bar{d}_w$, and d_a are determined from the fingering images when the fingertip radius reaches 60 mm. Figure 4.5 (in the Results and Discussion section below) provides an image illustrating the dimensions used in the analysis. The recorded

video frames were processed in MATLAB to identify interfaces and obtain various quantitative values for fingering patterns.

4.2 Results and Discussion

The fingering experiments were carried out by radially displacing the foam by injecting air at constant pressures between 0.5 and 10.0 psi (3.45 and 68.95 kPa) above atmosphere into the center of the Hele-Shaw cell. Figure 4.2 depicts time sequences of the air-foam interface at different air injection pressures of 0.5, 1.0, 2.0, 3.0, and 4.0 psi (3.45, 6.89, 13.79, 20.68, and 27.58 kPa), and air-foam images are presented in Figure 4.3. At low pressures (0.5 psi and 1.0 psi), the foam was displaced slowly by plug flow with apparent slip at the walls with the result of no residual foam bubbles remaining on the surfaces. This implies there is a thin wetting liquid layer between the surface and foam bubbles (Plateau borders touching the wall) that lubricates the foam flow within the gap [90] [91]. It also implies that the cohesive strength of the foam arising from the interfacial tension is sufficiently strong so that as a unit, the foam remains intact and moves as a ‘solid’ body within the gap. The observations show that there is no relative motion of the bubbles relative to each in the cross-gap direction. However, there is relative motion between the bubbles in the horizontal directions due to the expansion of the fingers both radially and laterally within the gap.

(a) 0.5 psi

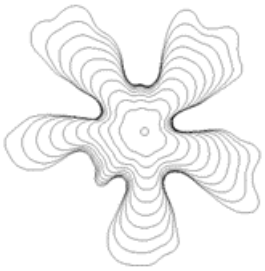

$t = 23.746\ s$
$r_{tip} = 60.9\ mm$

(b) 1.0 psi

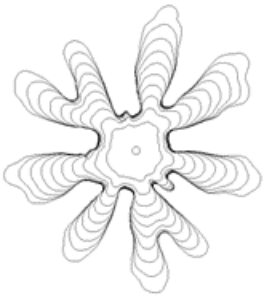

$t = 9.163\ s$
$r_{tip} = 59.7\ mm$

(c) 2.0 psi

$t = 0.625\ s$
$r_{tip} = 61.3\ mm$

(d) 3.0 psi

$t = 0.208\ s$
$r_{tip} = 59.3\ mm$

(e) 4.0 psi

$t = 0.125\ s$
$r_{tip} = 67.0\ mm$

Figure 4.2. Time sequences of the viscous fingering interface at different air injection pressures (a) 0.5 psi, $\Delta t = 2.371\ s$, (b) 1.0 psi, $\Delta t = 0.913\ s$, (c) 2.0 psi, $\Delta t = 0.063\ s$, (d) 3.0 psi, $\Delta t = 0.021\ s$, and (e) 4.0 psi, $\Delta t = 0.013\ s$. Δt is the time intervals between interfaces shown in the images.

The evolution of the fingers at low pressures follows a typical immiscible radial viscous fingering pattern where the initial fingers spread and some of them split when the finger width becomes large enough as shown in Figure 4.2 [35] [13]. The fingering pattern at 0.5 psi exhibits wide fingers and ‘gentle’ tip splitting is observed at the last interface displayed in the image. At 1.0 psi, the finger width becomes narrower and tip splitting starts at an earlier stage. A different

viscous fingering pattern with even more narrower fingers and greater finger velocity is observed at 2.0 psi. At this pressure, the time for the fingertip to reach the same radial distance is about 15 times faster than that at 1.0 psi. The VF pattern also shows multiple levels of tip splitting and many ‘daughter’ branches. In addition, at 2.0 psi, a layer of foam bubbles remains on the Hele-Shaw cell walls where the foam is displaced by air. Park and Durian also observed that residues of foam bubbles is left behind only at higher growth rate and that it is never more than two or three bubble diameters thick [54]. This means that slipping occurs mainly between bubble layers touching the wall and the next bubble layer at higher pressures. In this case, the resistance forces for motion between the wall and the first layer of bubbles adjacent to the wall are larger than the deformation and flow resistance of the internal layers of bubbles and thus, a plug flow occurs within the internal layers of bubbles. A similar fingering evolution pattern is observed at 3.0 psi and 4.0 psi. However, the higher the pressure, the thinner is the finger width and greater the number of daughter branches.

Another significantly different fingering evolution is observed at 10.0 psi as shown in Figure 4.4. At this high pressure, some of the fingers evolve as more narrow channels which then fill larger air invaded zones downstream of the channel. This is due to the reduction of the gas velocity as the air moves radially outward leading to a widening of the fingers away from the injection point. The faster the gas velocity, the greater the shear amongst bubble layers, and as a result, the narrower the finger emerging outwards. As the gas velocity drops, the lower the shear, and the wider the finger. This means the foam bubbles behaved elastically within initial deformation (forming the narrow channels) that can subsequently ‘heal’ restoring an intact foam where the channel once existed. The evolution of the narrow channels and ‘healing’ of the channels is a

dynamic behavior that depends on where the air is invading the foam at a given point of time – for those channels that become starved of air, the foam ‘heals’ the channel and the air pocket downstream becomes isolated and the fingers receiving the air extend. The observations also reveal that some channels are not visible in the image, which means they are in the middle of the foam layer within the gap. In addition, the number of ‘parent’ fingers is lower than that at lower injection pressure but each one of the parent fingers has a greater number of ‘daughter’ fingers emitting from the ‘parent’ fingers. Isolated air pockets appear to form either within the entire gap or partially fill the gap of the Hele-Shaw cell.

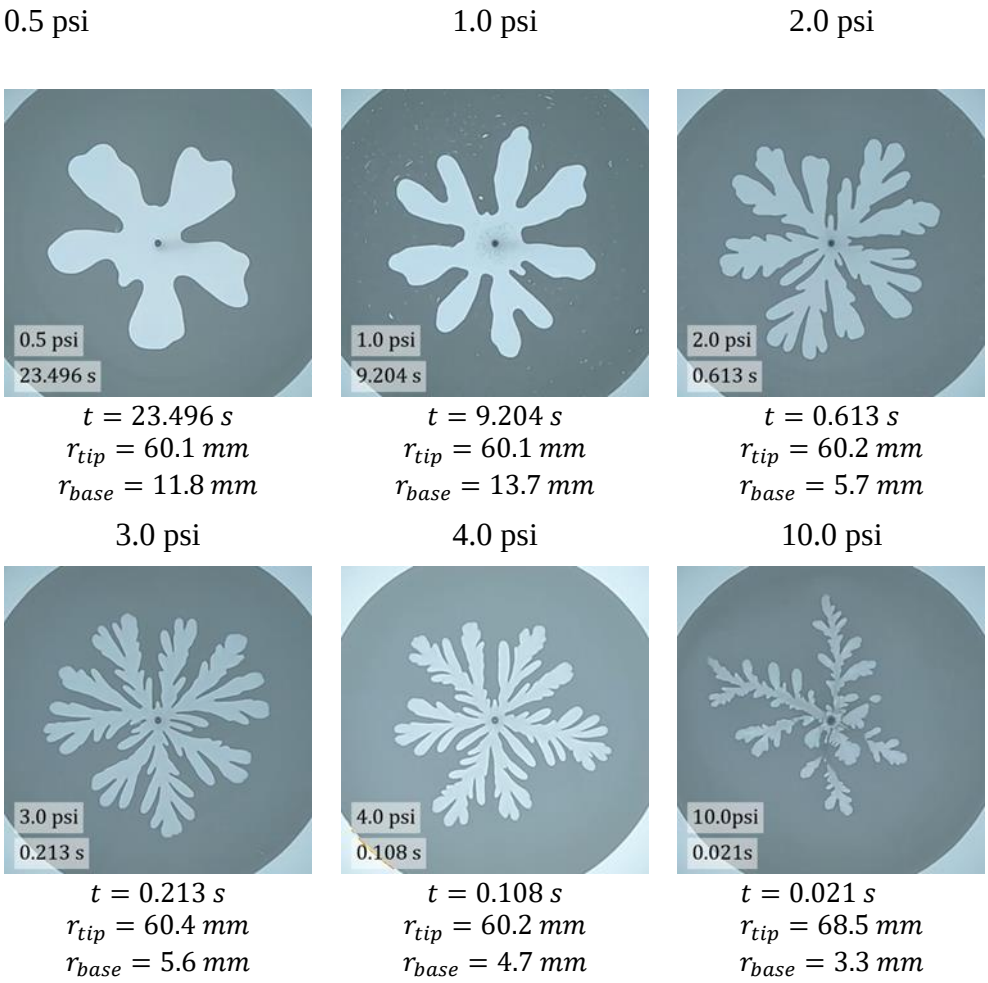

Figure 4.3. Viscous fingering images at different air injection pressures.

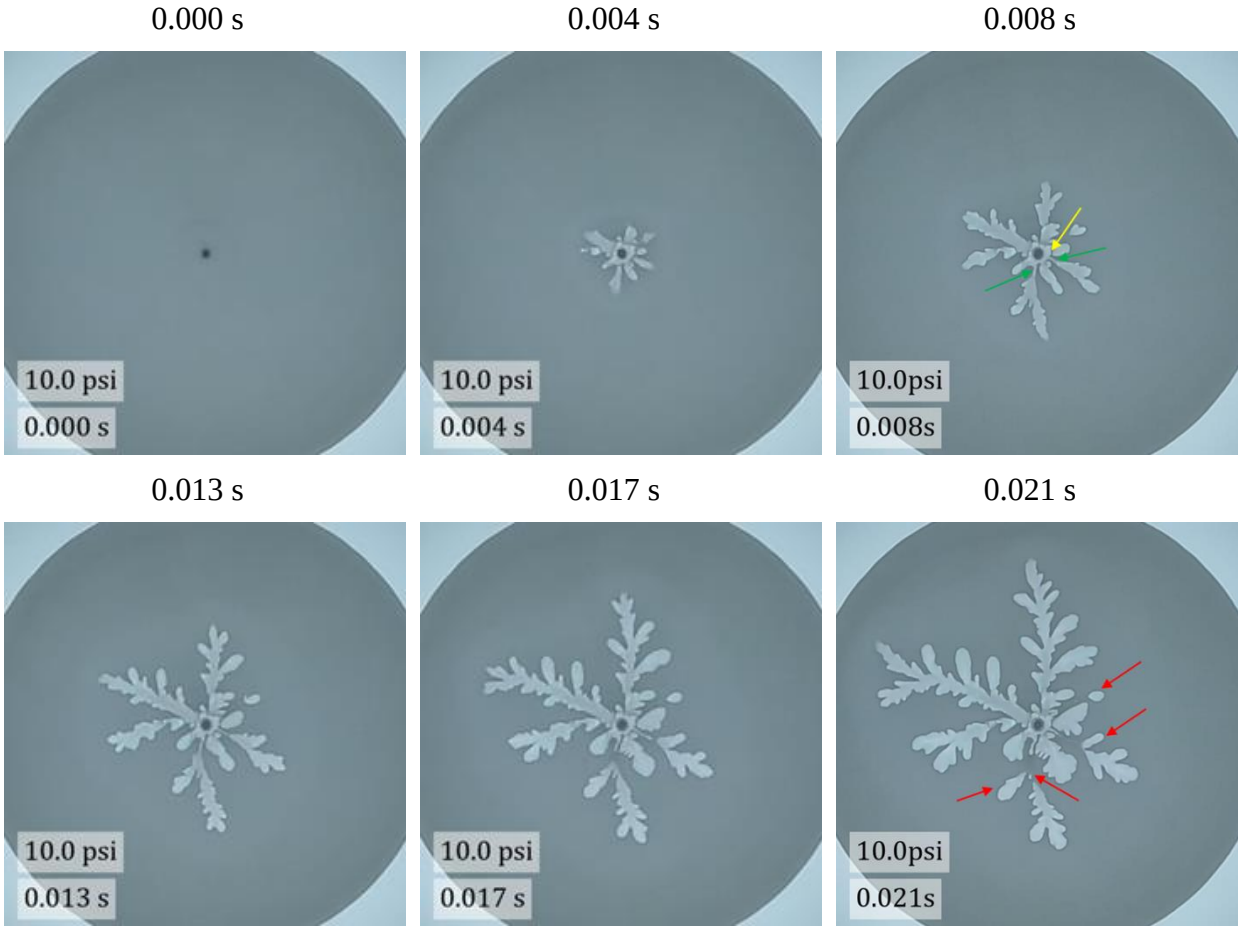

Figure 4.4. Evolution of viscous fingering at high driving pressure of 10.0 psi. Narrow channels are marked using a green arrow. The yellow arrow marks the presumed location of a narrow channel that is still feeding a growing finger, despite there being no visible connection between the finger and the inlet within the plane of the figure. The invisible channel is presumably in a different plane somewhere within the interior of the gap, so is necessarily narrower than the thickness of the Hele-Shaw gap. The red arrows highlight isolated finger tips.

Figure 4.5 illustrates how the effective number of fingers, the finger area density, the representative finger width density, and representative fingertip velocity are obtained using fingering patterns at air injection pressures of 0.5, 1.0, and 2.0 psi. As shown in Figure 4.5, there

is only one dominant wave number at ~5 with the largest amplitude for the fingering pattern at 0.5 psi, and the effective number of fingers is determined as $k_{eff} = 5.11$. In the case of the fingering pattern at 1.0 psi, wave numbers at ~7 and ~9 are dominant resulting in $k_{eff} = 7.78$. The Fourier spectrum at 2.0 psi represents five main fingering groups and many side branches. The effective number of fingers at 2,0 psi is $k_{eff} = 9.96$ which is 2.18 times greater than that at 1.0 psi.

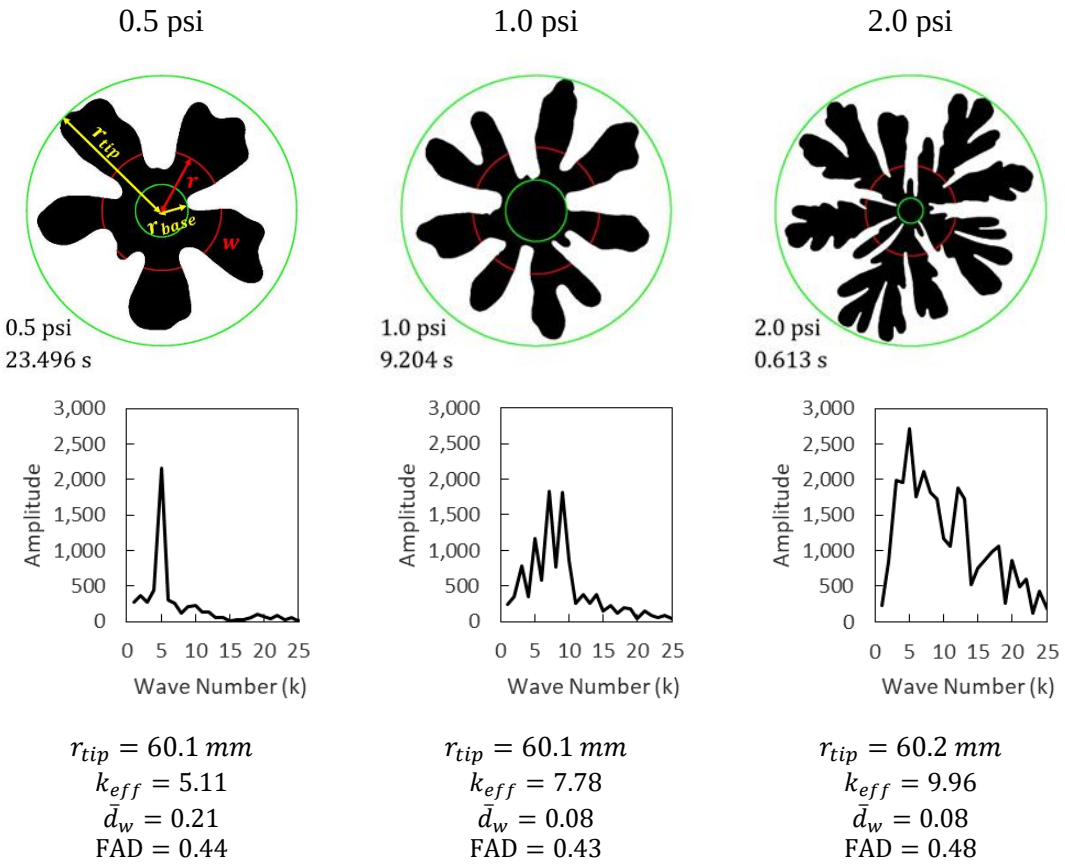

Figure 4.5. Viscous fingering image analysis, Fourier transform spectra of the interfaces, and calculated quantitative values for different air injection pressures.

The representative fingertip velocity v_{tip} is determined by fitting a line to the time series of the fingertip radius r_{tip} as shown in Figure 4.6. The fingertip velocities determined from the fitting lines are plotted as a function of pressure on a log-log scale in Figure 4.7(a). We identify three flow regimes according to how the foam is displaced. The three flow regimes with corresponding representative fingertip velocities v_{tip} and capillary numbers [92], $Ca^* = \mu v_{tip}/\gamma$, are listed in Table 4.1.

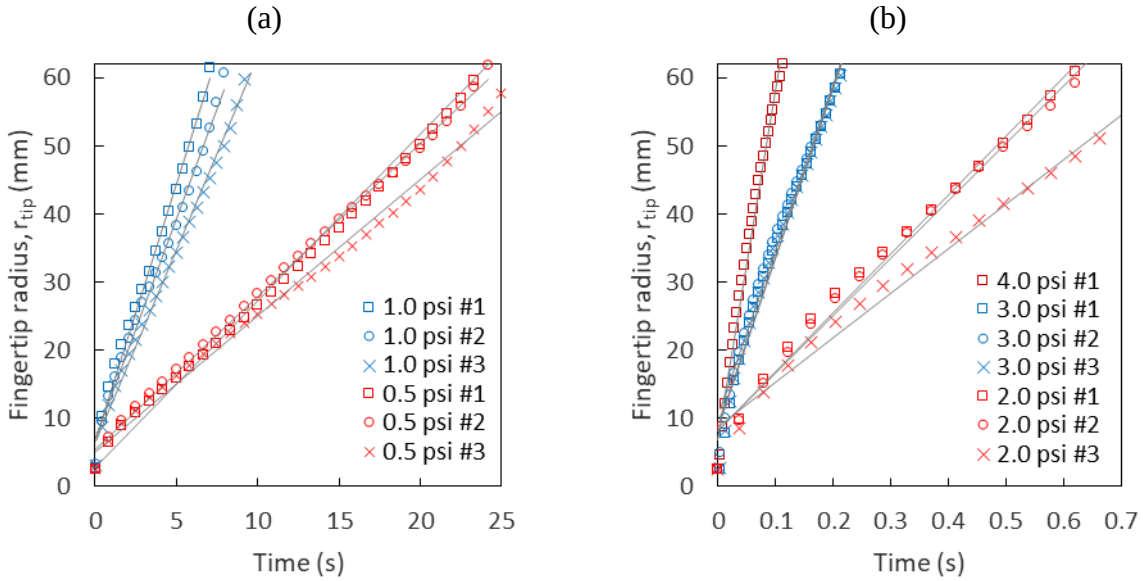

Figure 4.6. Fingertip radius r_{tip} as a function of time for repeated experiments at (a) low and (b) high injection pressures. Fitting lines for each experiment are shown as gray lines.

The liquid fraction and the size distribution can be the source of errors in each measurement shown in Figure 4.6. As a finger propagates, the existing foam bubbles are displaced and rearranged. The liquid fraction and the size distributions affect how the bubbles move and the

time it takes for them to rearrange [53] [88]. If there is a difference in the liquid fraction and the size distribution in each experiment, this will affect the evolution of fingering pattern. At lower pressures, we can expect more error because the growth of finger and the rearrangement of bubbles happen together slowly.

Table 4.1. Representative fingertip velocities v_{tip} and wall capillary numbers, $Ca^* = \mu v_{tip}/\gamma$, for the three flow regimes.

Flow regime	$v_{tip}\ (mm/s)$	Ca^*
#1	$1.9 < v_{tip} < 7.5$	$1.5 \times 10^{-4} < Ca^* < 5.7 \times 10^{-4}$
#2	$65.6 < v_{tip} < 516.6$	$5.0 \times 10^{-3} < Ca^* < 4.0 \times 10^{-2}$
#3	3212.5	2.5×10^{-1}

The pressure drop for bubbles moving with a velocity V in a cylindrical or polygonal capillary is found to be proportional to a power of V [91] [93] [94]:

$$\Delta P \propto V^{\alpha} \quad \text{with} \quad \alpha = \frac{2}{3}. \tag{4.3}$$

This is consistent with other research in the literature where it was experimentally shown that the power law with the exponent $\alpha = 2/3$ also applies to a layer of foam bubbles slipping in a rectilinear Hele-Shaw cell [95]. This relationship also means that the viscous friction between the sliding bubbles and confining wall is proportional to a power of V [27]. According to the study on the effects of surfactant type on the foam-wall viscous friction, the power law index $\alpha = 1/2$

for foams with high surface modulus including Gillette shaving foams, and $\alpha = 2/3$ for foams with low surface modulus [27]. As mentioned earlier, the relative motion of foam bubbles with respect to other bubbles in longitudinal directions was observed near the advancing fingertip. Therefore, the radial displacement flow of foam sliding on the walls involves both foam interface-cell wall friction and the viscous friction between foam bubbles. It was reported that the viscous stress in sheared foams is much higher for foams with high surface modulus than for foams with low surface modulus [96]. In this study, two power law exponents are identified by fitting two lines to the data points in Figure 4.7(a). The equations for the two lines are shown in Figure 4.7(a), and the slope is $1/\alpha$. The flow regime #1 where the foam is displaced slowly by plug flow slipping at the walls has the power law exponent $\alpha = 0.65 \approx 2/3$. This means that the radial displacement of foam by air in a Hele-Shaw cell is also in good agreement with the power law with the exponent $\alpha = 2/3$.

In flow regime #2 where the shaving foam is rapidly displaced leaving a layer of foam bubbles behind, the power law exponent is determined as $\alpha = 0.36$. The remaining layer of bubbles on the plate indicates that there is some modification of structure in the two layers of bubbles adjacent to the boundary so that the viscous force between the two layers becomes less than the viscous force between the wall and bubbles. As a result, the foam bubbles slip on the first layer of bubbles adjacent to the boundary instead of slipping on the wall.

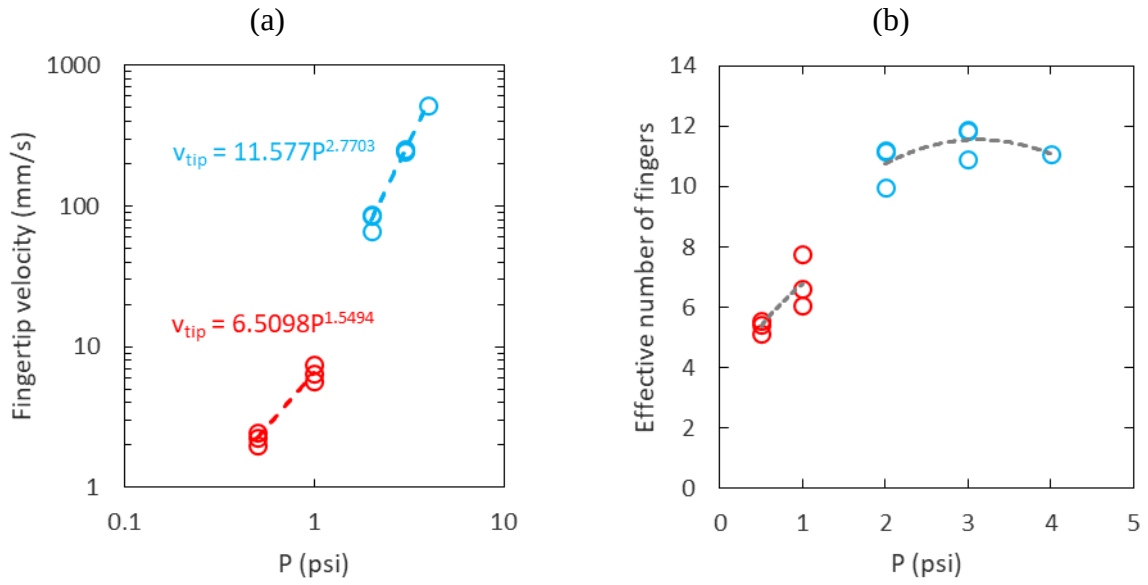

Figure 4.7. (a) Fingertip velocity as a function of air injection pressure and (b) effective number of fingers versus air injection pressure.

Figure 4.7(b) depicts the effective number of fingers versus air injection pressure. In the low velocity regime, the effective number of fingers increases from 5 to 7 due to tip splitting of main fingers as the pressure is raised from 0.5 to 1.0 psi. On the other hand, there is a noticeable increase of the effective number of fingers in the high velocity regime due to multiple levels of tip splitting and many daughter branches. However, the effective number of fingers gradually increases from 10 to 11 as the pressure increases from 2.0 to 4.0 psi.

Figure 4.8(a) depicts the average finger width density versus air injection pressure. Unlike fingertip velocity, effective number of fingers, and finger area density, which show discontinuous or distinct patterns of change with respect to pressure in two flow regimes, the average finger width density continuously scales with air injection pressure regardless of the

flow regimes as shown in Figure 4.8(a). The average finger width density scaling is $\bar{d}_w \propto P^{-0.58}$ from the fitting curve. This is consistent with the finger width scaling, $\lambda \propto (P/R)^{-0.5}$ where λ is the finger width and R is the sample radius, found by Park and Durian [54]. Figure 4.8(b) shows the finger area density versus air injection pressure. In both flow regimes, the finger area density starts at approximately 0.45 and decreases as the air injection pressure increases. It also shows noticeable discontinuity with respect to pressure between the two flow regimes. At 1.0 psi, the FAD is 0.4, and it increases to 0.48 at 2.0 psi as shown in Figure 4.8(b).

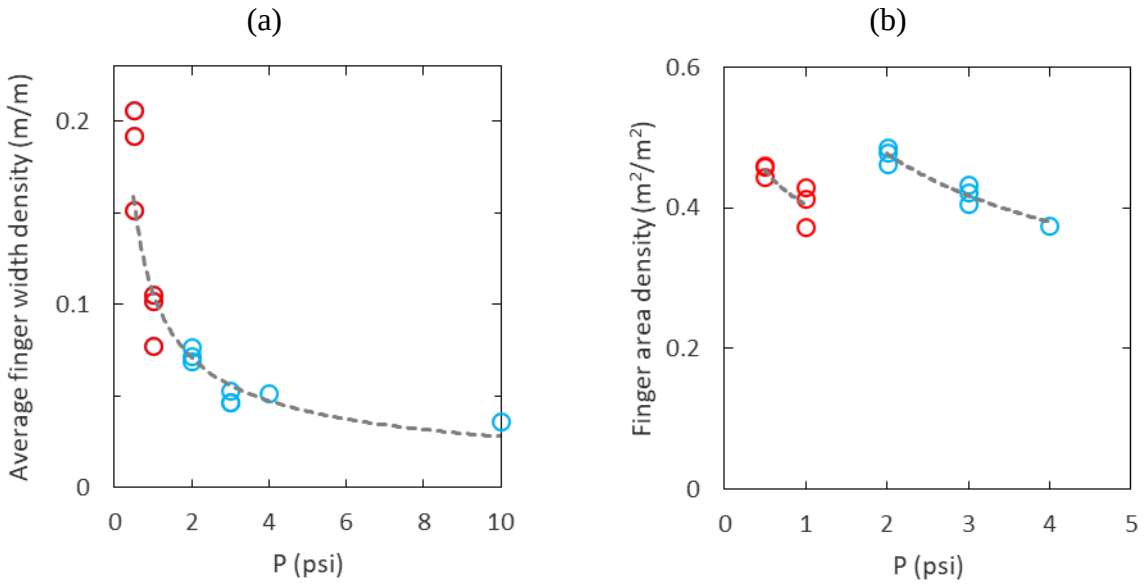

Figure 4.8. (a) Average finger width density (m/m) versus air injection pressure and (b) finger area density (m^2/m^2) versus air injection pressure.

Schematics of foam displacement flow in Hele-Shaw cell for the flow regimes #1, #2, and #3 are depicted in Figure 4.9. As shown in Figure 4.9(a), the foam bubbles first respond elastically by

deforming their shapes against the restoring force of surface tension and tilting in the direction of the shear stress from the wall as the air pressure pushes the foam bubbles in Hele-Shaw cell [94] [27]. Then, they start sliding slowly at the walls. As the air pressure increases, the velocity at which the bubbles slide increases, and as a result, the foam-wall friction increases, causing the bubbles at the layers of bubbles adjacent to the boundary to deform more. As shown in Figure 4.9(b), the foam films between the two boundary layers are flattened, resulting in reduced viscous friction between the two layers. When the viscous friction between two layers of bubbles adjacent to the boundary is less than the foam-wall friction, the foam slides over the first layers of bubbles adjacent to the boundary. The foam can move faster because the viscous friction between two layers of bubbles adjacent to the boundary is less than the foam-wall friction. The foam bubbles that are directly adjacent to the walls are observed in some cases to move slowly along the walls at a velocity significantly lower than that of the core bubbles. As shown in Figure 4.9(c), air can flow through a narrow channel within the internal layers of bubbles in flow regime #3. In addition, air can split an interface leading to a bubble 'poking' its way along bubble interfaces with little displacement of the bulk of the foam as shown in Figure 4.9(d).

Arif et al. observed a fracture like brittle crack by breaking films at much higher crack tip velocity of 10-20 m/s [29]. Yanagisawa et al. reported that a liquid film of foam bubble bursts with a velocity greater than 20 m/s [97]. In addition, finer, needle like fractures at the fingertips signal the onset of film ruptures in a radial Hele-Shaw cell [48]. In this study, the fingertip velocities are 0.5 m/s at 4.0 psi and 3.2 m/s at 10.0 psi. In addition, the fingering patterns show swelling shapes not the needle like fractures. As a result, the dynamics of foam displacement flows seen in this study are dominated by the T1 process.

(a)

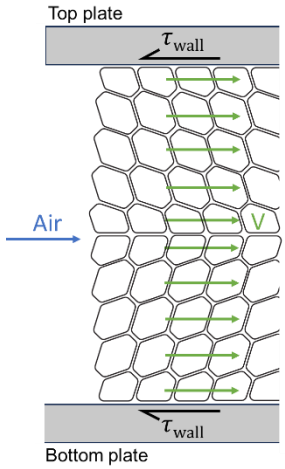

Slip at the walls (complete plug flow)

(b)

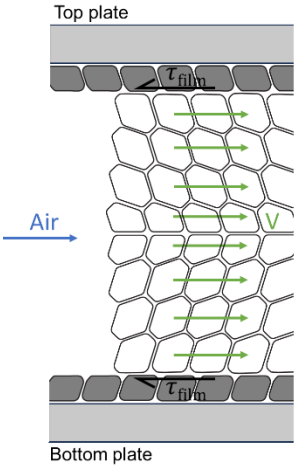

A layer of bubbles remains on the surface. Near the injection hole, the layer looks thicker.

(c)

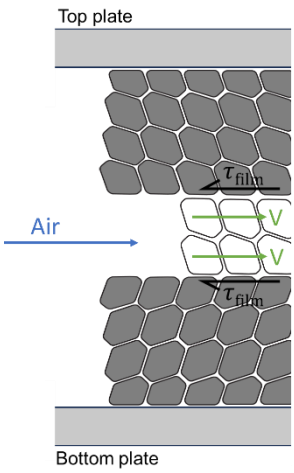

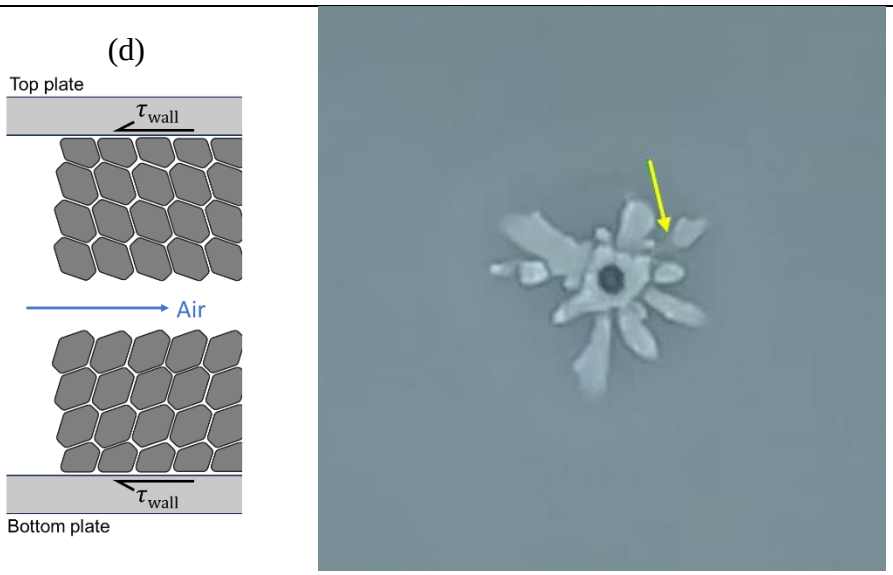

Figure 4.9. Schematics of foam displacement flows in Hele-Shaw cell in the cross-gap plane: (a) slip at the walls (complete plug flow), (b) slip at the first layer of bubbles adjacent to the boundary (internal plug flow), (c) slipping within internal layers of bubbles (internal plug flow), and (d) splitting of bubble interfaces (bubbles do not move).

4.3 Conclusions

The evolution of the viscous fingering interface for the immiscible radial displacement flows of air invading foam in Hele-Shaw cell has been examined. A commercial shaving foam, Gillette Foamy Regular, initially filled the cell. The foam was radially displaced by injecting air at constant pressures between 0.5 and 10.0 psi above atmosphere into the center of the Hele-Shaw cell. Three different flow regimes were identified. In a flow regime with low fingertip velocities at low air injection pressures, the foam is displaced slowly by plug flow with slip at the walls. In this regime, the air injection pressure is found to be proportional to the power of fingertip velocity with the exponent $\alpha = 0.65$. This shows that the radial displacement flow with low velocities is in good agreement with the power law with the exponent $\alpha = 2/3$ for bubbles moving in a cylindrical or polygonal capillary or a layer of bubbles slipping in a rectilinear Hele-

Shaw cell. In a flow regime with high fingertip velocities at higher air injection pressures, the foam is displaced more rapidly leaving a layer of foam bubbles behind on the surface. The power law exponent is determined as $\alpha = 0.36$ in this flow regime. Another flow regime was observed at 10.0 psi. At this high air injection pressure, some of the fingers developed as narrower channels where some of the air pockets formed in the foam became isolated as channels were 'healed' due to starvation (the air invaded other channels). The viscous fingering interfaces were quantitatively evaluated using the effective number of fingers, finger area density, and representative finger width density. The effective number of fingers and finger area density showed discontinuous or distinct patterns of change with respect to pressure in different flow regimes. On the other hand, the average finger width density continuously scaled with air injection pressure regardless of the flow regimes. The average finger width density scaling was determined as $\bar{d}_w \propto P^{-0.58}$, in agreement with the finger width scaling reported in the prior literature [54].

Chapter Five: Viscous fingering and interface splitting instabilities in air-water-oil systems

In this chapter, an experimental study to examine the effects of water in viscous fingering instabilities of air displacing mineral oil in a radial Hele-Shaw cell was examined. The displaced fluids consist of a small volume of water at the center, surrounded by mineral oil. Air is injected at constant pressures to displace both the water and surrounding mineral oil. The evolution of fingering patterns is then compared with reference cases in which air displaces only mineral oil without water. The presence of a small volume of water leads to significantly different fingering patterns than that when no water is present. In the water, a less unstable interface between air and water is observed until the point at which air contacts the mineral oil. Upon contacting the mineral oil, the air begins to propagate along the boundary between water and mineral oil resulting in the development of more intricate fingering patterns. Another notable distinction is that the fingertip radius propagates a greater distance with water than when air displaces only mineral oil. In addition, the fingertip moves faster with the presence of water displaying a discontinuity in fingertip velocities across the water and mineral oil regions. Furthermore, a greater volume of air is injected with water, compared to the cases without water.

5.1 Experiments

In this research, experiments on viscous fingering (VF) were conducted by using a radial Hele-Shaw cell apparatus. The cell used two square borosilicate glass plates measuring 304.8 mm ×

304.8 mm × 19 mm, made of SCHOTT Borofloat® 33, as illustrated in Figure 5.1(a). To control the gap thickness, the two plates were firmly secured together using stainless steel shims, each 0.127 mm (0.005 inches) thick. These shims were evenly positioned at eight locations between the plates. At the center of the top plate, there was an injection hole with a 3.175 mm (1/8 inch) diameter. The precision of the gap thickness was confirmed by comparing the volume of injected water with the area covered by the water, multiplied by the gap thickness. A longer evolution of the viscous fingering interface can be observed by using a high aspect ratio of the cell's width to the gap thickness [70] [71] [98]. Mineral oil supplied from VWR, colored with Sudan Red G at a concentration 0.1 wt.%, was initially introduced into the Hele-Shaw cell's gap as an existing more viscous liquid. The mineral oil was gradually injected into the Hele-Shaw cell using a syringe pump until it reached a sample radius of $R_{oil} = 101.0 \pm 2.3\ mm$ and a volume of $V_{oil} = 4.08 \pm 0.15\ cc$ as shown in Figure 5.1(b). In the experiment where air displaced water and mineral oil, a small amount of deionized water, $V_{water} = 0.19 \pm 0.02\ cc$, colored with Trypan blue at a concentration 0.06 wt.% was injected slowly after the injection of mineral oil as illustrated in Figure 5.1(c). During the air displacement process, constant pressure air was injected into the Hele-Shaw cell through the upper plate. This was accomplished by employing a 15-gallon (56.8 L) reservoir tank at the specified pressure. To improve wettability and ensure uniformity, the inner surfaces of the Hele-Shaw cell underwent careful polishing using a random orbital polisher equipped with a fine steel wool pad (Grade #00). Furthermore, a light-diffusing film was attached to the top of the Hele-Shaw cell, positioned beneath the LED lighting to enhance the visibility of viscous fingering (VF) patterns during the experiments.

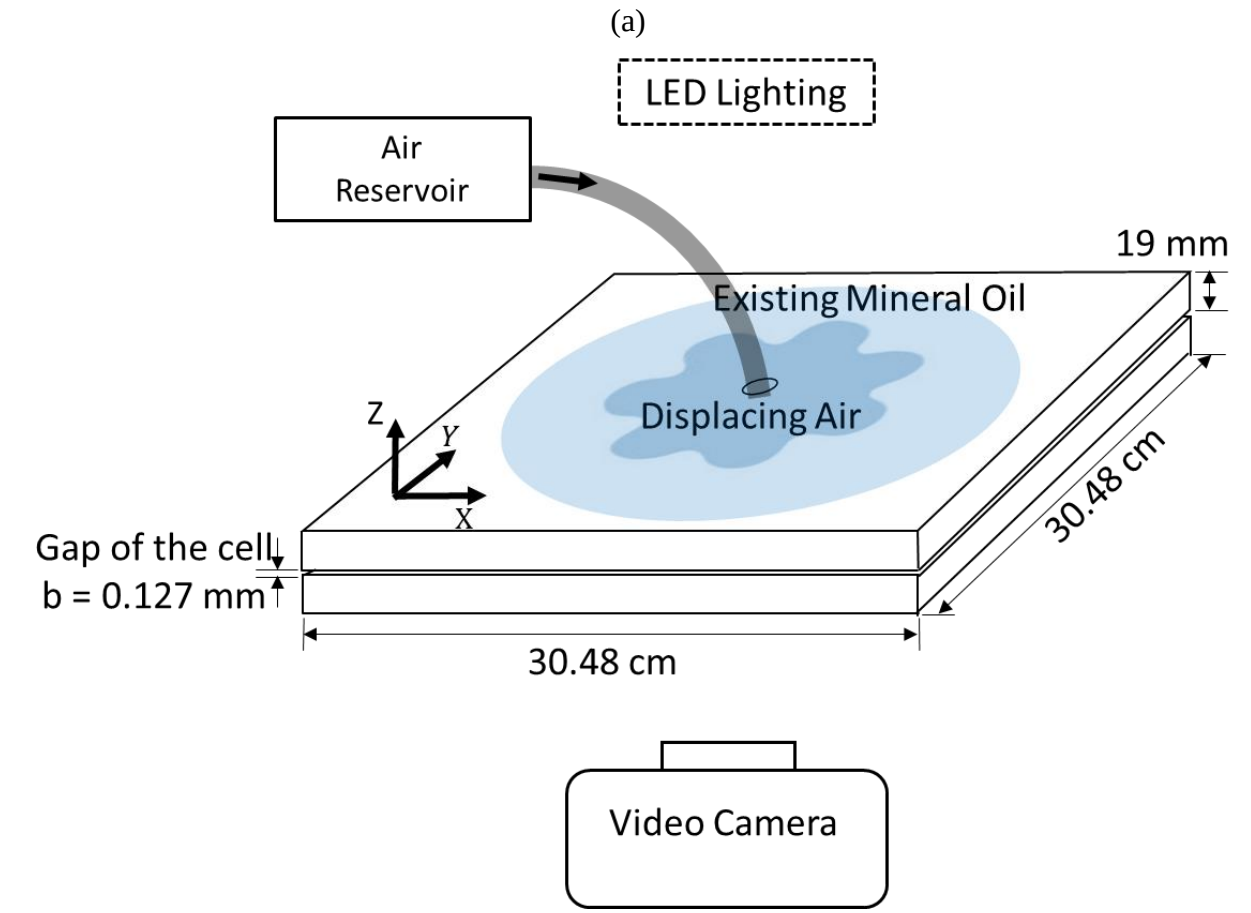

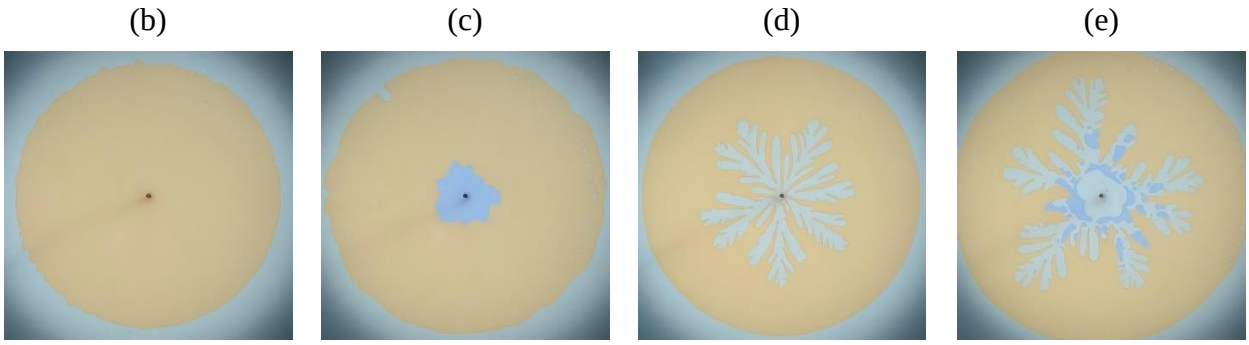

Figure 5.1. (a) Schematic of the radial viscous fingering experimental setup for air displacing mineral oil, (b) mineral oil is slowly injected using a syringe pump to a sample volume, $V_{oil} = 4.08 \pm 0.15\ cc$ or a sample radius, $R_{oil} = 101.0 \pm 2.3\ mm$, (c) small amount of water, $V_{water} = 0.19 \pm 0.02\ cc$, is injected slowly after the injection of mineral oil, and (d)(e) air is injected into the cell from a reservoir tank at constant pressure.

The experiments were recorded with a video camera (GoPro HERO 10 Black) operating at a rate of 240 frames per second (with a time interval of ~4 milliseconds between each frame). The camera was fixed vertically below the Hele-Shaw cell. The density of the mineral oil is $\rho_{oil} = 0.872\ g/cm^3$ at 20℃. The mineral oil's surface tension was measured at $\gamma_o = 26.3 \pm 0.3\, mN/m$ at 25°C, and the interfacial tension between deionized water and mineral oil was determined as $\gamma_{wo} = 45.2 \pm 0.3\, mN/m$ at 25°C using a Du Noüy ring. The viscosity of the mineral oil was determined as $\mu_o = 69.5 \pm 0.5\, cP$ at 23°C using a TA Instruments DHR-2 rheometer with a double gap rotor and cup geometry within a Peltier temperature system under steady shear conditions.

To quantitatively examine the instability of nonlinear VF interfaces, several criteria are employed. These criteria include the effective number of fingers [82] [98], the finger area density [35] [89] [83], and the representative finger width density [83]. Figure 5.2 below provides an image illustrating the quantitative criteria utilized in the analysis.

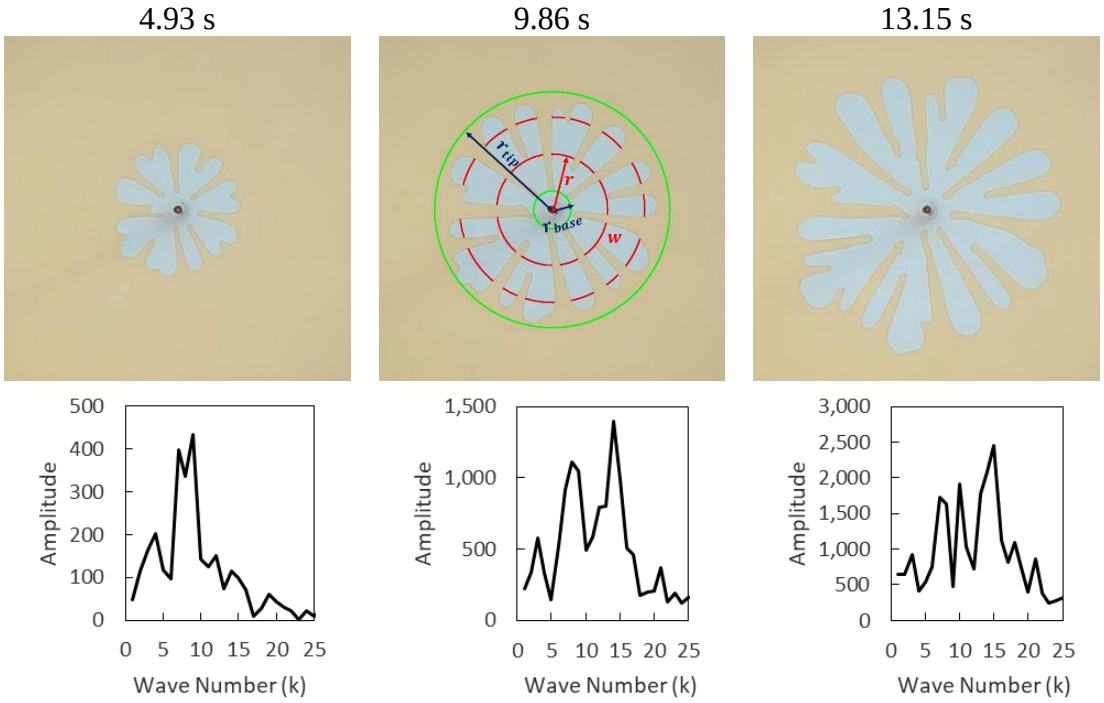

$k_{eff} = 8.40$
$\bar{d}_w = 0.11$
$d_a = 0.58$

$k_{eff} = 11.61$
$\bar{d}_w = 0.07$
$d_a = 0.55$

$k_{eff} = 12.78$
$\bar{d}_w = 0.06$
$d_a = 0.52$

Figure 5.2. Viscous fingering image analysis, Fourier transform spectra of the interfaces, and calculated quantitative values at three different time points for air displacing mineral oil under an air injection pressure of 0.5 psi.

The effective number of fingers, denoted as k_{eff}, is computed based on the Fourier spectrum of the radial interface position. In detail, the interface is represented as a vector of radial distances of the points on the interface in order, denoted as X. The discrete Fourier transform of this vector is calculated using the Matlab function fft(X), resulting in F(k), where F(k) represents the discrete Fourier transform and k is the wave number (the number of cycles in the input data, X). The amplitude spectrum is denoted as |F(k)| and is measured in units of cm. The effective number of fingers, k_{eff}, is subsequently determined through the following expression:

$$k_{eff} = \frac{\sum_k |F(k)|^2 k}{\sum_k |F(k)|^2} \tag{5.1}$$

The finger area density, d_a, is defined as the ratio of the finger area to the area of circle, ${\pi r_{tip}}^2$, where r_{tip} represents the radius of the point on the interface farthest from the center of the domain [35] [89] [83]. A d_a value of 1 corresponds to a perfectly stable circular interface, while lower d_a values indicate a more intricate fingering structure such as narrow fingers with many side branches. The representative finger width density, denoted as $\bar{d}_w$, is computed by averaging the average finger width density, $d_w(r)$, within the range from r_{base} to r_{tip}. The average finger width density, $d_w(r)$, for a given r is determined as $\overline{w}/2\pi r$, where $\overline{w}$ represents the average finger width [83]. Here, r_{base} signifies the radius of the point on the interface closest to the center of the domain. The average finger width, $\overline{w}$, is calculated as the ratio of the total widths of the fingers in a circle of radius r to the number of fingers encountered in the circle. The recorded video frames were analyzed using MATLAB to identify interfaces and determine the quantitative values from fingering patterns.

5.2 Results and Discussion

The radial viscous fingering experiments were conducted by injecting air at four different constant pressures ranging from 0.5 to 2.0 psi (3.45 to 13.79 kPa) above atmospheric pressure through the injection hole at the center of the top plate. The fingering patterns from air displacing water and mineral oil are compared to the fingering patterns observed when air displaces only mineral oil. As described above, to investigate the effects of water in viscous fingering instabilities of air displacing mineral oil, a small amount of water, $V_{water} = 0.19 \pm 0.02\ cc$, was

introduced in Hele-Shaw cell before injecting air. In this analysis, VF images captured at 10 distinct equally spaced time points are examined. The observation period extends until the fingertip radius reaches approximately 68 mm in the reference cases where air displaces only mineral oil. Figure 5.3 illustrates the time sequences of air-mineral oil interface under different air injection pressures. The experimental images of air displacing only mineral oil are presented in Figure 5.4.

The evolution of the VF interface of air displacing only mineral oil exhibits a typical characteristic of immiscible radial VF pattern. The initial fingers spread out and transform into a fan shape, and some of these fingers split as their width reaches a certain threshold [13] [35]. As the pressure increases, the width of the finger decreases, and the number of side branches increases as shown in Figure 5.3. In the early stage, the first VF images in Figure 5.4 show a narrowing of finger width as the air injection pressure increases. Simultaneously, there is an increase in the number of fingers due to tip splitting as the pressure increases. In addition, the base radius r_{base} decreased from 4.8 mm to 3.5 mm as the pressure increased from 0.5 psi to 2.0 psi as shown in the first VF images in Figure 5.4.

(a) 0.5 psi

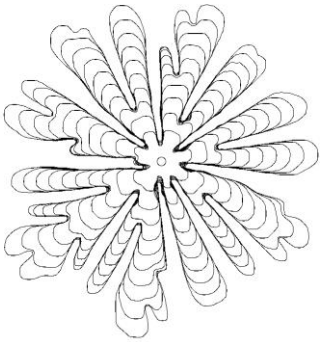

$t = 16.43\ s$
$r_{tip} = 67.7\ mm$

(b) 1.0 psi

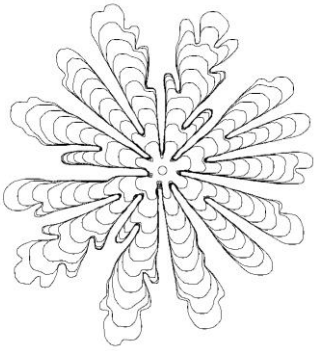

$t = 9.18\ s$
$r_{tip} = 67.6\ mm$

(c) 1.5 psi

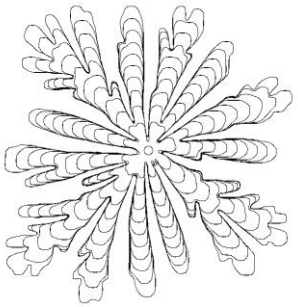

$t = 4.55\ s$
$r_{tip} = 67.7\ mm$

(d) 2.0 psi

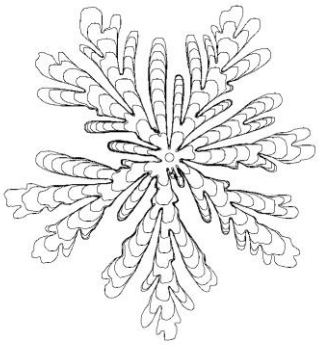

$t = 3.00\ s$
$r_{tip} = 67.9\ mm$

Figure 5.3. Air displacing mineral oil: time sequences of the viscous fingering interface at different air injection pressures (a) 0.5 psi, $\Delta t = 1.64\ s$, (b) 1.0 psi, $\Delta t = 0.92\ s$, (c) 1.5 psi, $\Delta t = 0.45\ s$, (d) 2.0 psi, $\Delta t = 0.30\ s$. Δt is the time interval between interfaces shown in the images.

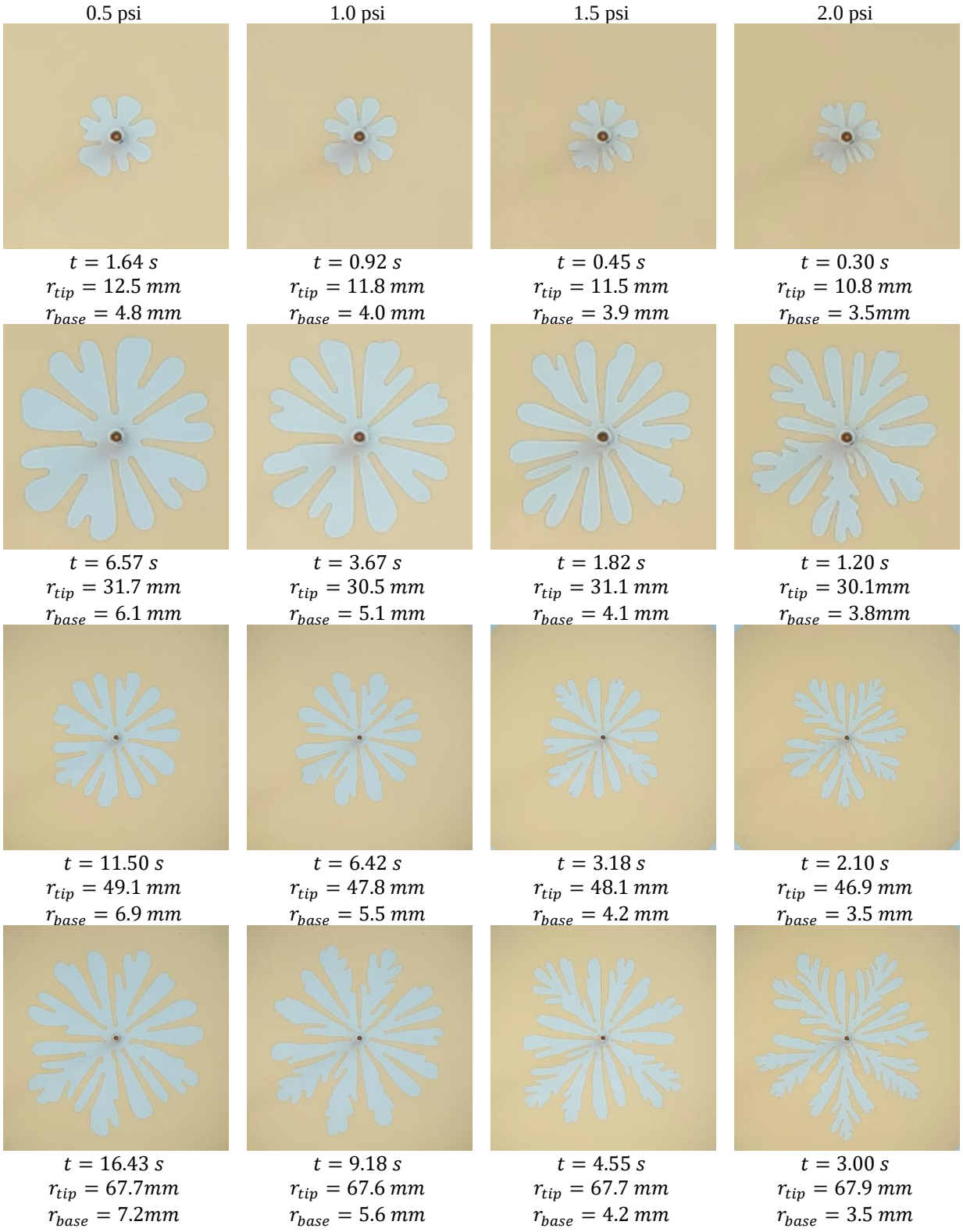

Figure 5.4. Air displacing mineral oil: viscous fingering images at different injection pressures.

Figure 5.5 depicts the evolution of air-water and air-mineral oil interfaces under different air injection pressures obtained at the same time points as in the reference cases where water only displaces mineral oil. As illustrated in Figure 5.5, the presence of a small amount of water surrounding the injection hole prior to air injection significantly influences the formation of more intricate fingering patterns.

As shown in Figure 5.5, the fingering patterns exhibit two very different types of interfaces: a less unstable interface in the initial stage and, after the air encounters the mineral oil, a more unstable one. In the early stage until air encounters oil, the initial VF images presented in Figure 5.6 show much less unstable interfaces than the initial interfaces shown in Figure 5.4 when only air and oil are present. Once air encounters mineral oil at certain points, the less unstable growth of interface between air and water comes to a halt, and the air starts to spread along the boundary between water and mineral. Then, fingers of air begin to form into mineral oil in radial direction from the air that has spread along the interface. At some points, it is observed that air passes through water through narrow channels instead of spreading along the water-mineral oil boundary. As seen in the final fingering images of Figure 5.5, the fingertips have advanced a greater distance in the same pressure and time compared to the reference cases.

(a) 0.5 psi

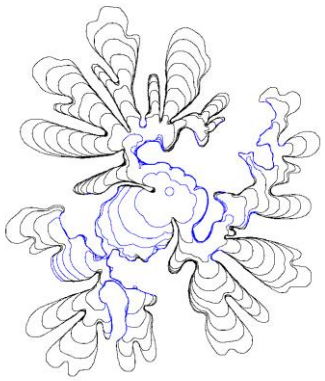

$t = 16.43\ s$
$r_{tip} = 78.4\ mm$

(b) 1.0 psi

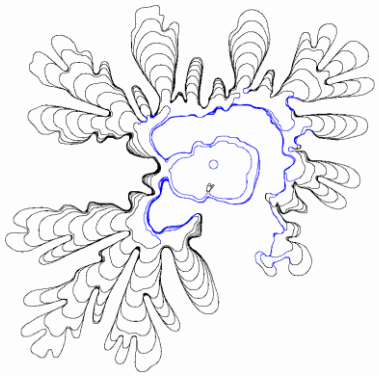

$t = 9.18\ s$
$r_{tip} = 97.1\ mm$

(c) 1.5 psi

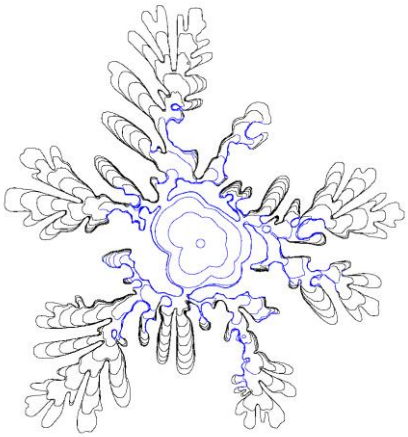

$t = 4.55\ s$
$r_{tip} = 90.8\ mm$

(d) 2.0 psi

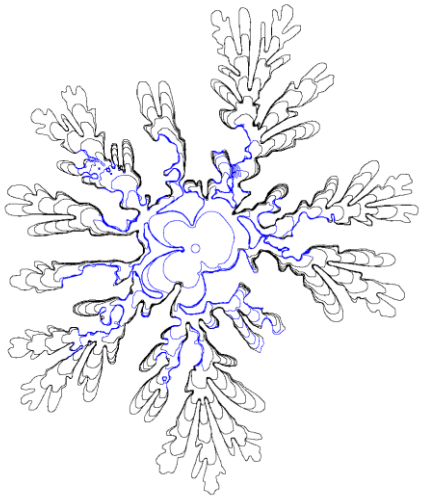

$t = 3.00\ s$
$r_{tip} = 96.7\ mm$

Figure 5.5. Time sequences of the viscous fingering interface of air at different air injection pressures (a) 0.5 psi, $\Delta t = 1.64\ s$, (b) 1.0 psi, $\Delta t = 0.92\ s$, (c) 1.5 psi, $\Delta t = 0.45\ s$, (d) 2.0 psi, $\Delta t = 0.30\ s$. Δt is the time interval between interfaces shown in the images. The interface between air and mineral oil is shown in black, whereas the interface between air and water is depicted in blue.

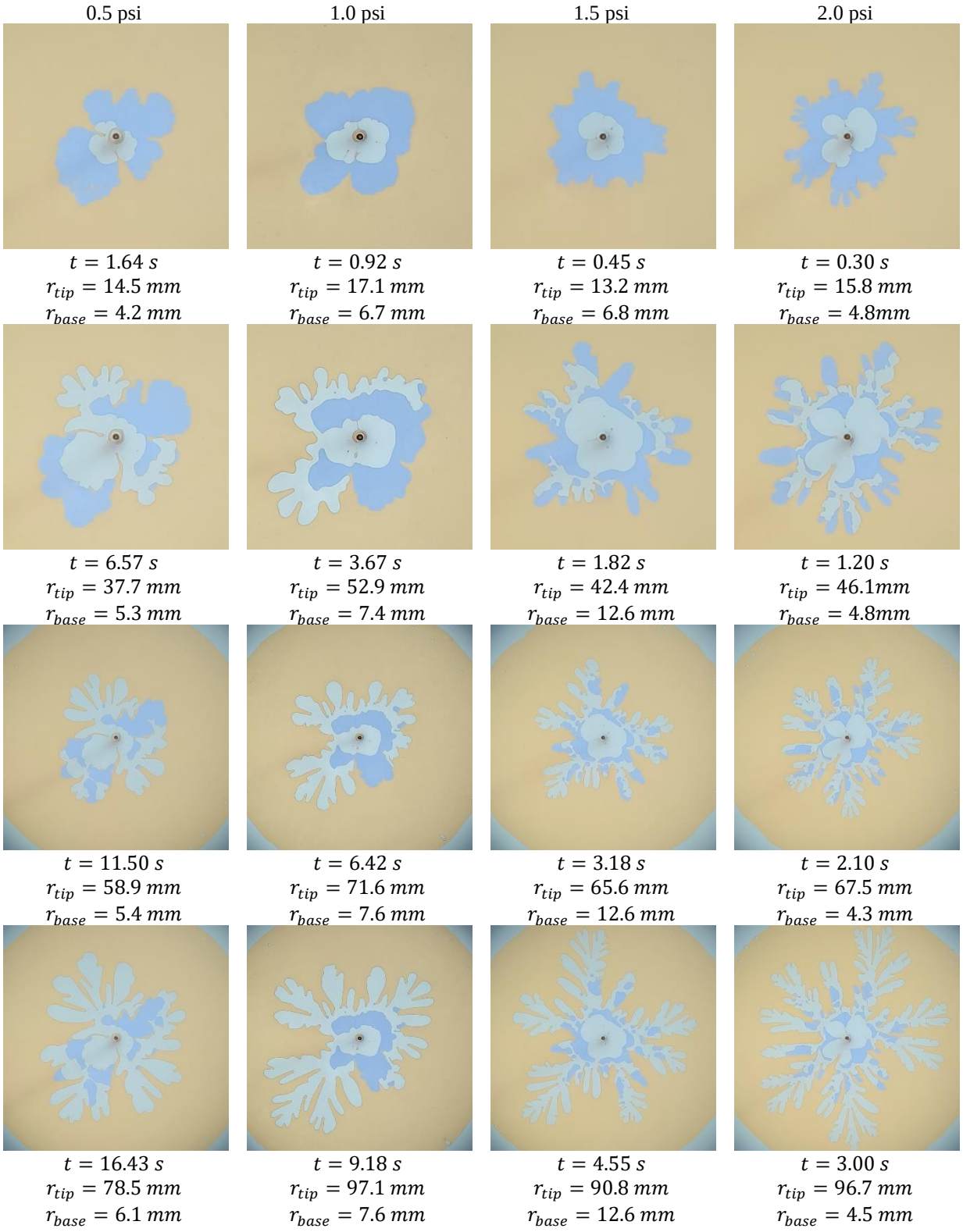

Figure 5.6. Viscous fingering images of air displacing water and mineral oil at different injection pressures.

Quantitative values are evaluated from the experimental VF images at 10 evenly distributed time points, as depicted in Figure 5.3 and 5.5. The effective number of fingers k_{eff} and the representative finger width density $\bar{d}_w$ are not computed for air displacing water and mineral oil due to the complexity of the fingering pattern. Figure 5.7 shows the variation of (a) effective number of fingers k_{eff} and (b) representative finger width density $\bar{d}_w$ as a function of time at four different air injection pressures during the displacement of mineral oil by air. In the early and intermediate stages, the higher the air injection pressure, the more effective number of fingers are observed. In the later stage, the effective number of fingers gradually increases approaching similar values of around 13 for all pressures.

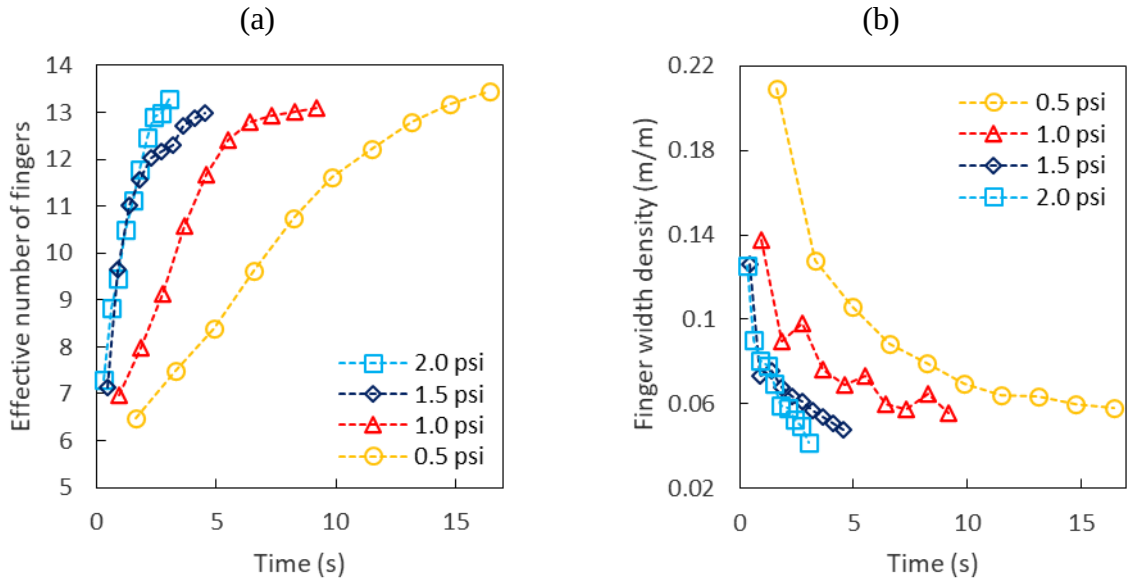

Figure 5.7. (a) Effective number of fingers k_{eff} and (b) representative finger width density $\bar{d}_w$ as a function of time at different air injection pressures for air displacing mineral oil.

As shown in Figure 5.7 (b), the representative finger width density $\bar{d}_w$ decreases rapidly initially and then gradually decreases in the later stage. In the early stage, there is a significant decrease in $\bar{d}_w$ as the pressure changes from 0.5 psi to 1.0 psi, but there is not much difference between 1.0 psi, 1.5 psi, and 2.0 psi. Figure 5.8 illustrates the finger area density over time for (a) air displacing mineral oil and (b) air displacing water and mineral oil. As shown in Figure 5.8(a), the displacement of mineral oil by air exhibits nearly linear decreases in finger area density over time, with the rate of decline amplifying as the air injection pressure rises.

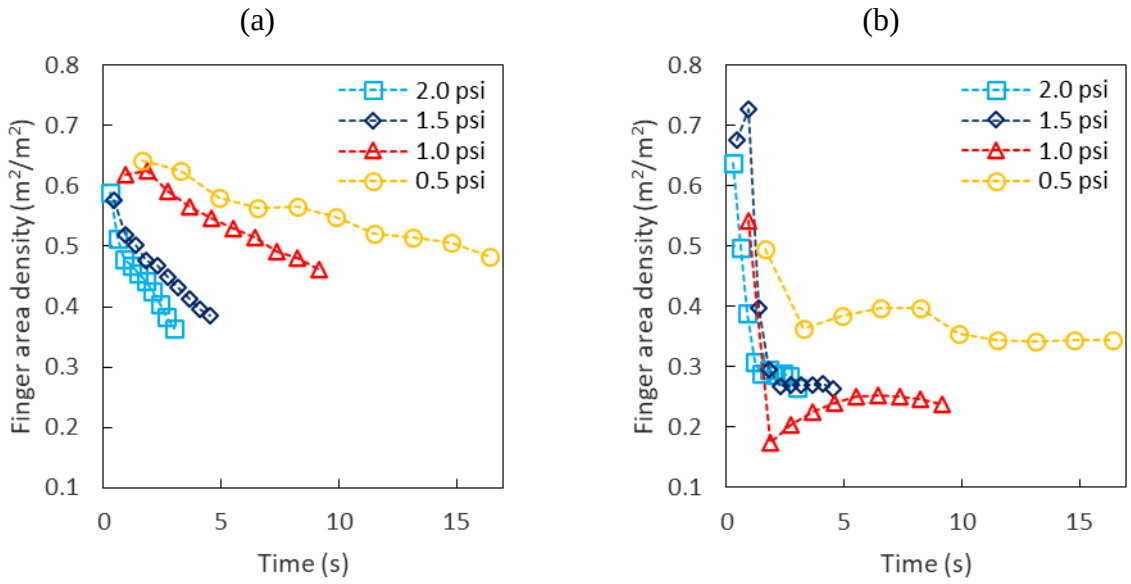

Figure 5.8. Finger area density (d_a) versus time for (a) air displacing mineral oil and (b) air displacing water and mineral oil.

Figure 5.8(b) shows a significantly distinct pattern in finger area density when air displaces both water and mineral oil. In all injection pressures, the finger area density undergoes a rapid and brief decline, after which it remains consistently low for an extended period. As illustrated in Figure 5.6, the finger area density is initially higher when air touches only water. Nevertheless, the finger area density, d_a, rapidly diminishes as soon as air meets mineral oil, as the air begins

to propagate along the boundary between air and water rather than displacing water radially. Figure 5.9 depicts fingertip radius r_{tip} as a function of time for (a) air displacing mineral oil and (b) air displacing water and mineral oil. As shown in Figure 5.9(a), air displacing mineral oil shows a linear growth of fingertip radius. The figure includes fitted lines and corresponding equations, where the slope represents the fingertip velocity v_{tip} measured in mm/s. The fingertip velocities fit well to an exponential equation, $v_{tip} = 2.08e^{1.17P}$, where P denotes the air injection pressure.

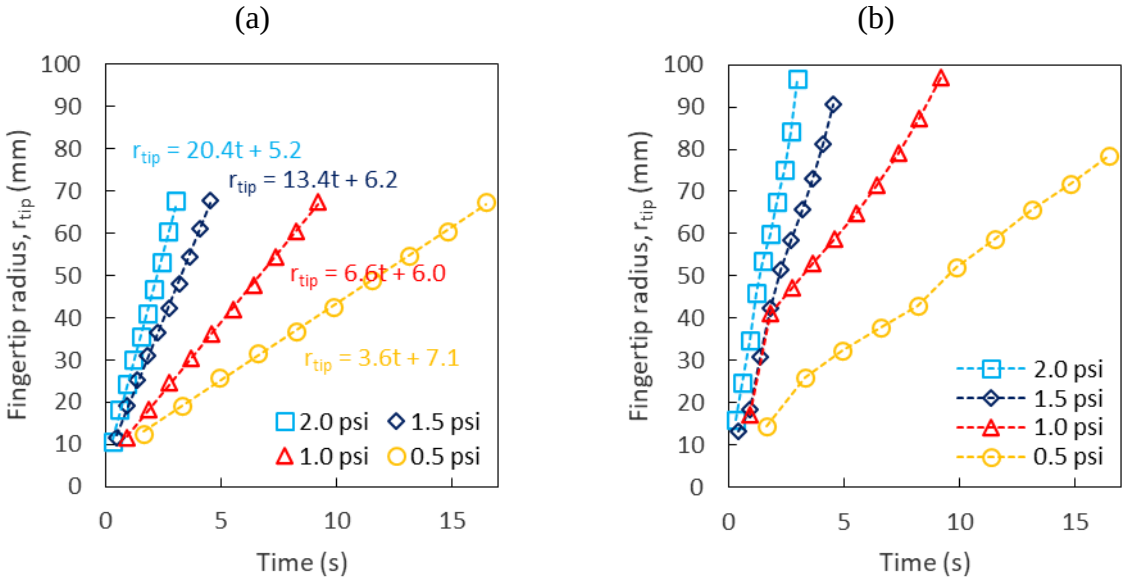

Figure 5.9. Fingertip radius r_{tip} as a function of time for (a) air displacing mineral oil and (b) air displacing water and mineral oil. Fitting lines and equations are shown only for (a).

In Figure 5.9(b), a markedly different pattern is observed in the growth of fingertip radius when air displaces both water and mineral oil. One notable distinction is that the fingertip radius r_{tip} propagated a greater distance than when air displaced only mineral oil. In addition, Figure 5.9(b)

shows a discontinuity in fingertip velocities. Initially, during the displacement of water by air, the fingertip moves faster. However, as air encounters mineral oil and displaces it, the fingertip velocity decreases. The fingertip velocities determined from the fitting lines are presented in Table 5.1.

Table 5.1. Fingertip velocities at different air injection pressures for air displacing mineral oil and air displacing water and mineral oil.

Pressure (psi)	Air displacing mineral oil	Air displacing water and mineral oil	
	$v_{tip}\ in\ mineral\ oil$ (mm/s)	$v_{tip}\ in\ water$ (mm/s)	$v_{tip}\ in\ mineral\ oil$ (mm/s)
0.5	3.6	6.9	4.1
1.0	6.6	26.1	7.7
1.5	13.4	22.0	17.2
2.0	20.4	31.4	27.2

Figure 5.10 depicts finger area (FA) as a function of time for (a) air displacing mineral oil and (b) air displacing water and mineral oil. As shown in Figure 5.9(a), the finger area is proportional to the power of time with the exponent of approximately 1.4.

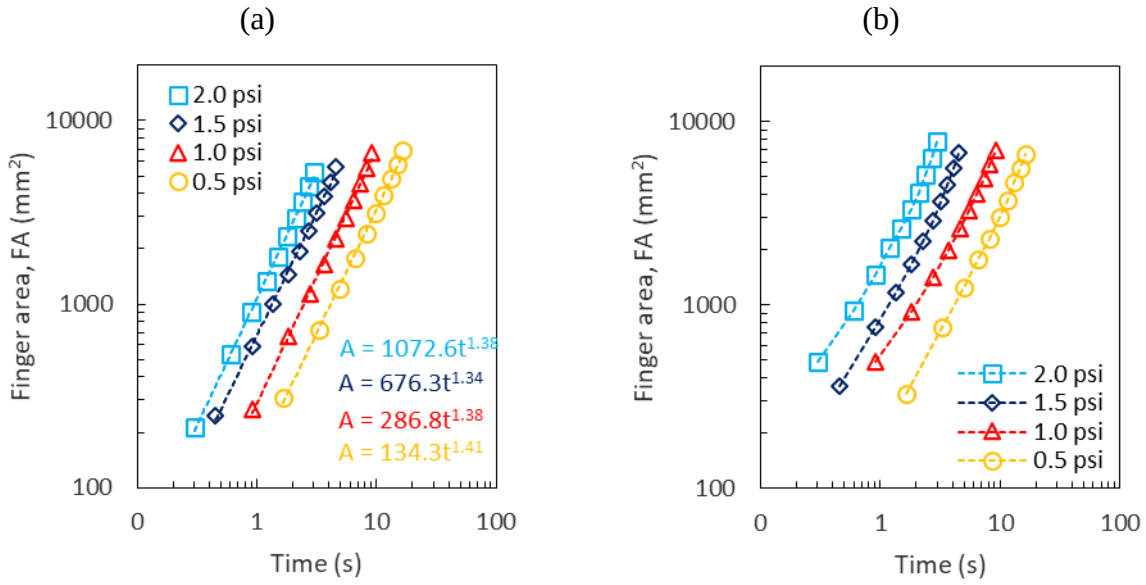

Figure 5.10. Finger area (FA) versus time as a function of time for (a) air displacing mineral oil and (b) air displacing water and mineral oil. Fitting lines and equations are shown only for (a).

As shown in Figure 5.10, there is no noticeable difference in FA between air displacing mineral oil and air displacing water and mineral oil at an air injection pressure of 0.5 psi. However, a noticeable initial increase in FA is observed at other pressures of 1.0, 1.5, and 2.0 psi for air displacing water and mineral oil. Additionally, air displacing water and mineral oil at 1.5 and 2.0 psi exhibits an increase in FA in the later stages as well.

5.3 Conclusions

The effects of water in viscous fingering instabilities of air displacing mineral oil and air displacing water surrounded by mineral oil in a radial Hele-Shaw cell was examined. For the second set of experiments, the displaced fluids consisted of a small volume of water, about 5

percent of the volume of mineral oil, at the center, surrounded by mineral oil. The reference cases contained the same volume of mineral oil without water. Air was injected at four different constant pressures ranging from 0.5 to 2.0 psi (3.45 to 13.79 kPa) to displace mineral oil or water/mineral oil. The fingering patterns resulting from air displacing both water and mineral oil were compared with the fingering patterns observed when air displaces only mineral oil. The evolution of the VF interface, with air displacing only mineral oil, exhibited a typical immiscible radial VF pattern in which the initial fingers spread out and transform into a fan shape, with some of these fingers splitting. The presence of a small volume of water led to significantly different fingering patterns. In the water, a less unstable interface between air and water was observed until the point at which air contacts the mineral oil. Upon contacting the mineral oil, the air began to propagate along the boundary between water and mineral oil resulting in the development of more intricate fingering patterns. At some locations, it was observed that air passed through water via narrow channels instead of spreading along the water-mineral oil boundary. Another notable distinction is that the fingertip radius propagates a greater distance than when air displaced only mineral oil. In addition, the fingertip moved faster with the presence of water displaying a discontinuity in fingertip velocities across the water and mineral oil regions. At low air injection pressure of 0.5 psi, there was no noticeable difference in finger area (FA) between air displacing mineral oil and air displacing water and mineral oil. However, a noticeable initial increase in FA was observed at pressures of 1.0, 1.5, and 2.0 psi for air displacing water and mineral oil. Additionally, an increase in FA was observed in the later stages as well at 1.5 and 2.0 psi. As a result, a more volume of air was injected when water was present, compared to the cases without water.

Chapter Six: Instability of parallel flow of two immiscible liquids in a pore and application to Steam-Assisted Gravity Drainage

The instability at the interface between two parallel flows of immiscible liquids through a uniform planar pore is studied by using linear stability analysis. A characteristic equation determines the growth rate versus wavenumber and instability conditions are determined. The instability is governed by a dimensionless group relating the ratio of gravity to interfacial tension. Interfacial tension has a stabilizing effect resisting the destabilizing gravitational force, limiting the range of wavelengths of unstable disturbances to be longer than a minimum critical wavelength. Application to flow of steam condensate and mobilized bitumen in the Steam-Assisted Gravity Drainage (SAGD) process shows that the instability is possible only over a specific range of temperatures given the densities of the steam condensate and oil in the reservoir. This instability may help in forming an emulsion which could help support oil drainage if the oil is hosted by the more mobile water phase.

Steam-Assisted Gravity Drainage (SAGD) is the most used recovery process for oil sands reservoirs. In this method, displayed schematically in Figure 6.1, steam injected into an upper horizontal well releases its latent heat to the cold bitumen at the edge of the depletion chamber which is then mobilized (its viscosity falls by about five orders of magnitude) and drains under the action of gravity to the production well at the base of the steam chamber. The key challenge faced by SAGD is in its thermal efficiency – heat transfer at the edge of the steam chamber – as yet this has not been fully resolved. The greater the thermal efficiency, the lower the

environmental emissions intensity as well as the lower the costs per unit volume bitumen produced.

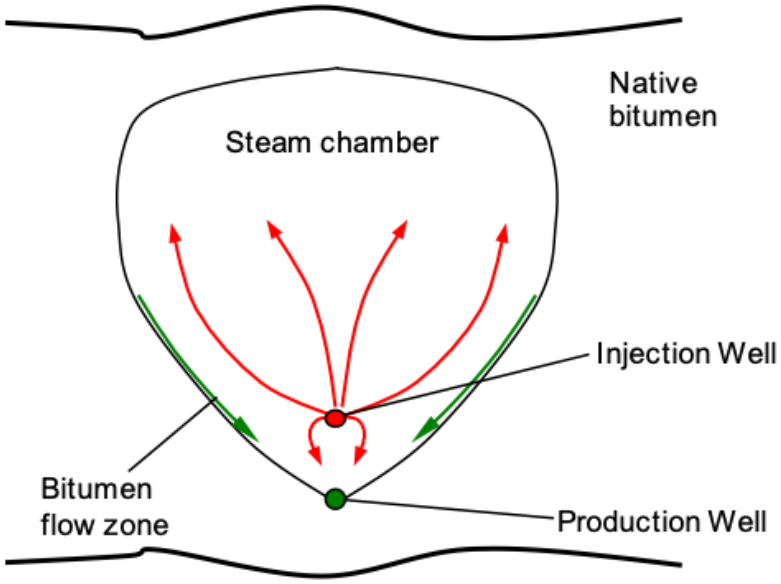

Figure 6.1. Cross-section schematic of the Steam-Assisted Gravity Drainage (SAGD) process.

6.1 Method

In a two-phase system, each fluid, as it flows in the porous medium, interferes with the flow of the other fluid [99]. For example, one fluid may flow through gaps between sands which are covered with a wetting phase fluid. It is also possible that one fluid displaces another fluid through a pore channel. In some cases, one fluid may plug some pore channels if the pressure gradient is insufficient to overcome the adverse capillary force acting on the interface. Another possible flow of two fluids is the parallel flow through a pore channel, under gravity drainage, which is depicted in Figure 6.2. In this figure, the two fluids of different densities, viscosities, and effective permeabilities flow parallel to each other with different velocities through a pore

channel; in the base case, the two fluids are separated by a flat interface. In oil sands reservoirs, the sands tend to be rounded with generally high aspect ratio channel-like pores with intersections between multiple grains [100].

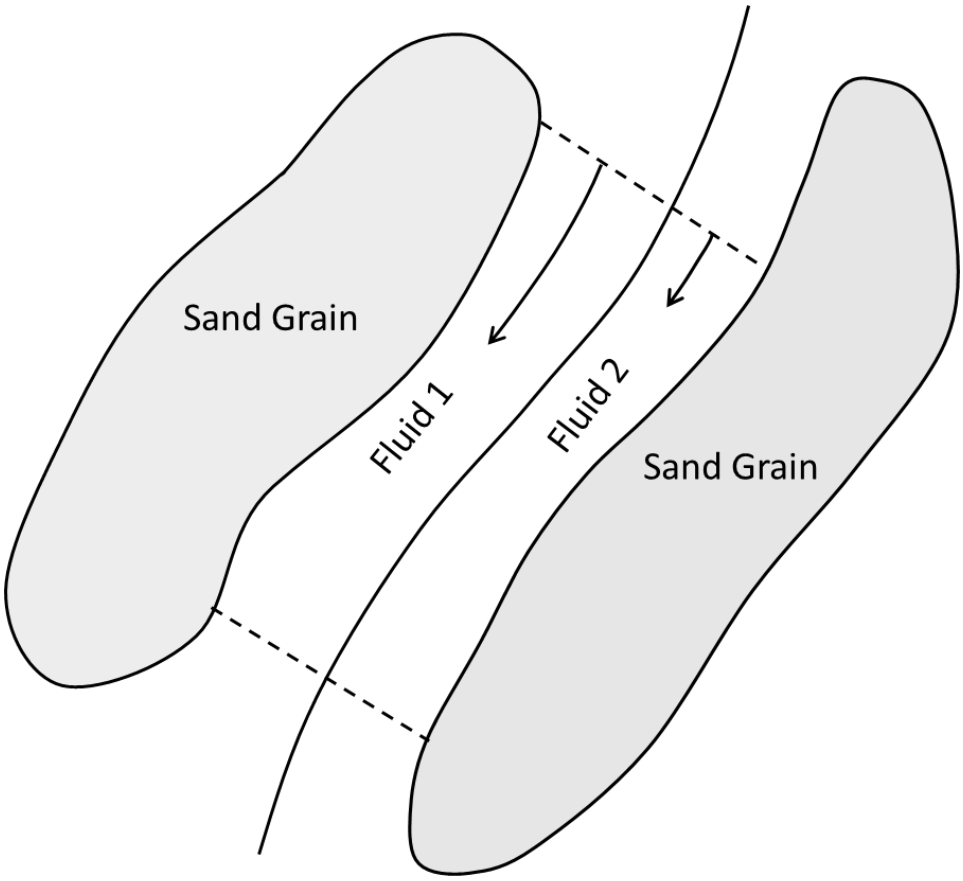

Figure 6.2. Schematic of the parallel flow of two fluids of different densities, viscosities, and effective permeabilities flowing through pore space with different velocities.

Figure 6.3 shows a simple two-dimensional model for the parallel flow of two fluids under gravity drainage through a gap between sands shown in Figure 6.2. This model can also be used to represent a macroscopic parallel flow in porous media. In this case, there is a transition zone of steep saturation gradients of the two fluids between two parallel flows, and this transition zone is replaced by a sharp, planar, macroscopic interface in the model [32].

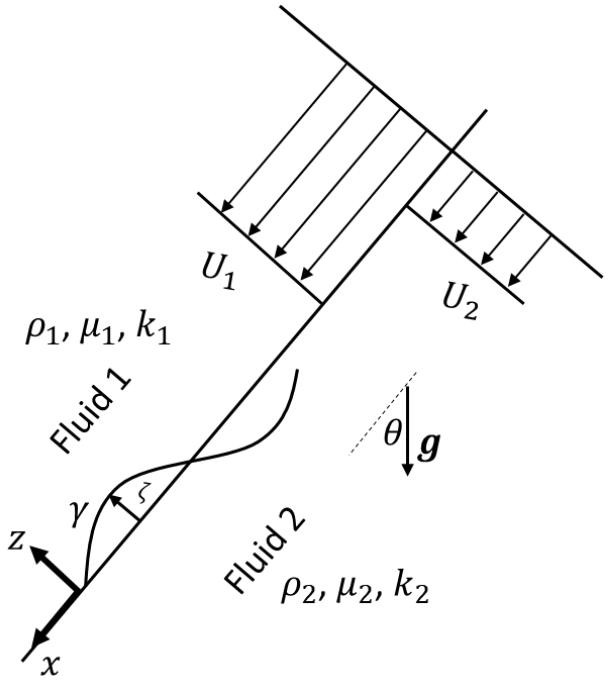

Figure 6.3. Schematic of the parallel flow of two fluids of different velocities U_1 and U_2, densities ρ_1 and ρ_2, viscosities μ_1 and μ_2, and effective permeabilities k_1 and k_2; the x-axis is at an angle θ to the gravitational acceleration **g**, the interfacial tension is γ, and the sinusoidal perturbation of the interface is $\zeta(x,t)$.

The parallel flow of two fluids of different velocities U_1 and U_2 along the positive x-direction is shown in Figure 6.3. The two fluids have different densities ρ_1 and ρ_2, viscosities μ_1 and μ_2, effective permeabilities k_1 and k_2. The gravitational acceleration **g** is at an angle θ to the x-axis, and the interfacial tension between two fluids is γ. The unperturbed interface at a base state is on the x-axis with $\zeta = 0$. In the following analysis, the following assumptions have been made:

1. base state velocities U_1 and U_2 are constant and uniform,
2. effective permeabilities k_1 and k_2 are constant and uniform,
3. flows are irrotational,
4. porous media is uniform, homogeneous, and isotropic,

5. fluids are immiscible, incompressible, and Newtonian,
6. perturbation banishes at z $= \pm\infty$, and
7. sand walls are not considered.

The governing equations are Darcy's law with the Boussinesq approximation and the continuity equation. A perturbation velocity can be obtained by subtracting a base state velocity from a perturbed state velocity and can be written as a velocity potential as follows:

$$\bar{v}_1 = -grad\left\{\frac{\kappa_1}{\mu_1}\left(p_1 + \frac{\mu_1}{\kappa_1}U_1 x - \rho_1 g\cos(\theta)\,x + \rho_1 g\sin(\theta)\,z\right)\right\} = grad\;\phi_1 \qquad (6.1a)$$

$$\bar{v}_2 = -grad\left\{\frac{\kappa_2}{\mu_2}\left(p_2 + \frac{\mu_2}{\kappa_2}U_2 x - \rho_2 g\cos(\theta)\,x + \rho_2 g\sin(\theta)\,z\right)\right\} = grad\;\phi_2 \qquad (6.1b)$$

where $\bar{v}_1$ and $\bar{v}_2$ are perturbation velocities, ϕ_1 and ϕ_2 are velocity potentials, and p_1 and p_2 are the phase pressures for fluid 1 and fluid 2, respectively. Integrating both sides and solving for the pressures gives

$$p_1 = -\frac{\mu_1}{\kappa_1}\phi_1 - \frac{\mu_1}{\kappa_1}U_1 x + \rho_1 g\cos(\theta)\,x - \rho_1 g\sin(\theta)\,z + P_1(t) \qquad (6.2a)$$

$$p_2 = -\frac{\mu_2}{\kappa_2}\phi_2 - \frac{\mu_2}{\kappa_2}U_2 x + \rho_2 g\cos(\theta)\,x - \rho_2 g\sin(\theta)\,z + P_2(t). \qquad (6.2b)$$

In the above equations, p_1 and p_2 represents the total phase pressures which includes the base state pressure and perturbation pressure. However, each velocity potential is only for each perturbation velocity. Substituting the velocity potential into the continuity equation gives the Laplace equation:

$$div\;\bar{\boldsymbol{v}} = 0 \qquad (6.3a)$$

$$\nabla^2\phi_1 = 0 \qquad (6.3b)$$

$$\nabla^2 \phi_2 = 0. \tag{6.3c}$$

In this study, the effects of sand walls are not considered, and it is assumed that the perturbation vanishes far from the interface:

$$\phi_1 \to 0 \text{ as } z \to +\infty \tag{6.4a}$$

$$\phi_2 \to 0 \text{ as } z \to -\infty. \tag{6.4b}$$

The kinematic boundary condition at the interface is that a fluid particle at the interface moves with the interface and never leaves the interface [101]. In this system, the interface equation which gives 0 on the interface is

$$F(x, z, t) = z - \zeta(x, t). \tag{6.5a}$$

The total derivative of the interface equation is 0 at the interface:

$$\frac{DF}{Dt} = 0 \text{ at } z = \zeta. \tag{6.5b}$$

Removing non-linear terms gives the kinematic boundary conditions:

$$\frac{\partial \zeta}{\partial t} = -U_1 \frac{\partial \zeta}{\partial x} + \frac{\partial \phi_1}{\partial z} \text{ at } z = \zeta \tag{6.5c}$$

$$\frac{\partial \zeta}{\partial t} = -U_2 \frac{\partial \zeta}{\partial x} + \frac{\partial \phi_2}{\partial z} \text{ at } z = \zeta. \tag{6.5d}$$

The dynamic boundary condition at the interface is the pressure difference through the interface due to the interfacial tension:

$$(p_1 - p_2) = \gamma c + P_c(t) \text{ at } z = \zeta \tag{6.6a}$$

$$c \cong \frac{\partial^2 \zeta}{\partial \mathrm{x}^2} \tag{6.6b}$$

where γ is the interface tension, and c is the curvature which is negative when the center of curvature is in fluid 2. $P_c(t)$ is added to the pressure difference because there are physical conditions which can cause a pressure difference other than that arising from the curvature of the interface. The perturbations can be decomposed into fundamental Fourier perturbation modes and each mode can be investigated separately. Fourier perturbation modes are assumed to be in the following forms:

$$\zeta = \hat{\zeta} e^{i\alpha(x-ct)} \tag{6.7a}$$

$$\phi_1 = \hat{\phi}_1 e^{i\alpha(x-ct)} \tag{6.7b}$$

$$\phi_2 = \hat{\phi}_2 e^{i\alpha(x-ct)} \tag{6.7c}$$

where α is the wavenumber, and c is the complex speed. The behaviors of perturbations are to be examined for all possible wavenumbers once the eigenvalue relation $c(\alpha)$ is determined. The temporal growth rate σ_r is obtained by multiplying the imaginary part of c by the wavenumber α:

$$c = c_r + c_i i \tag{6.7d}$$

$$e^{i\alpha(x-ct)} = e^{\alpha c_i t} e^{i\alpha(x-c_r t)} \tag{6.7e}$$

$$\sigma_r = \alpha c_i. \tag{6.7f}$$

From the Laplace equation (3b) and (3c) and the boundary condition (4a) and (4b), $\hat{\phi}_1$ and $\hat{\phi}_2$ are

$$\hat{\phi}_1 = A e^{-\alpha z} \tag{6.8a}$$

$$\hat{\phi}_2 = B e^{\alpha z}. \tag{6.8b}$$

From the kinematic boundary conditions (5c) and (5d), the constants A and B become

$$A = -i(U_1 - c)\hat{\zeta} \tag{6.8c}$$

$$B = i(U_2 - c)\hat{\zeta}. \tag{6.8d}$$

Combining (2a) and (2b) with (6a) gives

$$\begin{aligned} -\frac{\mu_1}{\kappa_1}(\phi_1)_{z=\zeta} + \frac{\mu_2}{\kappa_2}(\phi_2)_{z=\zeta} - \frac{\mu_1}{\kappa_1}U_1 x + \frac{\mu_2}{\kappa_2}U_2 x + \rho_1 g\cos(\theta)\, x \\ - \rho_2 g\cos(\theta)\, x - \rho_1 g\sin(\theta)\,\zeta + \rho_2 g\sin(\theta)\,\zeta + P_1(t) \\ - P_2(t) = P_c(t) + \gamma\frac{\partial^2\zeta}{\partial \mathrm{x}^2}. \end{aligned} \tag{6.9a}$$

At the onset of the instability, ζ is very close to 0. The conditions at $z = \zeta$ can be evaluated at $z = 0$ by linearization using the Taylor series at 0 and neglecting quadratic terms. For $\zeta = 0$, (9a) becomes

$$-\frac{\mu_1}{\kappa_1}U_1 x + \frac{\mu_2}{\kappa_2}U_2 x + \rho_1 g\cos(\theta)\, x - \rho_2 g\cos(\theta)\, x + P_1(t) - P_2(t) = P_c(t). \tag{6.9b}$$

Equation (9b) leads to the following eigenvalue relation $c(\alpha)$:

$$-i(U_1 - c)\frac{\mu_1}{\kappa_1} - i(U_2 - c)\frac{\mu_2}{\kappa_2} + \rho_1 g\sin(\theta) - \rho_2 g\sin(\theta) - \gamma\alpha^2 = 0. \tag{6.10a}$$

Solving for c gives:

$$\begin{aligned} c = \left(\frac{\mu_1}{\kappa_1} + \frac{\mu_2}{\kappa_2}\right)^{-1}\left(U_1\frac{\mu_1}{\kappa_1} + U_2\frac{\mu_2}{\kappa_2}\right) \\ + \left(\frac{\mu_1}{\kappa_1} + \frac{\mu_2}{\kappa_2}\right)^{-1}\left((\rho_1 - \rho_2)g\sin(\theta) - \gamma\alpha^2\right)i. \end{aligned} \tag{6.10b}$$

The real part of c is the phase velocity of the perturbation waves:

$$c_r = \left(\frac{\mu_1}{\kappa_1} + \frac{\mu_2}{\kappa_2}\right)^{-1}\left(U_1\frac{\mu_1}{\kappa_1} + U_2\frac{\mu_2}{\kappa_2}\right). \tag{6.10c}$$

The temporal growth rate of the perturbation waves is:

$$\sigma_r = \alpha c_i = \left(\frac{\mu_1}{\kappa_1} + \frac{\mu_2}{\kappa_2}\right)^{-1} [(\rho_1 - \rho_2) g \sin(\theta)\, \alpha - \gamma \alpha^3]. \quad (6.10d)$$

Using the permeability of a Hele-Shaw cell and gravity at right angles, the phase velocity (10c) and the temporal growth rate (10d) become the same as those in Gondret and Rabaud [69]. Also, the growth rate (10d) is the same as the one for an interface between two immiscible fluids in a base state of no motion in Sharma and Gates [62]. This shows that imposed tangential velocities do not affect the growth rate of the perturbed interface between two immiscible fluids in porous media according to the first-order theory derived here [32]. The perturbation modes are unstable and growing if the growth rate σ_r is positive for some wavenumbers. In other words, the interface is unstable and growing to the disturbances of those wavenumbers. The instability condition that makes σ_r positive is:

$$\frac{(\rho_1 - \rho_2) g \sin(\theta)}{\gamma} > \alpha^2. \quad (6.11a)$$

Eq. (11a) can be rewritten using the wavelength $\lambda = 2\pi / \alpha$:

$$\frac{(\rho_1 - \rho_2) g \sin(\theta)\, \lambda^2}{4\pi^2 \gamma} > 1. \quad (6.11b)$$

Eq. (11b) shows that the instability happens only when top fluid is heavier than bottom fluid and is governed by the dimensionless group which is the ratio of gravitational force to interfacial tension. The interfacial tension has a stabilizing effect resisting the gravitational force, and it limits the range of the wavenumber of unstable disturbances to be less than a maximum critical wavenumber. The maximum critical wavenumber is:

$$\alpha_c = \sqrt{\frac{(\rho_1 - \rho_2) g \sin(\theta)}{\gamma}}. \quad (6.11c)$$

In other words, the wavelength of unstable disturbances must be longer than the minimum critical wavelength:

$$\lambda_c = \frac{2\pi}{\alpha_c} = 2\pi\sqrt{\frac{\gamma}{(\rho_1 - \rho_2)g\sin(\theta)}}. \quad (6.11d)$$

The maximum growth rate occurs at

$$\alpha_m = \frac{\alpha_c}{\sqrt{3}} \quad (6.11e)$$

$$\lambda_m = \sqrt{3}\lambda_c. \quad (6.11f)$$

6.2 Results and Discussion

In this section, the instability conditions are applied to two types of parallel flows of steam condensate and mobilized bitumen in a pore during the Steam-Assisted Gravity Drainage (SAGD) process for recovering bitumen from an oil sands reservoir.

6.2.1 Steam condensate above and mobilized bitumen below

As shown in the instability condition (11a), the interface becomes unstable only when the top fluid is heavier than the bottom fluid. In this case, the density of steam condensate needs to be higher than the density of mobilized bitumen to have an unstable interface. As shown in Figure 6.4, the bitumen density can be higher or lower than that of steam condensate depending on the temperature [61]. For example, at 120°C, the density of 14°API oil is 910.02 kg/m^3, which is less than the density of steam condensate, 944.58 kg/m^3; however, at 220°C, the density of the oil,

851.44 kg/m^3 is greater than the density of steam condensate, 839.34 kg/m^3. This means that the stability of the interface in this system can change depending on the temperature. In the area below the density line of saturated water, the density of bitumen is lower than that of steam condensate, and in the area above it, the density of bitumen is higher. As a result, the interface is stable in the upper area, and it is unstable in the lower area.

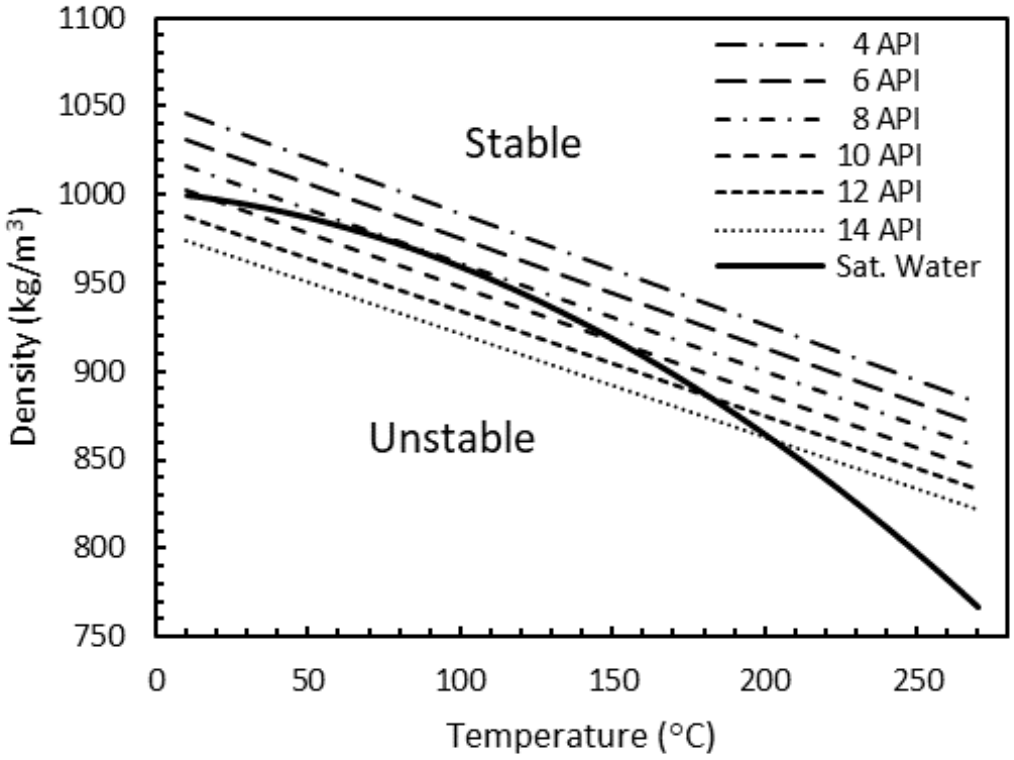

Figure 6.4. Density of oils and saturated water versus temperature; the stable/unstable regions are for the parallel flow of steam condensate above and mobilized bitumen below.

Figure 6.5 displays the growth rate versus wavenumber for different API gravities at 120°C. As shown in Eq. (7e) and (7f), the growth rate determines how fast a perturbation grows. If the

growth rate is greater than 0 at some wavenumber, any disturbance with that wavenumber on the interface grows exponentially. However, disturbances with negative growth rates shrink and disappear. The 4, 6, and 8°API oils, which are denser than water, have negative growth rates for all possible wavenumbers, which means that the interface is stable to any disturbance. On the other hand, the 10, 12, and 14°API oils, which are less dense than water, have positive growth rates over a range of wavenumbers. In these cases, the interface becomes unstable to disturbances of these wavenumbers. The range of unstable wavenumbers from 0 to the maximum wavenumber increases as the difference in density increases. The maximum growth rate also increases as the density difference rises. For 14°API oil, the minimum critical wavelength is 2.22 cm, and the maximum growth rate is 3.11×10^{-7} s^{-1} which happens at the wavelength of 3.85 cm. The time and length scales of the growth of unstable disturbances can be estimated by the growth rate and the minimum wavelength respectively. In the SAGD process, the greater the growth rate of the disturbance implies higher steam chamber expansion rate which implies larger oil production rate [62]; this implies that the instability, at pore scale, is beneficial and desired in the process. Furthermore, the instability at the steam-chamber edge can enhance heat transfer by developing a finger-shaped interface that enlarges the heat-transfer area [63]. This is consistent with the findings of Azom and Srinivasan [102] and Ezeuko et al. [103]. The operating saturation pressure (and consequent temperature) can be chosen to maximize the instability to maximally enhance the instability so as to obtain maximize SAGD performance.

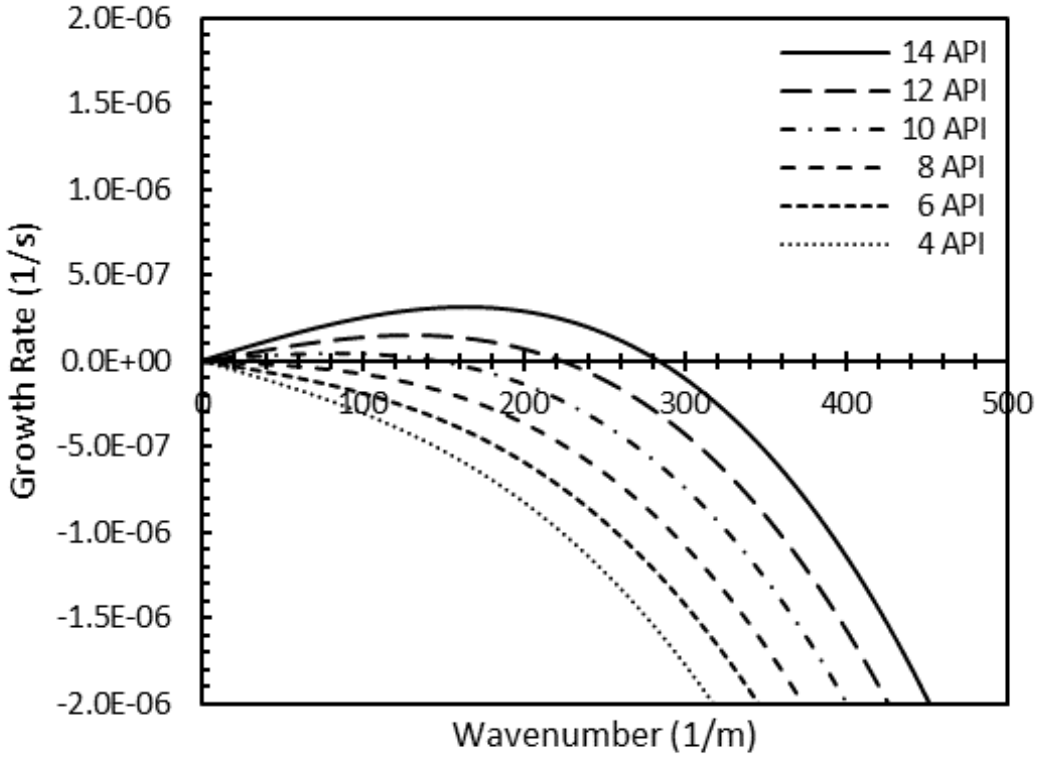

Figure 6.5. Growth rate σ_r versus wave number α versus API gravity at $T = 120$°C for the parallel flow of steam condensate above and mobilized bitumen below.

Figure 6.6 displays the growth rate versus wavenumber for different API gravities at 220°C. The results show that the growth rates are all negative for all wavenumbers. In other words, the interfaces are stable for all the disturbances. This is because all the 4 to 14°API oils are denser than saturated water at this temperature.

Figure 6.7 displays the growth rate versus wavenumber for different interfacial tensions from 1 to 6 mN/m at 120°C and 14°API. As shown in Eq. (11a) and (11b), interfacial tension stabilizes a disturbance on the interface by resisting the gravitational force acting on the fluid in the

disturbance. Larger interfacial tension can counteract a greater amount of denser fluid in a longer wavelength perturbation. On the other hand, smaller interfacial tension can resist a lower amount of denser fluid in a shorter wavelength perturbation from falling into the lower less dense fluid. As a result, the interfacial tension limits the range of the wavenumber of unstable disturbances to be less than a maximum critical wavenumber. In other words, it limits unstable disturbances to be longer than the minimum critical wavelength. As shown in Figure 6.7, the range of unstable wavenumbers increases as the interface tension decreases. For example, the critical minimum wavelength decreases from 2.22 to 1.28 cm when the interfacial tension decreases from 3 to 1 mN/m.

Figure 6.8 displays the growth rate versus wavenumber for different oil viscosities from 20 cP to 70 cP at 120°C and 14°API. As the oil viscosity decreases, the growth rate increases while the range of unstable wavenumbers remains unchanged. Eq. (10d) shows that the effects of the viscosities of two fluids add together and affect only the magnitude of the growth rate.

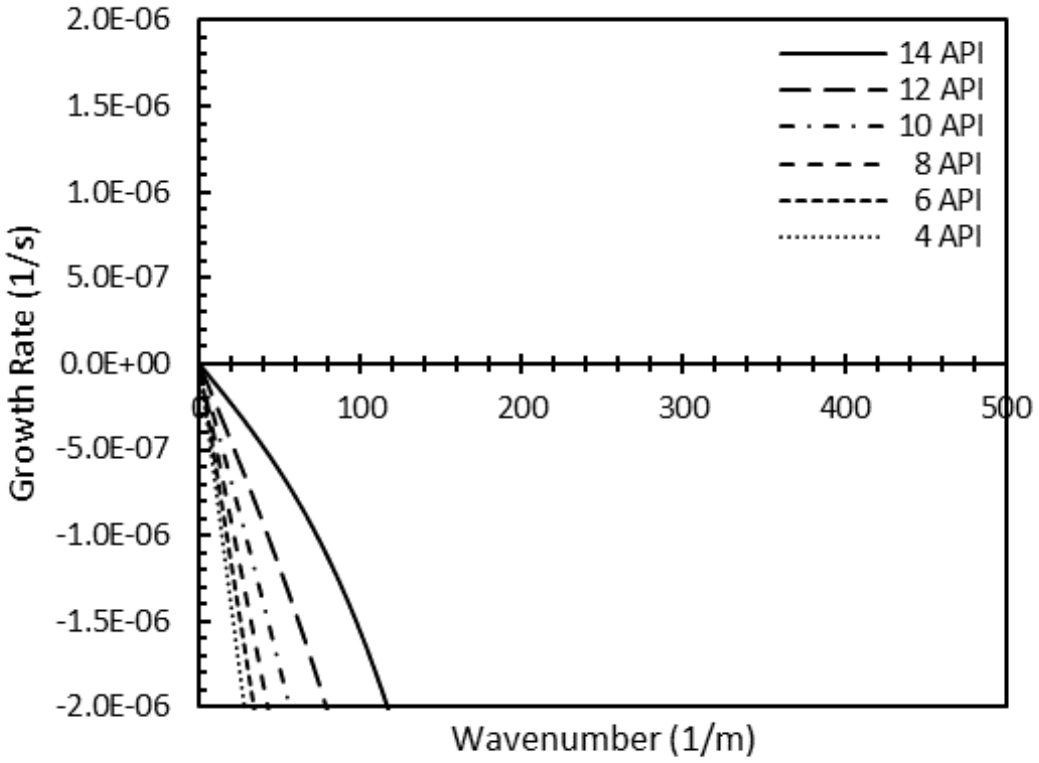

Figure 6.6. Growth rate σ_r versus wave number α versus API gravity at $T = 220$°C for the parallel flow of steam condensate above and mobilized bitumen below.

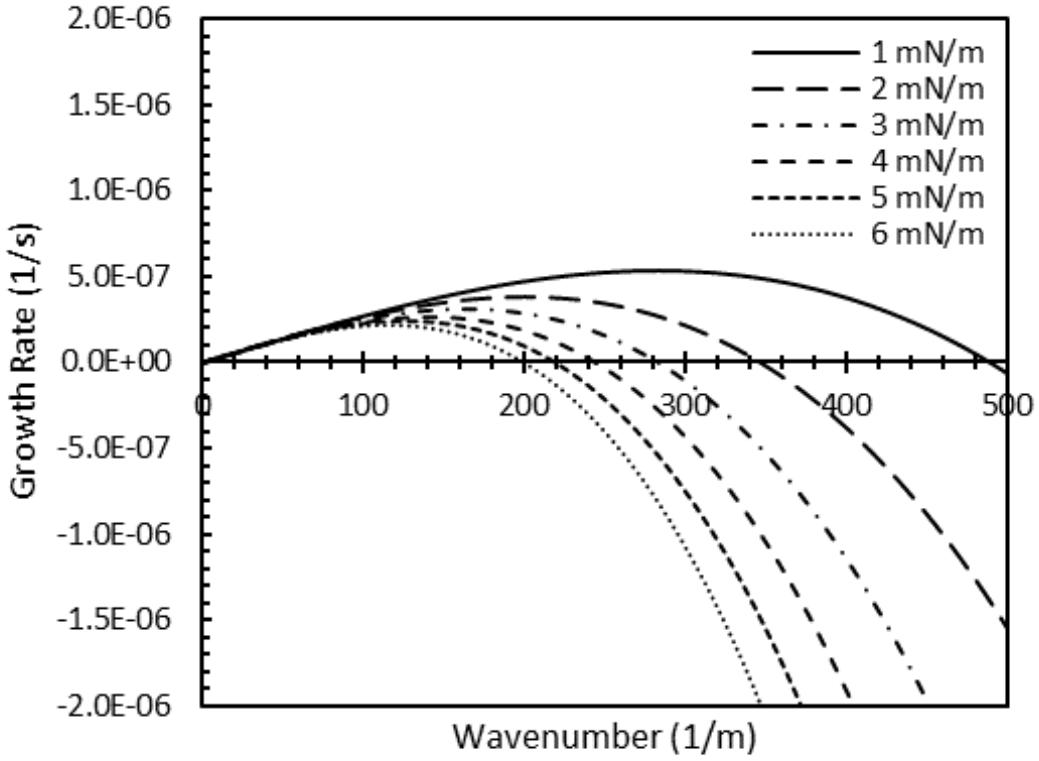

Figure 6.7. Growth rate σ_r versus wave number α versus interfacial tension at $T = 120$°C and 14°API for the parallel flow of steam condensate above and mobilized bitumen below.

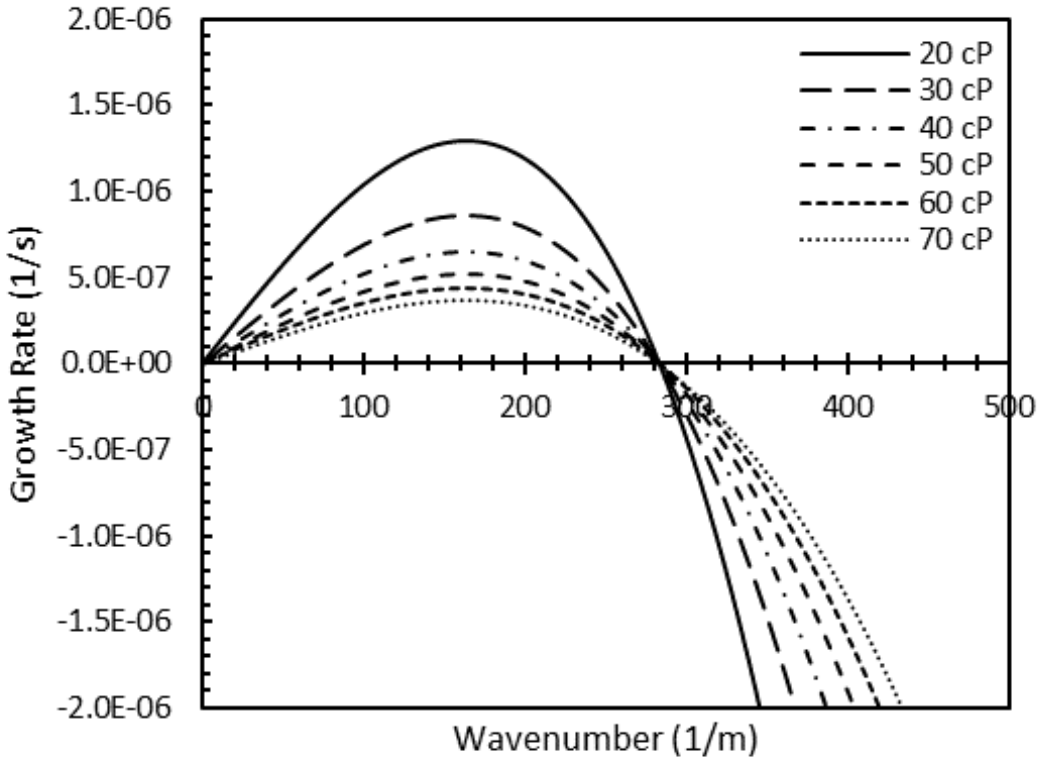

Figure 6.8. Growth rate σ_r versus wave number α versus oil viscosity at $T = 120$°C and 14°API for the parallel flow of steam condensate above and mobilized bitumen below.

Figure 6.9 displays the maximum growth rate versus temperature for the parallel flow of steam condensate above and mobilized bitumen below. The instability of the interface becomes maximum at T=124°C at the wavenumber of 78.7 m^{-1} for 10°API. At this temperature, it is expected that disturbances of the steam condensate-10°API bitumen interface grows at a maximum growth rate. This indicates that SAGD operating at this temperature can have benefits of the unstable interface such as enhanced heat transfer. However, most SAGD operations occur at between 200 and 230°C and thus, the steam condensate-10°API bitumen interface is stable because the steam condensate above is lighter than 10°API bitumen below at this temperature

range. 14°API bitumen shows more unstable interface with a maximum growth rate of 5.83×10^{-7} s^{-1} at T=158°C. However, the interface is stable at T=215°C for 10, 12, and 14°API bitumen.

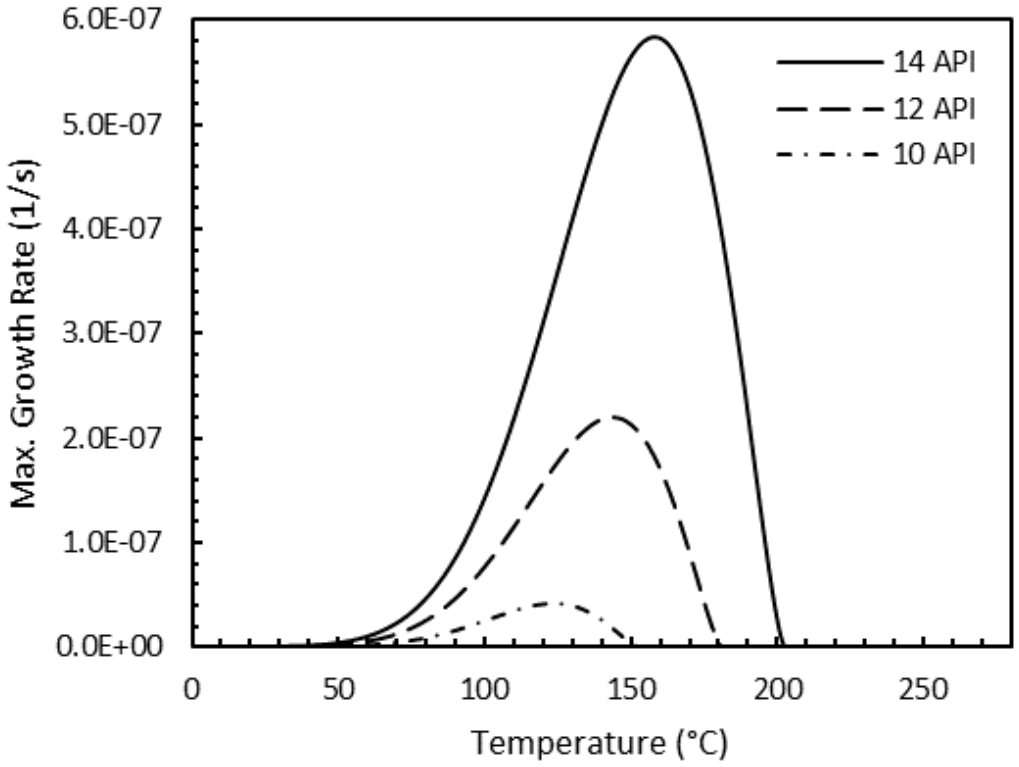

Figure 6.9. Maximum growth rate σ_r versus temperature for the parallel flow of steam condensate above and mobilized bitumen below.

6.2.2 Mobilized bitumen above and steam condensate below

In the case of the parallel flow of mobilized bitumen above and steam condensate below, the interface is stable in the lower area below the density line of saturated water, and the interface is unstable in the area above it. Figure 6.10 displays the growth rate versus wavenumber for

different API gravities at 120°C. 4, 6, and 8°API oils, which are denser than water, show positive growth rates over a range of wavenumbers. Figure 6.11 displays the growth rate versus wavenumber for different API gravities at 220°C. All the oils are heavier than steam condensate at this temperature, and all of them show positive growth rates over a range of wavenumbers.

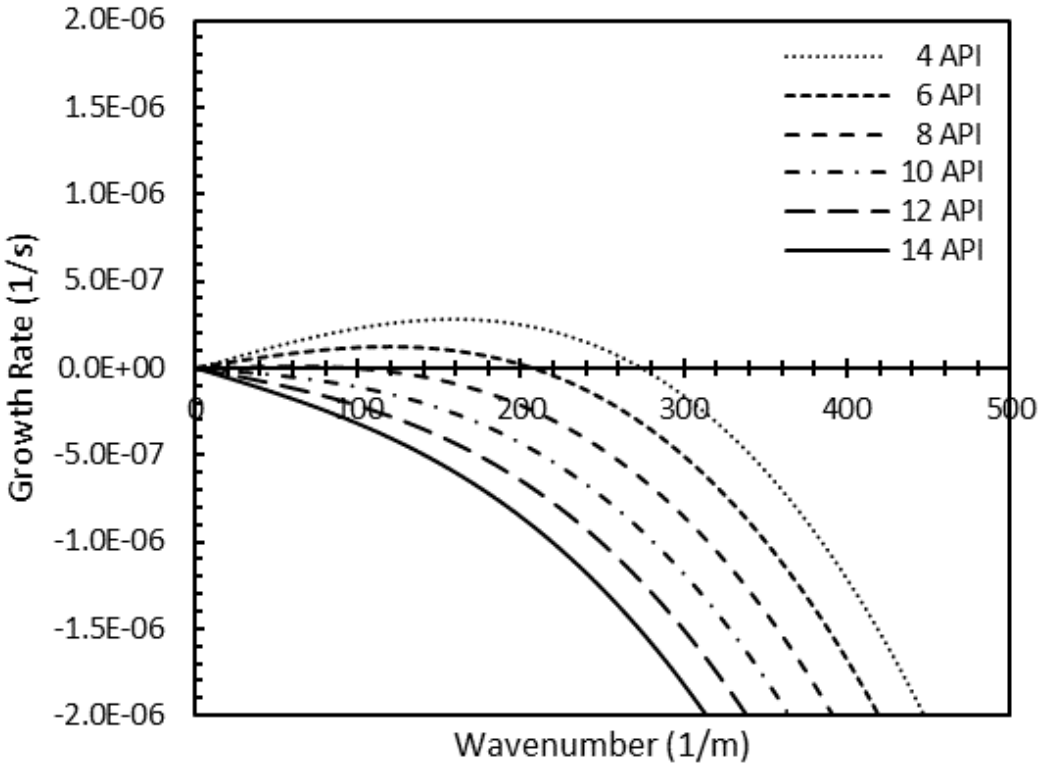

Figure 6.10. Growth rate σ_r versus wave number α versus API gravity at $T = 120℃$ for the parallel flow of mobilized bitumen above and steam condensate below.

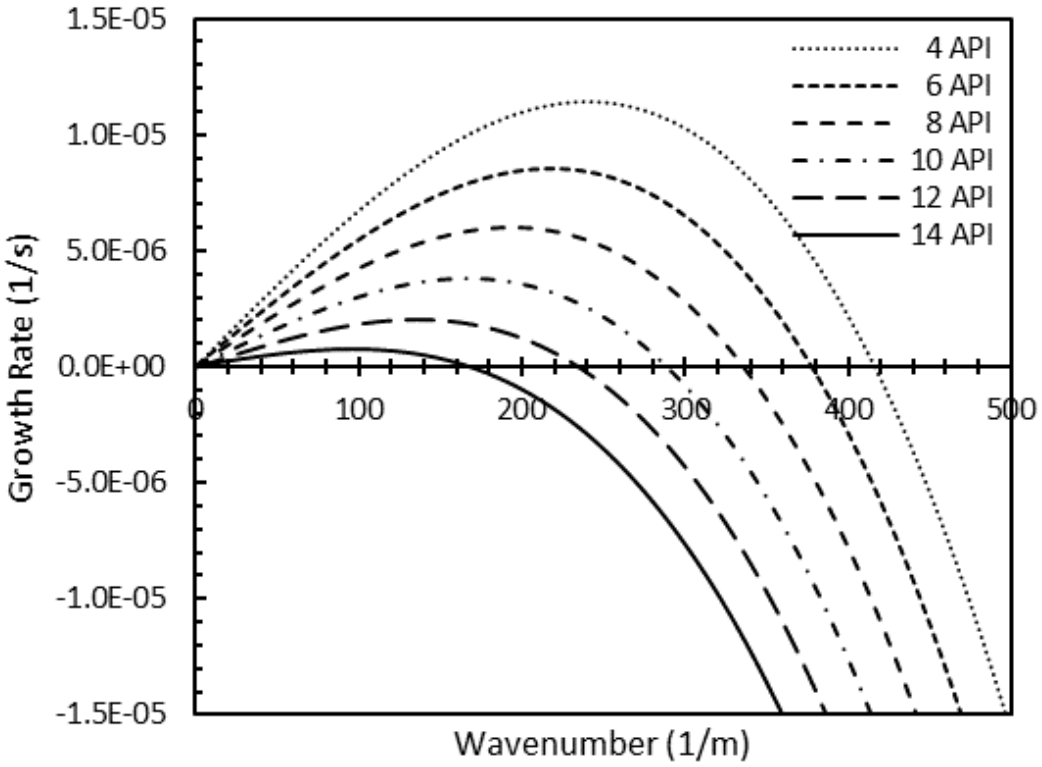

Figure 6.11. Growth rate σ_r versus wave number α versus API gravity at $T = 220℃$ for the parallel flow of mobilized bitumen above and steam condensate below.

Figure 6.12 displays the maximum growth rate versus temperature for the parallel flow of mobilized bitumen above and steam condensate below. For 10°API bitumen, the growth rate gradually increases from 0 starting at T=152.3°C where the two fluids have the same density, and it starts to increase rapidly around T=190°C. This shows that the operating temperature of SAGD needs to be reasonably higher than T=152.3°C to have benefits of the unstable interface such as enhanced heat transfer and emulsion formation for 10°API oil. At typical operating temperature of 200-230°C, the 10°API bitumen-steam condensate interface is quite unstable with a maximum growth rate of 1.42×10^{-6} to 5.80×10^{-6} s^{-1}. For 14°API oil, the interface is less

unstable at this temperature range, and it requires a higher operating temperature to achieve the same level of instability as 10°API oil. This suggests that there is a minimum temperature where instability occurs for the case of bitumen above and steam condensate below.

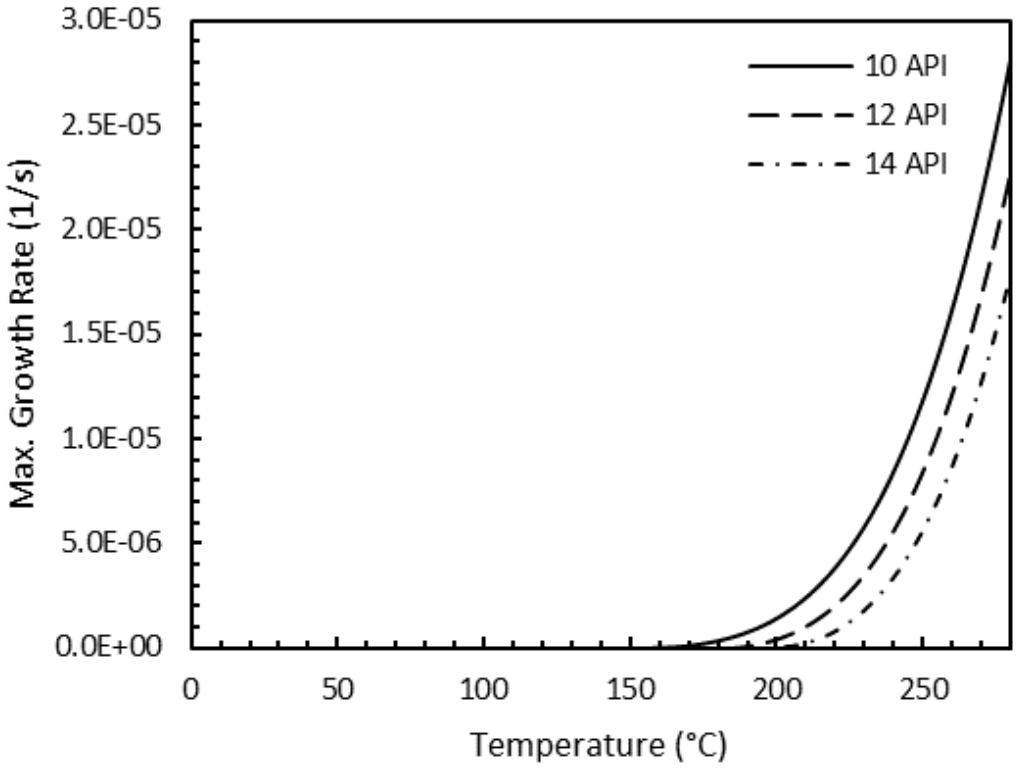

Figure 6.12. Maximum growth rate σ_r versus temperature for the parallel flow of mobilized bitumen above and steam condensate below.

Table 6.1. Reservoir and fluid properties.

Item	Value
Water viscosity, μ_w at 220°C	$1.24 \times 10^{-4}\ Pa\ s$
Water viscosity, μ_w at 120°C	$2.44 \times 10^{-4}\ Pa\ s$
Bitumen viscosity, μ_o at 220°C	$7.16 \times 10^{-3}\ Pa\ s$
Bitumen viscosity, μ_o at 120°C	$83.54 \times 10^{-3}\ Pa\ s$
Water/bitumen interface tension, γ	$3.0 \times 10^{-3}\ N/m$
Effective permeability of bitumen, k_o	$1.0 \times 10^{-12}\ m^2$
Effective permeability of water, k_w	$1.0 \times 10^{-12}\ m^2$
Angle between the base interface and gravity, θ	45°

Note: Interfacial tension of bitumen and water is assumed to be 3 mN/m based on the experiment results from Rajayi and Kantzas [104].

Table 6.2. List of correlations used in this study.

Density of water at saturation pressure[10] ρ_w in kg/m^3, T in °C	$\rho_w = 1001.7 - 0.1616T - 0.00262T^2$
Density of oil in the range of 0 to 15 °API[10] ρ in kg/m^3, T in °C	$\rho_o = \rho_{15}\left[1 - 0.0603\left(\frac{T-15}{100}\right)\right]$ $\rho_{15} = \left(\frac{141.5}{131.5 + °API}\right)(999)$
Viscosity of saturated water[10] T in °C, μ_w in cP	$\mu_w = \left(\frac{969 - T}{25.6T + 405.7}\right)$
Viscosity of Athabasca bitumen[10] T in °C, μ in cP	$\ln\ln(\mu) = -3.5738\ln(T + 273.15) + 22.8379$

6.3 Conclusions

The stability of the interface between two parallel flows of immiscible liquids through a uniform pore was examined by using linear stability analysis. The instability is governed by the dimensionless group governing the ratio of the gravitational force to interfacial tension, and the instability is only possible when the top fluid is denser than the bottom fluid. The results demonstrate that instability is possible only for a certain range of temperature given the densities of the steam condensate and oil in the reservoir. The interfacial tension has a stabilizing effect resisting the destabilizing gravitational force, and it limits the range of the wavenumber of unstable disturbances to be less than a maximum critical wavenumber. The parallel flow of steam condensate and mobilized bitumen in the Steam-Assisted Gravity Drainage (SAGD) process was examined by using the instability conditions. It was found that the stability of the interface can change depending on the temperature because the bitumen density can be higher or lower than that of steam condensate depending on the temperature. It was found that there is a temperature for SAGD where the growth rate becomes maximum for the case of steam condensate above and bitumen below and a minimum temperature where instability occurs for the case of bitumen above and steam condensate below. The results suggest that there is an optimal temperature where in situ oil-in-water emulsions form with consequent enhanced drainage rates.

Chapter Seven: Conclusions and Recommendations

7.1 Conclusions

This work investigated the effects of dilute low molecular weight poly(ethylene oxide) solutions in immiscible radial viscous fingering instabilities, the air invasion into three-dimensional foam inducing viscous fingering instabilities, the viscous fingering instabilities of air displacing water surrounded by mineral oil, and the instability of parallel flow of two immiscible liquids in a pore and application to Steam-Assisted Gravity Drainage.

7.1.1 Effects of dilute low molecular weight poly(ethylene oxide) solutions in immiscible radial viscous fingering instabilities

This research investigated the impact of normal stress differences on the immiscible radial viscous fingering instability within a Hele-Shaw cell. The focus was on elastic effects in dilute, low molecular weight poly(ethylene oxide) (PEO) solutions, excluding shear-thinning behavior. By varying the molecular weight of PEO, the influence of normal stress differences was examined. The experimental findings reveal nonmonotonic and contrasting effects, depending on both the molecular weight of PEO and the stage of radial viscous fingering evolution. Reductions in PEO molecular weight led to a decrease in the number of fingers and an expansion of finger width in the early stage. Conversely, an increase in PEO molecular weight promotes tip splitting and narrows finger width in the early stage but suppresses tip splitting in the intermediate stage. Weissenberg numbers at different stages of radial viscous fingering instabilities were estimated.

Tip splitting was observed at the highest Weissenberg number. Suppression of tip splitting occurred at intermediate Weissenberg numbers. At low Weissenberg numbers, there was an increase in finger width and a reduction in the number of fingers.

7.1.2 Air invasion into three-dimensional foam induces viscous fingering instabilities

The radial displacement flows of immiscible air invading a three-dimensional foam in a Hele-Shaw cell were experimentally explored. This research identified three distinct flow regimes. In the initial regime, characterized by relatively low fingertip velocities, the foam underwent a slow plug flow, with three-phase contact lines slipping at the cell walls. Notably, a proportional relationship between the air injection pressure and the power of the fingertip velocity was identified, fitting well with a power law where the exponent was determined to be 2/3. Transitioning to the second regime, higher velocities resulted in foam displacement as a plug within single layers of foam bubbles. Similar to the first regime, a power law exponent was found. In the third regime, which emerged at higher air injection pressures, air fingers developed through narrow channels, potentially isolating the air fingers as they underwent a "healing" process. Additionally, our results revealed a significant finding that the width of the air fingers exhibited continuous scaling with the air injection pressure, regardless of the flow regimes.

7.1.3 Viscous fingering instabilities of air displacing water surrounded by mineral oil in a radial Hele-Shaw cell

The impact of water on viscous fingering instabilities during the displacement of mineral oil by air in a radial Hele-Shaw cell was experimentally examined. The displaced fluids comprised a small central volume of water surrounded by mineral oil, with air injected at constant pressures to displace both the water and the surrounding mineral oil. The evolution of fingering patterns was compared with reference cases where air displaced only mineral oil, without water. The presence of water resulted in significantly different fingering patterns compared to cases without water. In the water region, a less unstable interface between air and water was observed until the point where air contacted the mineral oil. Upon contact with the mineral oil, the air propagated along the boundary between water and mineral oil, leading to the development of more intricate fingering patterns. Another notable difference was that the fingertip radius extended a greater distance in the presence of water compared to cases where air displaced only mineral oil. Additionally, the fingertip moved at a faster pace in the presence of water, displaying a discontinuity in fingertip velocities across the water and mineral oil regions. Furthermore, a greater volume of air was injected when water was present, in contrast to cases without water.

7.1.4 Instability of parallel flow of two immiscible liquids in a pore and application to Steam-Assisted Gravity Drainage

The instability occurring at the interface between two parallel flows of immiscible liquids passing through a uniform planar pore was investigated using linear stability analysis. A

characteristic equation was employed to determine the growth rate relative to wavenumber, and conditions for instability was established. The governing factor for this instability was a dimensionless group that represents the ratio of gravity to interfacial tension. Interfacial tension played a stabilizing role by counteracting the destabilizing gravitational force, thereby constraining the range of wavelengths of unstable disturbances to be longer than a minimum critical wavelength.

When applied to the flow of steam condensate and mobilized bitumen in the Steam-Assisted Gravity Drainage (SAGD) process, it was revealed that the instability occurs within a specific temperature range, considering the densities of the steam condensate and oil in the reservoir. This instability has the potential to contribute to the formation of an emulsion, which could aid in supporting oil drainage, particularly if the oil is hosted by the more mobile water phase.

7.2 Recommendations

Based on the findings of this research, several recommendations can be proposed for further study on viscous fingering instabilities in a radial Hele-Shaw cell.

- More experiments can be performed to investigate the effects of shear-thinning viscosity on the immiscible radial viscous fingering instability using both low and high molecular weight poly(ethylene oxide) solutions.
- Further exploration of the effects of dilute low molecular weight poly(ethylene oxide) solutions on immiscible radial viscous fingering instabilities can be conducted by

employing these solutions as the displacing fluid, rather than as the displaced existing fluid.

- Liquid-based foam can also be used as a displacing fluid to displace more viscous existing fluid in a radial Hele-Shaw cell.
- Additional experiments can be carried out by adding surfactants into water to reduce the interfacial tension in experiments where air displaces water surrounded by mineral oil.
- The radial Hele-Shaw cell can be improved by using more meticulous fabricating options from a specialty custom glass fabrication company for drilling the injection hole.
- The instability of parallel flow of two immiscible liquids can be experimentally studied by using a vertically configured Hele-Shaw cell.

References

[1] S. Hill, "Channelling in packed columns," *Chemical Engineering Science,* vol. 1, p. 247, 1952.

[2] P. G. Saffman and G. Taylor, "The penetration of a fluid into a porous medium or Hele-Shaw cell containing a more ciscous fluid," *Procedings of the Royal Society A,* vol. 245, p. 312, 1958.

[3] R. L. Slobod, B. H. Caudle, "X-Ray shadowgraph studies of areal sweepout efficiencies," *Society of Petroleum Engineers,* vol. 195, p. 265, 1952.

[4] P. Petitjeans, C.-Y. Chen, E. Meiburg and T. Maxworthy, "Miscible quarter five-spot displacements in a Hele-Shaw cell and the role of role of flow-induced dispersion," *Physics of Fluids,* vol. 11, p. 1705, 1999.

[5] B. H. Caudle and M. D. Witte, "Production potential changes during sweep-out in a five-spot system," *Journal of Petroleum Technology,* vol. 12, p. 63, 1959.

[6] B. Habermann, "The efficiency of miscible displacement as a function of mobility ratio," *Petroleum Transactions,* vol. 219, p. 264, 1960.

[7] L. Paterson, "Radial fingering in a Hele-Shaw cell," *Journal of Fluid Mechanics,* vol. 113, p. 513, 1981.

[8] J. D. Chen, "Radial viscous fingering patterns in Hele-Shaw cells," *Experiments in Fluids,* vol. 5, p. 363, 1987.

[9] A. G. Banpurkar, A. V. Limaye, S. B. Ogale, "Occurrence of coexisting dendrite morphologies: Immiscible fluid displacement in an anisotropic radial Hele-Shaw cell under a high flow rate regime," *Physical Review E*, vol. 61, p. 5507, 2000.

[10] R. Tsuzuki, R. Tanaka, T. Ban and Y. Nagatsu, "Deviation from capillary number scaling of nonlinear viscous fingering formed by the injection of Newtonian surfactant solution," *Physics of Fluids,* vol. 31, p. 042108, 2019.

[11] Y. Nagatsu, N. Fujita, Y. Kato, Y. Tada, "An experimental study of non-isothermal miscible displacements in a Hele-Shaw cell," *Experimental Thermal and Fluid Science,* vol. 33, p. 695, 2009.

[12] Y. Nagatsu, Y. Kondo, Y. Kato and Y. Tada, "Miscible viscous fingering involving viscosity increase by a chemical reaction with moderate Damköhler number," *Physics of Fluids,* vol. 23, p. 014109, 2011.

[13] G. M. Homsy, "Viscous fingering in porous media," *Annual Review of Fluid Mechanics,* vol. 19, p. 271, 1987.

[14] P. Fast, L. Kondic, M. J. Shelley and P. Palffy-Muhoray, "Pattern formation in non-Newtonian Hele-Shaw flow," *Physics of Fluids,* vol. 13, p. 1191, 2001.

[15] S. H. Hejazi and J. Aaziez, "Nonlinear simulation of transverse flow interactions with chemically driven convective mixing in porous media," *Water Resources Research,* vol. 49, p. 4607, 2013.

[16] D. H. Vlad and J. V. Maher, "Tip-splitting instabilities in the channel Saffman-Taylor flow of constant viscosity elastic fluids," *Physical Review E,* vol. 61, no. 5, p. 5439, 2000.

[17] M. Austin-Adigio and I. D. Gates, "Thermal viscous fingering in thermal recovery processes," *Energies,* vol. 13, p. 4986, 2020.

[18] H. Li, B. Maini and J. Azaiez, "Experimental and numerical anaysis of the viscous fingering instability of shear-thinning fluids," *The Canadian Journal of Chemical Engineering,* vol. 84, p. 52, 2006.

[19] M. Kawaguchi, K. Makino and T. Kato, "Viscous fingering patterns in polymer solutions," *Physica D,* vol. 109, p. 325, 1997.

[20] J. Nittmann, G. Daccord and H. E. Stanley, "Fractal growth of viscous fingers: quantitative characterization of a fluid instability phenomenon," *Nature,* vol. 314, p. 141, 1985.

[21] G. Daccord, J. Nittmann and H. E. Stanley, "Radial viscous fingers and diffusion-limited aggregation: Fractal dimension and growth sites," *Physical Review Letters,* vol. 56, p. 336, 1986.

[22] A. Lindner, P. Coussot and D. Bonn, "Viscous fingering in a yield stress fluid," *Physical Review Letters,* vol. 85, p. 314, 2000.

[23] A. Lindner, D. Bonn and J. Meunier, "Viscous fingering in a shear-thinning fluid," *Physics of Fluids,* vol. 12, p. 256, 2000.

[24] A. Lindner, D. Bonn, E. C. Poire, M. B. Amar and J. Meunier, "Viscous Fingering in non-Newtonian fluids," *Journal of Fluid Mechanics,* vol. 469, p. 237, 2002.

[25] D. Bonn and J. Meunier, "Viscoelastic free-boundary problems: non-Newtonian viscosity vs normal stress effects," *Physical Review Letters,* vol. 79, no. 14, p. 2662, 1997.

[26] D. J. Durian, D. A. Weitz and D. J. Pine, "Scaling behavior in shaving cream," *Physical Review A,* vol. 44, no. 12, p. R7902, 1991.

[27] N. D. Denkov, S. Tcholakova, K. Golemanov, K. P. Ananthpadmanabhan and A. Lips, "The role of surfactant type and bubble surface mobility in foam rheology," *The Royal Society of Chemistry,* vol. 5, p. 3389, 2009.

[28] S. Hilgenfeldt, S. Arif and J.-C. Tsai, "Foam: a multiphase system with many facets," *Philosophical Transactions of the Royal Society A,* vol. 366, p. 2145, 2008.

[29] S. Arif, J.-C. Tsai and S. Hilgenfeldt, "Speed of crack propagation in dry aqueous foam," *Europhysics Letters,* vol. 92, p. 38001, 2010.

[30] S. Chowdhury, M. Rakesh, S. Medhi, S. Shrivastava, R. Dehury and J. S. Sangwai, "Three-Phase Fluid Flow Interaction at Pore Scale during Water-and Surfactant-Alternating Gas (WAG/SAG) Injection Using Carbon Dioxide for Geo-Sequestration and Enhanced Oil Recovery," *Energy & Fuels,* vol. 37, p. 5270, 2023.

[31] P. D. McClure and B. E. Sleep, "Simulation of bioventing for soil and ground-water remediation," *Journal of Environmental Engineering,* vol. 122, p. 1003, 1996.

[32] R. L. Chuoke, P. van Meurs, and C. van der Poel, "The instability of slow, immiscible, viscous liquid-liquid displacements in permeable media," *Petroleum Transuctions,* vol. 216, p. 188, 1959.

[33] A. De Wit and G. M. Homsy, "Nonlinear interactions of chemical reactions and viscous fingering in porous media," *Physics of fluids,* vol. 11, p. 949, 1999.

[34] E. O. Dias, E. Alvarez-Lacalle, M. S. Carvalho and J. A. Miranda, "Minimization of viscous fluid fingering: A variational scheme for optimal flow rates," *Physical Review Letters,* vol. 109, p. 1144502, 2012.

[35] J. D. Chen, "Growth of radial viscous fingers in a Hele-Shaw cell," *Journal of Fluid Mechanics,* vol. 201, p. 223, 1989.

[36] S. D. R. Wilson, "A note on the measurement of dynamic contact angles," *Journal of Colloid and Interface Science,* vol. 51, p. 532, 1975.

[37] E. Allen and D. Boger, "The influence of rheological properties on mobility control in polymer-augmented waterflooding," *Society of Petroleum Engineers,* p. 449, 1988.

[38] S. Malhotra and M. M. Sharma, "Impact of fluid elasticityonmiscibleviscous fingering," *Chemical Engineering Science,* vol. 117, p. 125, 2014.

[39] P. Jangir, R. Mohan and P. Chokshi, "Experimental study on the role of polymer addition in Saffman–Taylor instability in miscible flow displacement," *Physics of Fluids,* vol. 34, p. 093102, 2022.

[40] R. B. Bird, R. C. Armstrong and O. Hassager, Dynamics of polymeric liquids volume 1 fluid mechanics, New York: John Wiley & Sons, 1987.

[41] K. Kang, S. S. Lee, S. J. Lee and J. M. Kim, "DNA-based highly tunable particle focuser," *Nature Communications,* vol. 4, p. 2567, 2013.

[42] G. Holzner, S. Stavrakis and A. DeMello, "Elasto-inertial focusing of mammalian cells and bacteria using low molecular, low viscosity PEO solutions," *Analytical Chemistry,* vol. 89, no. 21, p. 11653, 2017.

[43] H. Shokri, M. H. Kayhani and M. Norouzi, "Nonlinear simulation and linear stability analysis of viscous fingering instability of viscoelastic liquids," *Physics of Fluids,* vol. 29, p. 033101, 2017.

[44] S. Cohen-Addad and R. Hohler, "Rheology of foams and highly concentrated emulsions," *Current Opinion in Colloid & Interface Science,* vol. 19, p. 536, 2014.

[45] H. Manikantan and T. M. Squires, "Surfactant dynamics: hidden variables controlling fluid flows," *Journal of Fluid Mechanics,* vol. 892, p. P1, 2020.

[46] H. M. Princen, "Rheology of foams and highly concentrated emulsions. II. experimental study of the yield stress and wall effects for concentrated oil-in-water emulsions," *Journal of Colloid and Interface Science,* vol. 105, p. 150, 1985.

[47] S. Cohen-Addad, R. Hohler and Y. Khidas, "Origin of the slow linear viscoelastic response of aqueous foams," *Physical Review Letters,* vol. 93, p. 028302, 2004.

[48] P. S. Stewart and S. Hilgenfeldt, "Gas-liquid foam dynamics: From structural elements to continuum descriptions," *Annual Review of Fluid Mechanics,* vol. 55, p. 323, 2023.

[49] P. G. Saffman, G. I. Taylor, "The penetration of a fluid into a porous medium or Hele-Shaw cell containing a more viscous liquid," *Proceedings of the Royal Society of London A,* vol. 245, p. 312, 1958.

[50] I. B. Salem, I. Cantat and B. Dollet, "Response of a two-dimensional liquid foam to air injection: swelling rate, fingering and fracture," *Journal of Fluid Mechanics,* vol. 714, p. 258, 2013.

[51] P. S. Stewart, S. H. Davis and S. Hilgenfeldt, "Microstructural effects in aqueous foam fracture," *Journal of Fluid Mechanics,* vol. 785, p. 425, 2015.

[52] I. B. Salem, I. Cantat and B. Dollet, "Response of a two-dimensional liquid foam to air injection: Influence of surfactants, critical velocities and branched fracture," *Colloids and Surfaces A: Physicochemical and Engineering Aspects,* vol. 438, p. 41, 2013.

[53] N. Yanagisawa and R. Kurita, "Size distribution dependence of collective relaxation dynamics in a two-dimensional wet foam," *Scientific Reports,* vol. 11, p. 2786, 2021.

[54] S. S. Park and D. J. Durian, "Viscous and elastic fingering instabilities in foam," *Physical Review Letters,* vol. 72, p. 3347, 1994.

[55] D. L. Chen, L. Li, S. Reyes, D. N. Adamson and R. F. Ismagilov, "Using three-phase flow of immiscible liquids to prevent coalescence of droplets in microfluidic channels: criteria to identify the third liquid and validation with protein crystallization," *Langmuir,* vol. 23, p. 2255, 2007.

[56] A. Alhosani, B. Bijeljic and M. J. Blunt, "Pore-scale imaging and analysis of wettability order, trapping and displacement in three-phase flow in porous media with various wettabilities," *Transport in Porous Media,* vol. 140, p. 59, 2021.

[57] M. Dong, J. Foraie, S. Huang and I. Chatzis, "Analysis of immiscible water-alternating-gas (WAG) injection using micromodel tests," *Journal of Canadian Petroleum Technology,* vol. 44, p. 17, 2005.

[58] B. H. Caudle and A. B. Dyes, "Improving miscible displacement by gas-water injection," *Transactions of the AIME,* vol. 213, p. 281, 1958.

[59] W. Wang, C. Zhang, A. Patmonoaji, Y. Hu, S. Matsushita, T. Suekane and Y. Nagatsu, "Effect of gas generation by chemical reaction on viscous fingering in a Hele–Shaw cell," *Physics of Fluids,* vol. 33, p. 093104, 2021.

[60] C. C. Ezeuko, J. Wang and I. D. Gates, "Investigation of emulsion flow in SAGD and ES-SAGD," *Society of Petroleum Engineers,* 2012.

[61] D. R. Gotawala and I. D. Gates, "Stability of the edge of a SAGD steam chamber in a bitumen reservoir," *Chemical Engineering Science,* vol. 66, p. 1802, 2011.

[62] J. Sharma and I. D. Gates, "Interfacial stability of in-situ bitumen thermal solvent recovery processes," *Society of Petroleum Engineers,* 2011.

[63] M. Irani and I. Gates, "On the stability of the edge of a steam-assisted-gravity-drainage steam chamber," *Society of Petroleum Engineers,* 2014.

[64] R. M. Butler, Thermal recovery of oil and bitumen, Calgary: GravDrain, 1997.

[65] D. Zhu, J. A. Bergerson and I. D. Gates, "On fingering of steam chambers in steam-assisted heavy oil recovery," *AIChE Journal,* vol. 62, no. 4, p. 1364, 2016.

[66] R. Raghavan and S. S. Marsden, "A theoretical study of the instability in the parallel flow of immiscible liquids in a porous medium," *The Quarterly Journal of Mechanics and Applied Mathematics,* vol. 26, p. 205, 1973.

[67] H. H. Bau, "Kelvin-Helmholtz instability for parallel flow in porous media: a linear theory," *Physics of Fluids,* vol. 25, p. 1719, 1982.

[68] M. Zeybek and Y. C. Yortsos, "Parallel flow in Hele-Shaw cells," *Journal of Fluid Mechanics,* vol. 241, p. 421, 1992.

[69] P. Gondret and M. Rabaud, "Shear instability of two-fluid parallel flow in a Hele-Shaw cell," *Physics of Fluids,* vol. 9, p. 3267, 1997.

[70] B. Abedi, L. S. Berghe, B. S. Fonseca, E. C. Rodrigues and R. M. Oliveira, "Influence of wall slip in the radial displacement of a yield strength material in a Hele–Shaw cell," *Physics of Fluids,* vol. 34, p. 113102, 2022.

[71] P. Singh and S. Mondal, "Viscous fingering to fracturing transition in Hele–Shaw flow of shear-thickening fluid," *Physics of Fluids,* vol. 35, p. 064116, 2023.

[72] F. Bossard, N. El Kissi, A. D'aprea, F. Alloin, J. Y. Sanchez and A. Dufresne, "Influence of dispersion procedure on rheological properties of aqueous solutions of high molecular weight PEO," *Rheologica acta,* vol. 49, p. 529, 2010.

[73] B. R. Elbing, E. S. Winkel, M. J. Solomon and S. L. Ceccio, "Degradation of homogeneous polymer solutions in high shear turbulent pipe flow," *Experiments in fluids,* vol. 47, p. 1033, 2009.

[74] B. R. Elbing, M. J. Solomon, M. Perlin, D. R. Dowling and S. L. Ceccio, "Flow-induced degradation of drag-reducing polymer solutions within a high-Reynolds-number turbulent boundary layer," *Journal of Fluid Mechanics,* vol. 670, p. 337, 2011.

[75] C. W. McGary Jr, "Degradation of poly (ethylene oxide)," *Journal of Polymer Science,* vol. 46, p. 51, 1960.

[76] S. A. Vanapalli, M. T. Islam and M. J. Solomon, "Scission-induced bounds on maximum polymer drag reduction in turbulent flow," *Physics of Fluids,* vol. 17, p. 095108, 2005.

[77] D. Rivero, L. M. Gouveia, A. J. Müller and A. E. Sáez, "Shear-thickening behavior of high molecular weight poly (ethylene oxide) solutions," *Rheologica Acta,* vol. 51, p. 13, 2012.

[78] B. H. Cao and M. W. Kim, "Molecular weight dependence of the surface tension of aqueous poly(ethylene oxide) solutions," *Faraday Discuss,* vol. 98, p. 245, 1994.

[79] V. Tirtaatmadja, G. H. McKinley and J. J. Cooper-White, "Drop formation and breakup of low viscosity elastic fluids: Effects of molecular weight and concentration," *Physics of Fluids,* vol. 18, p. 043101, 2006.

[80] A. R. Kopf-Sill and G. M. Homsy, "Nonlinear unstable viscous fingers in Hele–Shaw flows. I. Experiments," *Physics of Fluids,* vol. 31, no. 2, p. 242, 1988.

[81] L. Kondic, M. J. Shelley and P. Palffy-Muhoray, "Non-Newtonian Hele-Shaw flow and the Saffman-Taylor instability," *Physical Review Letters,* vol. 80, p. 1433, 1998.

[82] Y. H. Lee, J. Azaiez and I. D. Gates, "Interfacial instabilities of immiscible non-Newtonian radial displacements in porous media," *Physics of Fluids,* vol. 31, no. 4, 2019.

[83] R. Tsuzuki, T. Ban, M. Fujimura and Y. Nagatsu, "Dual role of surfactant-producing reaction in immiscible viscous fingering evolution," *Physics of Fluids,* vol. 31, p. 022102, 2019.

[84] T. F. Lins and J. Azaiez, "Flow instabilities of Time-Dependent Injection Schemes in Immiscible Displacements," *The Canadian Journal of Chemical Engineering,* vol. 94, p. 2061, 2016.

[85] J. C. Earnshaw and D. J. Sharpe, "Surface viscoelasticity of a foam-forming solution," *Journal of the Chemical Society. Faraday Transactions,* vol. 92, p. 611, 1996.

[86] A. D. Gopal and D. J. Durian, "Shear-induced "melting" of an aqueous foam," *Journal of Colloid and Interface Science,* vol. 213, p. 169, 1999.

[87] Y. Furuta, N. Oikawa and R. Kurita, "Close relationship between a dry-wet transition and a bubble rearrangement in two-dimensional foam," *Scientific reports,* vol. 6, p. 37506, 2016.

[88] N. Yanagisawa and R. Kurita, "Cross over to collective rearrangements near the dry-wet transition in two-dimensional foams," *Scientific Reports,* vol. 13, p. 4939, 2023.

[89] Y. Nagatsu, Y. Kondo, Y. Kato and Y. Tada, "Effects of moderate Damköhler number on miscible viscous fingering involving viscosity decrease due to a chemical reaction," *Journal of fluid mechanics,* vol. 625, p. 97, 2009.

[90] A. M. Kraynik, "Foam flows," *Annual Review of Fluid Mechanics,* vol. 20, p. 325, 1988.

[91] I. Cantat, N. Kern and R. Delannay, "Dissipation in foam flowing through narrow channels," *Europhysics Letters,* vol. 65, no. 5, p. 726, 2004.

[92] P. Stevenson, Foam engineering : fundamentals and applications, John Wiley & Sons, 2012.

[93] F. P. Bretherton, "The motion of long bubbles in tubes," *Journal of Fluid Mechanics,* vol. 10, p. 166, 1961.

[94] G. J. Hirasaki and J. B. Lawson, "Mechanisms of foam flow in porous media: apparent viscosity in smooth capillaries," *Society of Petroleum Engineers Journal,* p. 176, 1985.

[95] C. Raufaste, A. Foulon and B. Dollet, "Dissipation in quasi-two-dimensional flowing foams," *Physics of Fluids,* vol. 21, p. 053102, 2009.

[96] N. D. Denkov, V. Subramanian, D. Gurovich and A. Lips, "Wall slip and viscous dissipation in sheared foams: Effect of surface mobility," *Colloids and Surfaces A: Physicochemical and Engineering Aspects,* vol. 263, p. 129, 2005.

[97] N. Yanagisawa, M. Tani and R. Kurita, "Dynamics and mechanism of liquid film collapse in a foam," *Soft Matter,* vol. 17, p. 1738, 2021.

[98] Y. H. Lee, J. Wang and I. D. Gates, "Effects of dilute low molecular weight poly (ethylene oxide) solutions in immiscible radial viscous fingering instabilities," *Physics of Fluids,* vol. 35, 2023.

[99] I. D. Gates, Basic reservoir engineering, Dubuque: Kendall Hunt Publishing Company, 2011.

[100] J. C. Sproule, "The McMurray formation in its relation to oil occurrence," in *Athabasca oil sands conference,* Edmonton, 1951.

[101] P. K. Kundu and I. M. Cohen, Fluid Mechanics, 4 ed., Academic Press, 2008.

[102] P. N. Azom and S. Srinivasan, "Mechanistic modeling of emulsion formation and heat transfer during the steam-assisted gravity drainage (SAGD) process," *SPE Annual Technical Conference and Exhibition,* p. SPE 124930, 2009.

[103] C. C. Ezeuko, J. Wang and I. D. Gates, "Investigation of emulsion flow in steam-assisted gravity drainage," *SPE Journal,* vol. 18, p. 440, 2013.

[104] M. Rajayi and A. Kantzas, "Effect of temperature and pressure on contact angle and interfacial tension of quartz/water/bitumen systems," *Society of Petroleum Engineers,* 2011.

Appendix A: Further information on Hele-Shaw cell experiments

The glass plates (SCHOTT Borofloat 33) were supplied from McMaster-Carr. Abrisa Technologies (https://abrisatechnologies.com/) was the fabricator of the borosilicate glass plates for McMaster-Carr. The injection hole was fabricated using a standard drilling option. However, Abrisa Technologies provides more meticulous options for making a hole in a borosilicate glass plate.

Deionized water and dilute PEO solutions were initially injected through a fixed length of Teflon tubing attached to the Hele-Shaw cell. As a result, a constant volume of water remained in the tubing before air from the mass flow controller is connected to the tubing. This gives some time for the mass flow controller to adjust to the pressure change and achieve constant volume flow rate of air. Non-water wetting Teflon tubing was employed to eliminate water remaining in the tubing during air injection.

The gap thickness is verified by comparing the actual volume of injected water and the area occupied by the water multiplied by the gap thickness. The volume of injected water was determined by measuring the mass of water from the same syringe with the same volume of water used in the experiments as shown in Table S1. The average volume of injected water is determined as $3.32 \pm 0.02\ cc$.

Table S1. Volume of injected water.

Mass of injected water (g)	Density of water (g/cm^3)	Volume of water (cm^3)
3.3269	0.99777	3.3343
3.2919	0.99777	3.2992

As shown in Table S2, the unit conversion factor, 0.178768 mm/pixel, is used to convert pixels to mm. The volume of water from an experiment image determined as $3.3061\ cc$ by multiplying the area occupied by the water by the gap thickness (d = 0.0762 mm) as shown in Table S3. This results in a percent error of -0.32% in the volume calculated from a captured image.

Table S2. Unit conversion factor for converting pixels to mm in experiment video frames.

Actual length (mm)	Pixels in image (pixel)	mm/pixel
304.8	1357623	0.178768

Table S3. Volume of water determined from an experiment video frame and a gap thickness.

Water area (pixel)	Water area (mm^3)	Water volume (cm^3)
1357623	43387.07	3.3061

Appendix B: Permissions

American Physical Society
Reuse and Permissions License

15-Mar-2024

T his license agreement between the American Physical Society ("APS") and Young Hoon Lee ("You") consists of your license details and the terms and conditions provided by the American Physical Society and SciPris.

Licensed Content Information

Lice nse Numbe r: RNP/24/MAR/077058
Lice nse date : 15-Mar-2024
DO I: 10.1103/PhysRevLett.109.144502
Title : Minimization of Viscous Fluid Fingering: A Variational Scheme for Optimal Flow Rates
Author: Eduardo O. Dias et al.
Publication: Physical Review Letters
Publishe r: American Physical Society
Cost: USD $ 0.00

Request Details

Doe s your re use re quire significant modifications: No
Spe cify inte nde d distribution locations:
Canada
Re use Cate gory: Reuse in a thesis/dissertation
Re que stor Type : Student
Ite ms for Re use : Figures/Tables
Numbe r of Figure /Table s: 1
Figure /Table s De tails: FIG. 4. Typical experimental patterns
Format for Re use : Electronic

Information about New Publication:

Unive rsity/Publishe r: University of Calgary
Title of disse rtation/the sis: Viscous Fingering Instability of Complex Fluids in a Radial Hele-Shaw Cell
Author(s): Young Hoon Lee
Expe cte d comple tion date : Mar. 2024

License Requestor Information

Name : Young Hoon Lee
Affiliation: Individual
Email Id: yhlee@ucalgary.ca
Country: Canada

American Physical Society
Reuse and Permissions License

TERMS AND CONDITIONS

T he American Physical Society (APS) is pleased to grant the Requestor of this license a non-exclusive, non-transferable permission, limited to Electronic format, provided all criteria outlined below are followed.

1. You must also obtain permission from at least one of the lead authors for each separate work, if you haven't done so already. T he author's name and affiliation can be found on the first page of the published Article.
2. For electronic format permissions, Requestor agrees to provide a hyperlink from the reprinted APS material using the source material's DOI on the web page where the work appears. T he hyperlink should use the standard DOI resolution URL, http://dx.doi.org/{DOI}. T he hyperlink may be embedded in the copyright credit line.
3. For print format permissions, Requestor agrees to print the required copyright credit line on the first page where the material appears: "Reprinted (abstract/excerpt/figure) with permission from [(FULL REFERENCE CITAT ION) as follows: Author's Names, APS Journal T itle, Volume Number, Page Number and Year of Publication.] Copyright (YEAR) by the American Physical Society."
4. Permission granted in this license is for a one-time use and does not include permission for any future editions, updates, databases, formats or other matters. Permission must be sought for any additional use.
5. Use of the material does not and must not imply any endorsement by APS.
6. APS does not imply, purport or intend to grant permission to reuse materials to which it does not hold copyright. It is the

requestor ’s sole responsibility to ensure the licensed material is original to APS and does not contain the copyright of another entity, and that the copyright notice of the figure, photograph, cover or table does not indicate it was reprinted by APS with permission from another source.
7. T he permission granted herein is personal to the Requestor for the use specified and is not transferable or assignable without express written permission of APS. T his license may not be amended except in writing by APS.
8. You may not alter, edit or modify the material in any manner.
9. You may translate the materials only when translation rights have been granted.
10. APS is not responsible for any errors or omissions due to translation.
11. You may not use the material for promotional, sales, advertising or marketing purposes.
12. T he foregoing license shall not take effect unless and until APS or its agent, Aptara, receives payment in full in accordance with Aptara Billing and Payment Terms and Conditions, which are incorporated herein by reference.
13. Should the terms of this license be violated at any time, APS or Aptara may revoke the license with no refund to you and seek relief to the fullest extent of the laws of the USA. Official written notice will be made using the contact information provided with the permission request. Failure to receive such notice will not nullify revocation of the permission.
14. APS reserves all rights not specifically granted herein.
15. T his document, including the Aptara Billing and Payment Terms and Conditions, shall be the entire agreement between the parties relating to the subject matter hereof.

AIP PUBLISHING LICENSE

TERMS AND CONDITIONS

Mar 15, 2024

This Agreement between Dr. Young Hoon Lee ("You") and AIP Publishing ("AIP Publishing") consists of your license details and the terms and conditions provided by AIP Publishing and Copyright Clearance Center.

License Number	5750391508425
License date	Mar 15, 2024
Licensed Content Publisher	AIP Publishing
Licensed Content Publication	Physics of Fluids
Licensed Content Title	Miscible quarter five-spot displacements in a Hele-Shaw cell and the role of flow-induced dispersion
Licensed Content Author	Petitjeans, Philippe; Chen, Ching-Yao
Licensed Content Date	Jul 1, 1999
Licensed Content Volume	11
Licensed Content Issue	7
Type of Use	Thesis/Dissertation
Requestor type	Student
Format	Electronic
Portion	Photograph/Image

Number of Photographs/Images	1
Will you be translating?	No
Title of new work	Viscous Fingering Instability of Complex Fluids in a Radial Hele-Shaw Cell
Institution name	University of Calgary
Expected presentation date	Mar 2024
Portions	FIG. 3. (a) Fingering patterns at the breakthrough time
Requestor Location	Dr. Young Hoon Lee 184 Sage Valley Cir NW Calgary, AB T3R0E7 Canada Attn: Dr. Young Hoon Lee
Total	**0.00 CAD**

Terms and Conditions

AIP Publishing -- Terms and Conditions: Permissions Uses

AIP Publishing hereby grants to you the non-exclusive right and license to use and/or distribute the Material according to the use specified in your order, on a one-time basis, for the specified term, with a maximum distribution equal to the number that you have ordered. Any links or other content accompanying the Material are not the subject of this license.

1. You agree to include the following copyright and permission notice with the reproduction of the Material:"Reprinted from [FULL CITATION], with the permission of AIP Publishing." For an article, the credit line and permission notice must be printed on the first page of the article or book chapter. For photographs, covers, or tables, the notice may appear with the Material, in a footnote, or in the reference list.
2. If you have licensed reuse of a figure, photograph, cover, or table, it is your responsibility to ensure that the material is original to AIP Publishing and does not contain the copyright of another entity, and that the copyright notice of the figure, photograph, cover, or table does not indicate that it was reprinted by AIP Publishing, with permission, from another source. Under no circumstances does AIP Publishing purport or intend to grant permission to reuse material to which it does not hold appropriate rights.
   You may not alter or modify the Material in any manner. You may translate the Material into another language only if you have licensed translation rights. You may not use the Material for promotional purposes.
3. The foregoing license shall not take effect unless and until AIP Publishing or its agent, Copyright Clearance Center, receives the Payment in accordance with Copyright Clearance Center Billing and Payment Terms and Conditions, which are incorporated herein by reference.
4. AIP Publishing or Copyright Clearance Center may, within two business days of granting this license, revoke the license for any reason whatsoever, with a full refund payable to you. Should you violate the terms of this license at any time, AIP Publishing, or Copyright Clearance Center may revoke the license with no refund to you. Notice of such revocation will be made using the contact information provided by you. Failure to receive such notice will not nullify the revocation.
5. AIP Publishing makes no representations or warranties with respect to the Material. You agree to indemnify and hold harmless AIP Publishing, and their officers, directors, employees or agents from and against any and all claims arising out of your use of the Material other than as specifically authorized herein.
6. The permission granted herein is personal to you and is not transferable or assignable without the prior written permission of AIP Publishing. This license may not be amended except in a writing signed by the party to be charged.
7. If purchase orders, acknowledgments or check endorsements are issued on any forms containing terms and conditions which are inconsistent with these provisions, such inconsistent terms and conditions shall be of no force and effect. This document, including the CCC Billing and Payment

Terms and Conditions, shall be the entire agreement between the parties relating to the subject matter hereof.

This Agreement shall be governed by and construed in accordance with the laws of the State of New York. Both parties hereby submit to the jurisdiction of the courts of New York County for purposes of resolving any disputes that may arise hereunder.

V1.2

Questions? E-mail us at customercare@copyright.com.

This is a License Agreement between Young Hoon Lee (“User”) and Copyright Clearance Center, Inc. (“CCC”) on behalf of the Rightsholder identified in the order details below. The license consists of the order details, the Marketplace Permissions General Terms and Conditions below, and any Rightsholder Terms and Conditions which are included below.

All payments must be made in full to CCC in accordance with the Marketplace Permissions General Terms and Conditions below.

Order Date

15-Mar-2024

Order License ID

1461907-1

ISSN

0081-1696

Type of Use

Republish in a thesis/dissertation

Publisher

THE SOCIETY,

Portion

Image/photo/illustration

LICENSED CONTENT

Publication Title

TRANSACTION- SOCIETY OF PETROLEUM ENGINEERS OF THE AMERICAN INSTITUTE OF MINING METALLURGICAL AND PETROLEUM ENGINEERS INCORPORATED

Author/Editor

SOCIETY OF PETROLEUM ENGINEERS OF AIME.

Date

01/01/1961

Language

English

Country

United States of America

Rightsholder

Society of Petroleum Engineers (SPE)

Publication Type

Journal

REQUEST DETAILS

Portion Type

Image/photo/illustration

Number of Images / Photos / Illustrations

1

Format (select all that apply)

Electronic

Who Will Republish the Content?

Author of requested content

Duration of Use

Life of current edition

Lifetime Unit Quantity

Up to 499

Rights Requested

Main product

Distribution

Canada

Translation

Original language of publication

Copies for the Disabled?

No

Minor Editing Privileges?

No

Incidental Promotional Use?

No

Currency

CAD

NEW WORK DETAILS

Title

Viscous Fingering Instability of Complex Fluids in a Radial Hele-Shaw Cell

Instructor Name

Young Hoon Lee

Institution Name

University of Calgary

Expected Presentation Date

2024-03-15

ADDITIONAL DETAILS

Order Reference Number

N/A

The Requesting Person / Organization to Appear on the License

Young Hoon Lee

REQUESTED CONTENT DETAILS

Title, Description or Numeric Reference of the Portion(s)

FIG. I-IN TABILITY OF A WATER·OIL I NTERFACE

Editor of Portion(s)

N/A

Volume / Edition

216

Page or Page Range of Portion

191

Title of the Article / Chapter the Portion Is From

The Instability of Slow, Immiscible, Viscous Liquid-Liquid Displacements in Permeable Media

Author of Portion(s)

SOCIETY OF PETROLEUM ENGINEERS OF AIME.

Issue, if Republishing an Article From a Serial

N/A

Publication Date of Portion

1959-10-01

Marketplace Permissions General Terms and Conditions

The following terms and conditions ("General Terms"), together with any applicable Publisher Terms and Conditions, govern User's use of Works pursuant to the Licenses granted by Copyright Clearance Center, Inc. ("CCC") on behalf of the applicable Rightsholders of such Works through CCC's applicable Marketplace transactional licensing services (each, a "Service").

- 1)**Definitions.**For purposes of these General Terms, the following definitions apply:

  "License" is the licensed use the User obtains via the Marketplace platform in a particular licensing transaction, as set forth in the Order Confirmation.

  "Order Confirmation" is the confirmation CCC provides to the User at the conclusion of each Marketplace transaction. "Order Confirmation Terms" are additional terms set forth on specific Order Confirmations not set forth in the General Terms that can include terms applicable to a particular CCC transactional licensing service and/or any Rightsholder-specific terms.

  "Rightsholder(s)" are the holders of copyright rights in the Works for which a User obtains licenses via the Marketplace platform, which are displayed on specific Order Confirmations.

  "Terms" means the terms and conditions set forth in these General Terms and any additional Order Confirmation Terms collectively.

  "User" or "you" is the person or entity making the use granted under the relevant License. Where the person accepting the Terms on behalf of a User is a freelancer or other third party who the User authorized to accept the General Terms on the User's behalf, such person shall be deemed jointly a User for purposes of such Terms.

  "Work(s)" are the copyright protected works described in relevant Order Confirmations.

- 2)**Description of Service.**CCC's Marketplace enables Users to obtain Licenses to use one or more Works in accordance with all relevant Terms. CCC grants Licenses as an agent on behalf of the copyright rightsholder identified in the relevant Order Confirmation.
- 3)**Applicability of Terms.**The Terms govern User's use of Works in connection with the relevant License. In the event of any conflict between General Terms and Order Confirmation Terms, the latter shall govern. User acknowledges that Rightsholders have complete discretion whether to grant any permission, and whether to place any limitations on any grant, and that CCC has no right to supersede or to modify any such discretionary act by a Rightsholder.
- 4)**Representations; Acceptance.**By using the Service, User represents and warrants that User has been duly authorized by the User to accept, and hereby does accept, all Terms.
- 5)**Scope of License; Limitations and Obligations.**All Works and all rights therein, including copyright rights, remain the sole and exclusive property of the Rightsholder. The License provides only those rights expressly set forth in the terms and conveys no other rights in any Works
- 6)**General Payment Terms.**User may pay at time of checkout by credit card or choose to be invoiced. If the User chooses to be invoiced, the User shall: (i) remit payments in the manner identified on specific invoices, (ii) unless otherwise specifically stated in an Order Confirmation or separate written agreement, Users shall remit payments upon receipt of the relevant invoice from CCC, either by delivery or notification of availability of the invoice via the Marketplace platform, and (iii) if the User does not pay the invoice within 30 days of receipt, the User may incur a service charge of 1.5% per month or the maximum rate allowed by applicable law, whichever is less. While User may exercise the rights in the License immediately upon receiving the Order Confirmation, the License is automatically revoked and is null and void, as if it had never been issued, if CCC does not receive complete payment on a timely basis.
- 7)**General Limits on Use.**Unless otherwise provided in the Order Confirmation, any grant of rights to User (i) involves only the rights set forth in the Terms and does not include subsequent or additional uses, (ii) is non-exclusive and non-transferable, and (iii) is subject to any and all limitations and restrictions (such as, but not limited to, limitations on duration of use or circulation) included in the Terms. Upon completion of the licensed use as set forth in the Order Confirmation, User shall either secure a new permission for further use of the Work(s) or immediately cease any new use of the Work(s) and shall render inaccessible (such as by deleting or by removing or severing links or other locators) any further copies of the Work. User may only make alterations to the Work if and as expressly set forth in the Order Confirmation. No Work may be used in any way that is unlawful, including without limitation if such use would violate applicable sanctions laws or regulations, would be defamatory, violate the rights of third parties (including such third parties' rights of copyright, privacy, publicity, or other tangible or intangible property), or is otherwise illegal, sexually explicit, or obscene. In addition, User may not conjoin a Work with any other material that may result in damage to the reputation of the Rightsholder. Any unlawful use will render any licenses hereunder null and void. User agrees to inform CCC if it becomes aware of any infringement of any rights in a Work and to cooperate with any reasonable request of CCC or the Rightsholder in connection therewith.
- 8)**Third Party Materials.**In the event that the material for which a License is sought includes third party materials (such as photographs, illustrations, graphs, inserts and similar materials) that are identified in such material as having been used by permission (or a similar indicator), User is responsible for identifying, and seeking separate licenses (under this Service, if

available, or otherwise) for any of such third party materials; without a separate license, User may not use such third party materials via the License.

- 9)**Copyright Notice.**Use of proper copyright notice for a Work is required as a condition of any License granted under the Service. Unless otherwise provided in the Order Confirmation, a proper copyright notice will read substantially as follows: "Used with permission of [Rightsholder's name], from [Work's title, author, volume, edition number and year of copyright]; permission conveyed through Copyright Clearance Center, Inc." Such notice must be provided in a reasonably legible font size and must be placed either on a cover page or in another location that any person, upon gaining access to the material which is the subject of a permission, shall see, or in the case of republication Licenses, immediately adjacent to the Work as used (for example, as part of a by-line or footnote) or in the place where substantially all other credits or notices for the new work containing the republished Work are located. Failure to include the required notice results in loss to the Rightsholder and CCC, and the User shall be liable to pay liquidated damages for each such failure equal to twice the use fee specified in the Order Confirmation, in addition to the use fee itself and any other fees and charges specified.
- 10)**Indemnity.**User hereby indemnifies and agrees to defend the Rightsholder and CCC, and their respective employees and directors, against all claims, liability, damages, costs, and expenses, including legal fees and expenses, arising out of any use of a Work beyond the scope of the rights granted herein and in the Order Confirmation, or any use of a Work which has been altered in any unauthorized way by User, including claims of defamation or infringement of rights of copyright, publicity, privacy, or other tangible or intangible property.
- 11)**Limitation of Liability.**UNDER NO CIRCUMSTANCES WILL CCC OR THE RIGHTSHOLDER BE LIABLE FOR ANY DIRECT, INDIRECT, CONSEQUENTIAL, OR INCIDENTAL DAMAGES (INCLUDING WITHOUT LIMITATION DAMAGES FOR LOSS OF BUSINESS PROFITS OR INFORMATION, OR FOR BUSINESS INTERRUPTION) ARISING OUT OF THE USE OR INABILITY TO USE A WORK, EVEN IF ONE OR BOTH OF THEM HAS BEEN ADVISED OF THE POSSIBILITY OF SUCH DAMAGES. In any event, the total liability of the Rightsholder and CCC (including their respective employees and directors) shall not exceed the total amount actually paid by User for the relevant License. User assumes full liability for the actions and omissions of its principals, employees, agents, affiliates, successors, and assigns.
- 12)**Limited Warranties.**THE WORK(S) AND RIGHT(S) ARE PROVIDED "AS IS." CCC HAS THE RIGHT TO GRANT TO USER THE RIGHTS GRANTED IN THE ORDER CONFIRMATION DOCUMENT. CCC AND THE RIGHTSHOLDER DISCLAIM ALL OTHER WARRANTIES RELATING TO THE WORK(S) AND RIGHT(S), EITHER EXPRESS OR IMPLIED, INCLUDING WITHOUT LIMITATION IMPLIED WARRANTIES OF MERCHANTABILITY OR FITNESS FOR A PARTICULAR PURPOSE. ADDITIONAL RIGHTS MAY BE REQUIRED TO USE ILLUSTRATIONS, GRAPHS, PHOTOGRAPHS, ABSTRACTS, INSERTS, OR OTHER PORTIONS OF THE WORK (AS OPPOSED TO THE ENTIRE WORK) IN A MANNER CONTEMPLATED BY USER; USER UNDERSTANDS AND AGREES THAT NEITHER CCC NOR THE RIGHTSHOLDER MAY HAVE SUCH ADDITIONAL RIGHTS TO GRANT.
- 13)**Effect of Breach.**Any failure by User to pay any amount when due, or any use by User of a Work beyond the scope of the License set forth in the Order Confirmation and/or the Terms, shall be a material breach of such License. Any breach not cured within 10 days of written notice thereof shall result in immediate termination of such License without further notice. Any unauthorized (but licensable) use of a Work that is terminated immediately upon notice thereof may be liquidated by payment of the Rightsholder's ordinary license price therefor; any unauthorized (and unlicensable) use that is not terminated immediately for any reason

(including, for example, because materials containing the Work cannot reasonably be recalled) will be subject to all remedies available at law or in equity, but in no event to a payment of less than three times the Rightsholder's ordinary license price for the most closely analogous licensable use plus Rightsholder's and/or CCC's costs and expenses incurred in collecting such payment.

- 14)**Additional Terms for Specific Products and Services.**If a User is making one of the uses described in this Section 14, the additional terms and conditions apply:
    - a)***Print Uses of Academic Course Content and Materials (photocopies for academic coursepacks or classroom handouts).***For photocopies for academic coursepacks or classroom handouts the following additional terms apply:
        - i) The copies and anthologies created under this License may be made and assembled by faculty members individually or at their request by on-campus bookstores or copy centers, or by off-campus copy shops and other similar entities.
        - ii) No License granted shall in any way: (i) include any right by User to create a substantively non-identical copy of the Work or to edit or in any other way modify the Work (except by means of deleting material immediately preceding or following the entire portion of the Work copied) (ii) permit "publishing ventures" where any particular anthology would be systematically marketed at multiple institutions.
        - iii) Subject to any Publisher Terms (and notwithstanding any apparent contradiction in the Order Confirmation arising from data provided by User), any use authorized under the academic pay-per-use service is limited as follows:
            - A) any License granted shall apply to only one class (bearing a unique identifier as assigned by the institution, and thereby including all sections or other subparts of the class) at one institution;
            - B) use is limited to not more than 25% of the text of a book or of the items in a published collection of essays, poems or articles;
            - C) use is limited to no more than the greater of (a) 25% of the text of an issue of a journal or other periodical or (b) two articles from such an issue;
            - D) no User may sell or distribute any particular anthology, whether photocopied or electronic, at more than one institution of learning;
            - E) in the case of a photocopy permission, no materials may be entered into electronic memory by User except in order to produce an identical copy of a Work before or during the academic term (or analogous period) as to which any particular permission is granted. In the event that User shall choose to retain materials that are the subject of a photocopy permission in electronic memory for purposes of producing identical copies more than one day after such retention (but

still within the scope of any permission granted), User must notify CCC of such fact in the applicable permission request and such retention shall constitute one copy actually sold for purposes of calculating permission fees due; and

- F) any permission granted shall expire at the end of the class. No permission granted shall in any way include any right by User to create a substantively non-identical copy of the Work or to edit or in any other way modify the Work (except by means of deleting material immediately preceding or following the entire portion of the Work copied).

- iv) Books and Records; Right to Audit. As to each permission granted under the academic pay-per-use Service, User shall maintain for at least four full calendar years books and records sufficient for CCC to determine the numbers of copies made by User under such permission. CCC and any representatives it may designate shall have the right to audit such books and records at any time during User's ordinary business hours, upon two days' prior notice. If any such audit shall determine that User shall have underpaid for, or underreported, any photocopies sold or by three percent (3%) or more, then User shall bear all the costs of any such audit; otherwise, CCC shall bear the costs of any such audit. Any amount determined by such audit to have been underpaid by User shall immediately be paid to CCC by User, together with interest thereon at the rate of 10% per annum from the date such amount was originally due. The provisions of this paragraph shall survive the termination of this License for any reason.

- b)***Digital Pay-Per-Uses of Academic Course Content and Materials (e-coursepacks, electronic reserves, learning management systems, academic institution intranets).***For uses in e-coursepacks, posts in electronic reserves, posts in learning management systems, or posts on academic institution intranets, the following additional terms apply:
  - i) The pay-per-uses subject to this Section 14(b) include:

    - A)**Posting e-reserves, course management systems, e-coursepacks for text-based content,**which grants authorizations to import requested material in electronic format, and allows electronic access to this material to members of a designated college or university class, under the direction of an instructor designated by the college or university, accessible only under appropriate electronic controls (e.g., password);
    - B)**Posting e-reserves, course management systems, e-coursepacks for material consisting of photographs or other still images not embedded in text,**which grants not only the authorizations described in Section 14(b)(i)(A) above, but also the following authorization: to include the requested material in course materials for use consistent with Section 14(b)(i)(A) above, including any necessary resizing, reformatting or modification of the resolution

of such requested material (provided that such modification does not alter the underlying editorial content or meaning of the requested material, and provided that the resulting modified content is used solely within the scope of, and in a manner consistent with, the particular authorization described in the Order Confirmation and the Terms), but not including any other form of manipulation, alteration or editing of the requested material;

- C)**Posting e-reserves, course management systems, e-coursepacks or other academic distribution for audiovisual content,**which grants not only the authorizations described in Section 14(b)(i)(A) above, but also the following authorizations: (i) to include the requested material in course materials for use consistent with Section 14(b)(i)(A) above; (ii) to display and perform the requested material to such members of such class in the physical classroom or remotely by means of streaming media or other video formats; and (iii) to "clip" or reformat the requested material for purposes of time or content management or ease of delivery, provided that such "clipping" or reformatting does not alter the underlying editorial content or meaning of the requested material and that the resulting material is used solely within the scope of, and in a manner consistent with, the particular authorization described in the Order Confirmation and the Terms. Unless expressly set forth in the relevant Order Conformation, the License does not authorize any other form of manipulation, alteration or editing of the requested material.

- ii) Unless expressly set forth in the relevant Order Confirmation, no License granted shall in any way: (i) include any right by User to create a substantively non-identical copy of the Work or to edit or in any other way modify the Work (except by means of deleting material immediately preceding or following the entire portion of the Work copied or, in the case of Works subject to Sections 14(b)(1)(B) or (C) above, as described in such Sections) (ii) permit "publishing ventures" where any particular course materials would be systematically marketed at multiple institutions.

- iii) Subject to any further limitations determined in the Rightsholder Terms (and notwithstanding any apparent contradiction in the Order Confirmation arising from data provided by User), any use authorized under the electronic course content pay-per-use service is limited as follows:

    - A) any License granted shall apply to only one class (bearing a unique identifier as assigned by the institution, and thereby including all sections or other subparts of the class) at one institution;

    - B) use is limited to not more than 25% of the text of a book or of the items in a published collection of essays, poems or articles;

    - C) use is limited to not more than the greater of (a) 25% of the text of an issue of a journal or other periodical or (b) two articles from such an issue;

- D) no User may sell or distribute any particular materials, whether photocopied or electronic, at more than one institution of learning;

- E) electronic access to material which is the subject of an electronic-use permission must be limited by means of electronic password, student identification or other control permitting access solely to students and instructors in the class;

- F) User must ensure (through use of an electronic cover page or other appropriate means) that any person, upon gaining electronic access to the material, which is the subject of a permission, shall see:

    - a proper copyright notice, identifying the Rightsholder in whose name CCC has granted permission,

    - a statement to the effect that such copy was made pursuant to permission,

    - a statement identifying the class to which the material applies and notifying the reader that the material has been made available electronically solely for use in the class, and

    - a statement to the effect that the material may not be further distributed to any person outside the class, whether by copying or by transmission and whether electronically or in paper form, and User must also ensure that such cover page or other means will print out in the event that the person accessing the material chooses to print out the material or any part thereof.

- G) any permission granted shall expire at the end of the class and, absent some other form of authorization, User is thereupon required to delete the applicable material from any electronic storage or to block electronic access to the applicable material.

- iv) Uses of separate portions of a Work, even if they are to be included in the same course material or the same university or college class, require separate permissions under the electronic course content pay-per-use Service. Unless otherwise provided in the Order Confirmation, any grant of rights to User is limited to use completed no later than the end of the academic term (or analogous period) as to which any particular permission is granted.

- v) Books and Records; Right to Audit. As to each permission granted under the electronic course content Service, User shall maintain for at least four full calendar years books and records sufficient for CCC to determine the numbers of copies made by User under such permission. CCC and any representatives it may designate shall have the right to audit such books and records at any time during User's ordinary business hours, upon two days' prior notice. If any

such audit shall determine that User shall have underpaid for, or underreported, any electronic copies used by three percent (3%) or more, then User shall bear all the costs of any such audit; otherwise, CCC shall bear the costs of any such audit. Any amount determined by such audit to have been underpaid by User shall immediately be paid to CCC by User, together with interest thereon at the rate of 10% per annum from the date such amount was originally due. The provisions of this paragraph shall survive the termination of this license for any reason.

- c)***Pay-Per-Use Permissions for Certain Reproductions (Academic photocopies for library reserves and interlibrary loan reporting) (Non-academic internal/external business uses and commercial document delivery).***The License expressly excludes the uses listed in Section (c)(i)-(v) below (which must be subject to separate license from the applicable Rightsholder) for: academic photocopies for library reserves and interlibrary loan reporting; and non-academic internal/external business uses and commercial document delivery.
  - i) electronic storage of any reproduction (whether in plain-text, PDF, or any other format) other than on a transitory basis;
  - ii) the input of Works or reproductions thereof into any computerized database;
  - iii) reproduction of an entire Work (cover-to-cover copying) except where the Work is a single article;
  - iv) reproduction for resale to anyone other than a specific customer of User;
  - v) republication in any different form. Please obtain authorizations for these uses through other CCC services or directly from the rightsholder.

  Any license granted is further limited as set forth in any restrictions included in the Order Confirmation and/or in these Terms.

- d)***Electronic Reproductions in Online Environments (Non-Academic-email, intranet, internet and extranet).***For "electronic reproductions", which generally includes e-mail use (including instant messaging or other electronic transmission to a defined group of recipients) or posting on an intranet, extranet or Intranet site (including any display or performance incidental thereto), the following additional terms apply:
  - i) Unless otherwise set forth in the Order Confirmation, the License is limited to use completed within 30 days for any use on the Internet, 60 days for any use on an intranet or extranet and one year for any other use, all as measured from the "republication date" as identified in the Order Confirmation, if any, and otherwise from the date of the Order Confirmation.
  - ii) User may not make or permit any alterations to the Work, unless expressly set forth in the Order Confirmation (after request by User and approval by Rightsholder); provided, however, that a Work consisting of photographs or other still images not embedded in text may, if necessary, be resized,

reformatted or have its resolution modified without additional express permission, and a Work consisting of audiovisual content may, if necessary, be "clipped" or reformatted for purposes of time or content management or ease of delivery (provided that any such resizing, reformatting, resolution modification or "clipping" does not alter the underlying editorial content or meaning of the Work used, and that the resulting material is used solely within the scope of, and in a manner consistent with, the particular License described in the Order Confirmation and the Terms.

- 15)**Miscellaneous.**
    - a) User acknowledges that CCC may, from time to time, make changes or additions to the Service or to the Terms, and that Rightsholder may make changes or additions to the Rightsholder Terms. Such updated Terms will replace the prior terms and conditions in the order workflow and shall be effective as to any subsequent Licenses but shall not apply to Licenses already granted and paid for under a prior set of terms.

    - b) Use of User-related information collected through the Service is governed by CCC's privacy policy, available online at www.copyright.com/about/privacy-policy/.

    - c) The License is personal to User. Therefore, User may not assign or transfer to any other person (whether a natural person or an organization of any kind) the License or any rights granted thereunder; provided, however, that, where applicable, User may assign such License in its entirety on written notice to CCC in the event of a transfer of all or substantially all of User's rights in any new material which includes the Work(s) licensed under this Service.

    - d) No amendment or waiver of any Terms is binding unless set forth in writing and signed by the appropriate parties, including, where applicable, the Rightsholder. The Rightsholder and CCC hereby object to any terms contained in any writing prepared by or on behalf of the User or its principals, employees, agents or affiliates and purporting to govern or otherwise relate to the License described in the Order Confirmation, which terms are in any way inconsistent with any Terms set forth in the Order Confirmation, and/or in CCC's standard operating procedures, whether such writing is prepared prior to, simultaneously with or subsequent to the Order Confirmation, and whether such writing appears on a copy of the Order Confirmation or in a separate instrument.

    - e) The License described in the Order Confirmation shall be governed by and construed under the law of the State of New York, USA, without regard to the principles thereof of conflicts of law. Any case, controversy, suit, action, or proceeding arising out of, in connection with, or related to such License shall be brought, at CCC's sole discretion, in any federal or state court located in the County of New York, State of New York, USA, or in any federal or state court whose geographical jurisdiction covers the location of the Rightsholder set forth in the Order Confirmation. The parties expressly submit to the personal jurisdiction and venue of each such federal or state court.

JOHN WILEY AND SONS LICENSE
TERMS AND CONDITIONS
Mar 15, 2024

This Agreement between Dr. Young Hoon Lee ("You") and John Wiley and Sons ("John Wiley and Sons") consists of your license details and the terms and conditions provided by John Wiley and Sons and Copyright Clearance Center.

License Number	5750400573767
License date	Mar 15, 2024
Licensed Content Publisher	John Wiley and Sons
Licensed Content Publication	Canadian Journal of Chemical Engineering
Licensed Content Title	Instability of parallel flow of two immiscible liquids in a pore and application to steam-assisted gravity drainage
Licensed Content Author	Ian D. Gates, Young H. Lee
Licensed Content Date	May 5, 2021
Licensed Content Volume	100
Licensed Content Issue	S1
Licensed Content Pages	10
Type of use	Dissertation/Thesis
Requestor type	Author of this Wiley article
Format	Electronic
Portion	Full article
Will you be translating?	No
Title of new work	Viscous Fingering Instability of Complex Fluids in a Radial Hele-Shaw Cell

Institution name	University of Calgary
Expected presentation date	Mar 2024
Requestor Location	Dr. Young Hoon Lee 184 Sage Valley Cir NW Calgary, AB T3R0E7 Canada Attn: Dr. Young Hoon Lee
Publisher Tax ID	EU826007151
Total	0.00 CAD
Terms and Conditions	

TERMS AND CONDITIONS

This copyrighted material is owned by or exclusively licensed to John Wiley & Sons, Inc. or one of its group companies (each a"Wiley Company") or handled on behalf of a society with which a Wiley Company has exclusive publishing rights in relation to a particular work (collectively "WILEY"). By clicking "accept" in connection with completing this licensing transaction, you agree that the following terms and conditions apply to this transaction (along with the billing and payment terms and conditions established by the Copyright Clearance Center Inc., ("CCC's Billing and Payment terms and conditions"), at the time that you opened your RightsLink account (these are available at any time at http://myaccount.copyright.com).

Terms and Conditions

- The materials you have requested permission to reproduce or reuse (the "Wiley Materials") are protected by copyright.
- You are hereby granted a personal, non-exclusive, non-sub licensable (on a stand-alone basis), non-transferable, worldwide, limited license to reproduce the Wiley Materials for the purpose specified in the licensing process. This license, **and any CONTENT (PDF or image file) purchased as part of your order,** is for a one-time use only and limited to any maximum distribution number specified in the license. The first

instance of republication or reuse granted by this license must be completed within two years of the date of the grant of this license (although copies prepared before the end date may be distributed thereafter). The Wiley Materials shall not be used in any other manner or for any other purpose, beyond what is granted in the license. Permission is granted subject to an appropriate acknowledgement given to the author, title of the material/book/journal and the publisher. You shall also duplicate the copyright notice that appears in the Wiley publication in your use of the Wiley Material. Permission is also granted on the understanding that nowhere in the text is a previously published source acknowledged for all or part of this Wiley Material. Any third party content is expressly excluded from this permission.

- With respect to the Wiley Materials, all rights are reserved. Except as expressly granted by the terms of the license, no part of the Wiley Materials may be copied, modified, adapted (except for minor reformatting required by the new Publication), translated, reproduced, transferred or distributed, in any form or by any means, and no derivative works may be made based on the Wiley Materials without the prior permission of the respective copyright owner.**For STM Signatory Publishers clearing permission under the terms of the STM Permissions Guidelines only, the terms of the license are extended to include subsequent editions and for editions in other languages, provided such editions are for the work as a whole in situ and does not involve the separate exploitation of the permitted figures or extracts,** You may not alter, remove or suppress in any manner any copyright, trademark or other notices displayed by the Wiley Materials. You may not license, rent, sell, loan, lease, pledge, offer as security, transfer or assign the Wiley Materials on a stand-alone basis, or any of the rights granted to you hereunder to any other person.

- The Wiley Materials and all of the intellectual property rights therein shall at all times remain the exclusive property of John Wiley & Sons Inc, the Wiley Companies, or their respective licensors, and your interest therein is only that of having possession of and the right to reproduce the Wiley Materials pursuant to Section 2 herein during the continuance of this Agreement. You agree that you own no right, title or interest in or to the Wiley Materials or any of the intellectual property rights therein. You shall have no rights hereunder other than the license as provided for above in Section 2. No right, license or interest to any trademark, trade name, service mark or other branding ("Marks") of WILEY or its

licensors is granted hereunder, and you agree that you shall not assert any such right, license or interest with respect thereto

- NEITHER WILEY NOR ITS LICENSORS MAKES ANY WARRANTY OR REPRESENTATION OF ANY KIND TO YOU OR ANY THIRD PARTY, EXPRESS, IMPLIED OR STATUTORY, WITH RESPECT TO THE MATERIALS OR THE ACCURACY OF ANY INFORMATION CONTAINED IN THE MATERIALS, INCLUDING, WITHOUT LIMITATION, ANY IMPLIED WARRANTY OF MERCHANTABILITY, ACCURACY, SATISFACTORY QUALITY, FITNESS FOR A PARTICULAR PURPOSE, USABILITY, INTEGRATION OR NON-INFRINGEMENT AND ALL SUCH WARRANTIES ARE HEREBY EXCLUDED BY WILEY AND ITS LICENSORS AND WAIVED BY YOU.

- WILEY shall have the right to terminate this Agreement immediately upon breach of this Agreement by you.

- You shall indemnify, defend and hold harmless WILEY, its Licensors and their respective directors, officers, agents and employees, from and against any actual or threatened claims, demands, causes of action or proceedings arising from any breach of this Agreement by you.

- IN NO EVENT SHALL WILEY OR ITS LICENSORS BE LIABLE TO YOU OR ANY OTHER PARTY OR ANY OTHER PERSON OR ENTITY FOR ANY SPECIAL, CONSEQUENTIAL, INCIDENTAL, INDIRECT, EXEMPLARY OR PUNITIVE DAMAGES, HOWEVER CAUSED, ARISING OUT OF OR IN CONNECTION WITH THE DOWNLOADING, PROVISIONING, VIEWING OR USE OF THE MATERIALS REGARDLESS OF THE FORM OF ACTION, WHETHER FOR BREACH OF CONTRACT, BREACH OF WARRANTY, TORT, NEGLIGENCE, INFRINGEMENT OR OTHERWISE (INCLUDING, WITHOUT LIMITATION, DAMAGES BASED ON LOSS OF PROFITS, DATA, FILES, USE, BUSINESS OPPORTUNITY OR CLAIMS OF THIRD PARTIES), AND WHETHER OR NOT THE PARTY HAS BEEN ADVISED OF THE POSSIBILITY OF SUCH DAMAGES. THIS LIMITATION SHALL APPLY NOTWITHSTANDING ANY FAILURE OF ESSENTIAL PURPOSE OF ANY LIMITED REMEDY PROVIDED HEREIN.

- Should any provision of this Agreement be held by a court of competent jurisdiction to be illegal, invalid, or unenforceable, that provision shall be

deemed amended to achieve as nearly as possible the same economic effect as the original provision, and the legality, validity and enforceability of the remaining provisions of this Agreement shall not be affected or impaired thereby.

- The failure of either party to enforce any term or condition of this Agreement shall not constitute a waiver of either party's right to enforce each and every term and condition of this Agreement. No breach under this agreement shall be deemed waived or excused by either party unless such waiver or consent is in writing signed by the party granting such waiver or consent. The waiver by or consent of a party to a breach of any provision of this Agreement shall not operate or be construed as a waiver of or consent to any other or subsequent breach by such other party.

- This Agreement may not be assigned (including by operation of law or otherwise) by you without WILEY's prior written consent.

- Any fee required for this permission shall be non-refundable after thirty (30) days from receipt by the CCC.

- These terms and conditions together with CCC's Billing and Payment terms and conditions (which are incorporated herein) form the entire agreement between you and WILEY concerning this licensing transaction and (in the absence of fraud) supersedes all prior agreements and representations of the parties, oral or written. This Agreement may not be amended except in writing signed by both parties. This Agreement shall be binding upon and inure to the benefit of the parties' successors, legal representatives, and authorized assigns.

- In the event of any conflict between your obligations established by these terms and conditions and those established by CCC's Billing and Payment terms and conditions, these terms and conditions shall prevail.

- WILEY expressly reserves all rights not specifically granted in the combination of (i) the license details provided by you and accepted in the course of this licensing transaction, (ii) these terms and conditions and (iii) CCC's Billing and Payment terms and conditions.

- This Agreement will be void if the Type of Use, Format, Circulation, or Requestor Type was misrepresented during the licensing process.

- This Agreement shall be governed by and construed in accordance with the laws of the State of New York, USA, without regards to such state's conflict of law rules. Any legal action, suit or proceeding arising out of or relating to these Terms and Conditions or the breach thereof shall be instituted in a court of competent jurisdiction in New York County in the State of New York in the United States of America and each party hereby consents and submits to the personal jurisdiction of such court, waives any objection to venue in such court and consents to service of process by registered or certified mail, return receipt requested, at the last known address of such party.

WILEY OPEN ACCESS TERMS AND CONDITIONS

Wiley Publishes Open Access Articles in fully Open Access Journals and in Subscription journals offering Online Open. Although most of the fully Open Access journals publish open access articles under the terms of the Creative Commons Attribution (CC BY) License only, the subscription journals and a few of the Open Access Journals offer a choice of Creative Commons Licenses. The license type is clearly identified on the article.

The Creative Commons Attribution License

The Creative Commons Attribution License (CC-BY) allows users to copy, distribute and transmit an article, adapt the article and make commercial use of the article. The CC-BY license permits commercial and non-

Creative Commons Attribution Non-Commercial License

The Creative Commons Attribution Non-Commercial (CC-BY-NC)License permits use, distribution and reproduction in any medium, provided the original work is properly cited and is not used for commercial purposes.(see below)

Creative Commons Attribution-Non-Commercial-NoDerivs License

The Creative Commons Attribution Non-Commercial-NoDerivs License (CC-BY-NC-ND) permits use, distribution and reproduction in any medium, provided the original work is properly cited, is not used for commercial purposes and no modifications or adaptations are made. (see below)

Use by commercial "for-profit" organizations